

---

# **SHM SENSORS OPTIMIZATION BASED ON THE INTEGRATION OF MULTIPLE APPROACH FOR BRIDGE DAMAGE DETECTION**

**(橋梁損傷同定のための多重手法統合による構造ヘル  
スモニタリングセンサー最適化)**

---

ABDUREHMAN MULETA BALI



**Department of Urban Innovation  
Yokohama National University  
Yokohama, Japan**

**February 2022**

---

# **SHM Sensors Optimization based on the Integration of Multiple Approach for Bridge Damage Detection**

**(橋梁損傷同定のための多重手法統合による構造ヘル  
スモニタリングセンサー最適化)**

**A DISSERTATION**

Submitted in partial fulfillment of the requirements for the degree of

**DOCTOR OF PHILOSOPHY (IN ENGINEERING)**

**ABDUREHMAN MULETA BALI**

**Academic Advisors:**

Prof. HIROSHI KATSUCHI

Prof. HITOSHI YAMADA

Assoc. Prof. HIROSHI TAMURA

**Department of Urban Innovation**

**Yokohama National University**

**Yokohama, Japan**

**February 2022**

---

# ABSTRACT

The social, economic, and political development of a country is majorly dependent on the transportation access, from which bridges play the most important role on land transportation. During their operational service, appropriate inspection and maintenance activities must be executed to ensure a prolonged operational life. Otherwise, bridge's failures can be catastrophic, both in terms of human life and economic loss.

Bridge management systems (BMSs) have been developed to assist decision makers in maximizing the safety, serviceability, and functionality of bridges within available budgets. Its system is mainly based on visual inspection, which is the traditional bridge condition assessment technique, to assess the bridges condition. The results of visual inspection are heavily dependent on the experience and judgment of bridge inspectors, yielding primarily qualitative and subjective results.

Hence, a robust condition assessment technique is essential to eliminate the drawbacks of visual inspection and produce quantitative and systematic results, that doesn't depend on the experience or judgment of the inspector.

Structural health monitoring (SHM) is one of non-destructive condition assessment technique. It uses sensors embedded in a structure to monitor and analyze the structure's response and detect abnormal behavior. There are several types of SHM techniques according to the objective of application. The vibration-based and displacement influence line-based damage identification techniques are part of the SHM application for damage identification.

The vibration-based technique uses the measured acceleration response from sensors to identify the modal parameters like; natural frequencies, mode-shapes, mode shape curvature and modal strain energy to identify the damage through change in these parameters.

The displacement-based method uses the measured displacement response of the bridge for the moving load and compare the change in displacement shape of the bridge in relation to displacement influence line to identify the damage location.

Even though, such damage identification methods are being introduced. The practical implementation in actual damage identification is not incorporated in bridge condition assessment. Hence, in this thesis, the improvement on the methods considering the practical implementation of these systems is studied. For reducing the uncertainty towards decision making the joint application of these two methods is recommended as a multi-approach damage identification technique.

Reviews on the SHM study also shows the limitation of optimization related studies. About 4.5% of the research papers on the area of SHM focus on sensor placement optimization. Hence, this thesis, in addition to improvement on the damage identification techniques, the optimized sensor placement is also conducted to further improve the SHM system.

Different cases scenarios are considered and the damage identification using the improved methods have been analyzed. The optimization of SHM sensors improves the damage identification by providing stable location for measuring responses with minimal noise effect.

The modification of SHM techniques improves the practical applicability of the system. The displacement-based index method, MDBI, improves the damage location identification in dynamically excited bridges. The FE-MSE method also shows good result by using finite element-based damage detection.

In the MDBI method, sensor's location shows to have impact on the result of damage identification. Sensors by the bridge entrance side have better damage identification than the sensors located at the bridge exit side. Hence, when observing cumulative MDBI, the direction of movement, it is recommended to take into consideration and only sensors corresponding to that direction.

Furthermore, the utilization of multi-approach technique is showing a promising result towards addressing diversification in damage identification and improving decision making.

**Dedicated to Kalid Muleta Bali**

My beloved and most respected brother

August 1987 - December 2019

# ACKNOWLEDGMENTS

*Alhamdulillah Rabil Alamin (all praise belongs to Allah)*

During the PhD study, the author has encountered a lot of difficulty in life and study. Especially, when the author lost his brother, who also was studying his PhD in India during the same period. It was a difficult time for the author to focus and continue his study. Without a kindly support and understanding from his supervisor and family, the author could not finish his study as well as enjoy the life here in Japan. Now is the time for author to express his gratitude to all of them.

The author would like to express his deepest and sincere gratitude to Professor Hiroshi Katsuchi of Yokohama National University, who has supported the author in both academic and non-academic matters. His kind support and encouragement lead to accomplishment of the dissertation.

The author wishes to express his appreciation to Professor Hitoshi Yamada, Associate Professor Hiroshi Tamura, and Associate Professor Dionysius Siringoringo of Yokohama National University and Associate Professor Mayuko Nishio of Tsukuba University for their constructive advice and recommendation during his study.

The author is grateful for the committee members Professor Koichi Maekawa and Associate Professor Chikako Fujiyama for their important comment and suggestions.

Next, the author is highly indebted and grateful to the Japanese Government and Peoples for their generous financial assistance through Ministry of Education, Culture, Sports, Science and Technology (Monbukagakusho) scholarship.

The contribution of voluntary group members, Hagiwara-san from RKK group and Yagi-san from Mitsui V-net have helped the author to understand the culture and lifestyle of Japanese people and able to communicate with daily conversation level.

Members of the Structural Laboratory of Yokohama National University also showed kind cooperation, support, and assistance for the author, which he is grateful for. Specially, the author would like to thank Dr. Khawaja Ali, for his guidance on various issues those occasionally appeared.

Finally, the author would like to show deepest gratitude to his family and friends who continuously encouraged and support him both academically and emotionally. My wife, Medina Assefa, you have played an important role during my study, I am happy and grateful to have you by my side. My son, Khalid Abdurehman, you have been a motivation for achieving more in my life and most of all a replacement for my brother. My friend, Addisu Desalegn, thank you for being there when I need you the most. My father, mother, brothers, and sisters, thank you very much for always remembering me in your prayers and supporting me emotionally, it has been a great drive for my accomplishment.

Abdurehman Muleta Bali

# CONTENTS

Chapter 1: Introduction .....	1
1.1 Background of the Research .....	1
1.2 Motivation of the Thesis .....	2
1.3 Objectives of the Study .....	2
1.4 Research Contribution.....	3
1.5 Research Methodology.....	3
1.6 Outline of the Thesis .....	4
Chapter 2: Literature Review .....	6
2.1 Bridge Condition Assessment .....	6
2.1.1 Visual Inspection.....	6
2.1.2 Load Testing.....	7
2.1.3 Non-Destructive Test .....	7
2.1.4 Structural Health Monitoring .....	7
2.2 Structural Health Monitoring (SHM) for Damage Identification.....	9
2.2.1 Displacement Influence Line Method .....	12
2.2.2 Modal Strain Energy Method .....	14
2.3 Multi-Objective Optimization with Genetic Algorithm .....	16
2.3.1 Non-dominated Sorting Genetic Algorithm (NSGA-III) .....	16
2.3.2 GA Operators .....	18
Chapter 3: Multi-Approach Damage Identification .....	19
3.1 Modified Displacement Based Index Method.....	20
3.1.1 Transfer of displacement data .....	21
3.2 Modified MSE Based Method.....	23
Chapter 4: Numerical Analysis using FE Modeling .....	26
4.1 Target Bridge Modeling .....	26
4.2 Bridge Vehicle Interaction .....	28
4.2.1 Road Surface Profile .....	28
4.2.2 Vehicle's Dynamic Load.....	30
4.3 Bridge Response Measurement.....	33
Chapter 5: SHM Sensors Optimization with NSGA-III.....	34
5.1 Problem Representation .....	34
5.2 Optimization Objective Functions.....	35
5.2.1 Displacement Sensors.....	35
5.2.2 Acceleration Sensors .....	38

5.3 Genetic Algorithm Coding .....	44
5.4 Optimization Flow.....	45
5.5 Optimality curve.....	46
Chapter 6: Damage Identification .....	48
6.1 Damage Modeling.....	48
6.2 Damage Scenarios .....	50
Chapter 7: Results and Discussion .....	52
7.1 Data collection and processing.....	52
7.2 Sensor Placement Optimization .....	56
7.2.1 Longitudinal direction displacement sensor optimization result.....	59
7.2.2 Vertical direction displacement sensor optimization result.....	61
7.2.3 Acceleration sensor optimization result .....	63
7.3 Vehicle's Transverse Position Identification .....	65
7.4 Damage Identification.....	68
7.4.1 Case-1 .....	69
7.4.2 Case – 2 .....	73
7.4.3 Case – 3 .....	75
7.4.4 Case – 4 .....	78
7.4.5 Case – 5 .....	80
7.4.6 Case – 6 .....	83
7.4.7 Case – 7 .....	85
7.4.8 Case – 8 .....	88
Chapter 8: Conclusion.....	94



## LIST OF FIGURES

Fig. 1 Research flow chart.....	4
Fig. 2 Displacement influence line of a structure to a moving load.....	12
Fig. 3 Reference points on a normalized reference plane [4].....	16
Fig. 4 Flow chart for identification of true transverse position of the vehicle .....	21
Fig. 5 Flow chart of damage identification with FE based MSE .....	25
Fig. 6 Target bridge information (a) Bridge dimensions (b) Bridge cross section (c) Panel arrangement.....	26
Fig. 7 Bridge Loading. (a) Loading Arrangement (b) Material property Validation .....	27
Fig. 8 Mode shapes of the target bridge .....	28
Fig. 9 Road surface profile.....	30
Fig. 10 Quarter car model .....	31
Fig. 11 Dynamic loading generated by the vehicle on the bridge .....	32
Fig. 12 Bridge loading with moving axel load.....	32
Fig. 13 Candidate node distribution under the slab and girder.....	33
Fig. 14 (a) Singular value plot. (b) location of sudden drop in singular value.....	40
Fig. 15 Genetic coding representation of individual in a population .....	44
Fig. 16 Flow diagram of the optimization process.....	45
Fig. 17 Flow diagram for the optimality curve updating .....	47
Fig. 18 Damage locations considered in the scenarios.....	49
Fig. 19 Panel arrangement of the slab .....	49
Fig. 20 Candidate sensor position and assigned notation.....	52
Fig. 21 Vertical acceleration response at node 116 (mid span) measured for full length of simulation.....	53
Fig. 22 Vertical acceleration response at node 116 after removing the section when the load is on bridge.....	53
Fig. 23 Longitudinal acceleration measured at node 116 after the vehicle leaves the bridge. ....	54
Fig. 24 Transversal acceleration measured at node 116 after the vehicle leaves the bridge .....	54
Fig. 25 Vertical displacement response measured at node 116.....	55
Fig. 26 Extracting vertical displacement response for section where the vehicle is on bridge ...	55

Fig. 27 Longitudinal displacement response for section where the vehicle is on bridge .....	56
Fig. 28 GA parameters comparison: two-point crossover vs mixed crossover .....	56
Fig. 29 GA parameters comparison: 1% mutation rate vs 2% mutation rate .....	57
Fig. 30 GA parameters comparison: 100 Generation vs 150 Generation.....	57
Fig. 31 Optimized non-dominate members through the search progress .....	58
Fig. 32 Strong relationship plot for sensor 10 with other candidate nodes .....	59
Fig. 33 Strong relationship plot for sensor 43 with other candidate nodes .....	60
Fig. 34 Strong relationship plot for sensor 54 with other candidate nodes .....	60
Fig. 35 Contour plot of sensor overlap.....	60
Fig. 36 Strong relationship plot for sensor 2 with other candidate nodes .....	61
Fig. 37 Strong relationship plot for sensor 6 with other candidate nodes .....	62
Fig. 38 Strong relationship plot for sensor 230 with other candidate nodes .....	62
Fig. 39 Contour plot of sensor overlap.....	62
Fig. 40 Optimality curve sample 1 .....	64
Fig. 41 Optimality curve sample 2 .....	64
Fig. 42 Transverse position measurement reference .....	65
Fig. 43 Strain response measurement location .....	66
Fig. 44 Influence surface calibrated for the left-side outer girder.....	66
Fig. 45 Influence surface calibrated for the right-side outer girder.....	66
Fig. 46 True transverse position identified at 1.604m shifted from reference point .....	67
Fig. 47 True transverse position identified at 3.011m shifted from reference point .....	67
Fig. 48 True transverse position identified at 4.217m shifted from reference point .....	68
Fig. 49 Sensor distribution under the target bridge a) 3D view b) Top view.....	68
Fig. 50 Case 1 damage location identification with DBI and M-DBI methods. ....	70
Fig. 51 Case 1 individual sensors estimation of the damage index with DBI method. ....	70
Fig. 52 Case 1 individual sensors estimation of the damage index with modified DBI method	71
Fig. 53 Case 1 identified damaged elements using FE-MSE method .....	71
Fig. 54: Integrated damage location identification for case 1. a) actual simulated damage, b) M-DBI estimation c) FE-MSE estimation. ....	72
Fig. 55 Case 2 damage location identification with DBI and MDBI methods.....	73

Fig. 56 Case 2 individual sensors' estimated damage index for DBI method.....	74
Fig. 57 Case 2 individual sensors' estimated damage Index for MDBI method.....	74
Fig. 58 Case 2 identified damaged elements using FE-MSE method .....	74
Fig. 59 Integrated damage location identification for case 2. a) actual simulated damage, b) M-DBI estimation c) FE-MSE estimation. ....	75
Fig. 60 Case 3 damage location identification with DBI and MDBI methods.....	76
Fig. 61 Case 3 individual sensors' estimated damage index for DBI method.....	76
Fig. 62 Case 3 individual sensors' estimated damage index for MDBI method .....	76
Fig. 63 Case 3 identified damaged elements using FE-MSE method .....	77
Fig. 64 Integrated damage location identification for case 3. a) actual simulated damage, b) M-DBI estimation c) FE-MSE estimation. ....	77
Fig. 65 Case 4 damage location identification with DBI and MDBI methods.....	78
Fig. 66 Case 4 individual sensors' estimated damage index for DBI method.....	78
Fig. 67 Case 4 individual sensors' estimated damage index for MDBI method .....	79
Fig. 68 Case 4 identified damaged elements using FE-MSE method .....	79
Fig. 69 Integrated damage location identification for case 4. a) actual simulated damage, b) M-DBI estimation c) FE-MSE estimation. ....	80
Fig. 70 Case 5 damage location identification with DBI and MDBI methods.....	81
Fig. 71 Case 5 individual sensors' estimated damage index for DBI method.....	81
Fig. 72 Case 5 individual sensors' estimated damage index for MDBI method .....	81
Fig. 73 Case 5 identified damaged elements using FE-MSE method .....	82
Fig. 74 Integrated damage location identification for case 5. a) actual simulated damage, b) M-DBI estimation c) FE-MSE estimation. ....	82
Fig. 75 Case 6 damage location identification with DBI and MDBI methods.....	83
Fig. 76 Case 6 individual sensors' estimated damage index for DBI method.....	83
Fig. 77 Case 6 individual sensors' estimated damage index for MDBI method .....	84
Fig. 78 Case 6 identified damaged elements using FE-MSE method .....	84
Fig. 79 Integrated damage location identification for case 6. a) actual simulated damage, b) M-DBI estimation c) FE-MSE estimation. ....	85
Fig. 80 Case 7 damage location identification with DBI and MDBI methods.....	86
Fig. 81 Case 7 individual sensors' estimated damage index for DBI method.....	86

Fig. 82 Case 7 individual sensors' estimated damage index for MDBI method .....	86
Fig. 83 Case 7 identified damaged elements using FE-MSE method .....	87
Fig. 84 Integrated damage location identification for case 7. a) actual simulated damage, b) M-DBI estimation c) FE-MSE estimation. ....	87
Fig. 85 Case 8 damage location identification with DBI and MDBI methods.....	88
Fig. 86 Case 8 individual sensors' estimated damage index for DBI method.....	88
Fig. 87 Case 8 individual sensors' estimated damage index for MDBI method .....	88
Fig. 88 Case 8 identified damaged elements using FE-MSE method .....	89
Fig. 89 Integrated damage location identification for case 8. a) actual simulated damage, b) M-DBI estimation c) FE-MSE estimation. ....	89
Fig. 90 Damage location identification for DBI and MDBI methods for evaluating optimized sensor location.....	92
Fig. 91 Damage location identification using individual sensors' estimation for DBI Method..	92
Fig. 92 Damage location identification using individual sensors' estimation for MDBI Method .....	92
Fig. 93 Displacement response in the longitudinal direction .....	93
Fig. 94 Damage location identification for DBI and MDBI methods for evaluating optimized sensor location.....	93

## LIST OF TABLES

Table 1 ISO 8608 $G_d(n_o)$ values .....	29
Table 2 Vehicle's dynamic characteristics .....	31
Table 3 Fast Greedy optimization algorithm .....	42
Table 4 Damage types general information .....	50
Table 5 Damage analysis scenarios .....	51
Table 6 Genetic algorithm parameters adopted for optimization .....	58
Table 7 Optimized longitudinal sensor locations .....	59
Table 8 Optimized vertical sensor locations .....	61
Table 9 Identified and FEM frequencies corresponding to the mode shapes .....	63
Table 10 Shift in transverse position of vehicle from the reference point .....	65
Table 11 Comparison of MDBI and DBI based on summary of case scenarios .....	90
Table 12 Summarized results of case scenarios for the integration of MDBI and FE-MSE methods .....	91

# Chapter 1: Introduction

## 1.1 Background of the Research

Bridges are valuable assets for a society to cross over barriers of connection. The social, economic, and political development of a country is majorly dependent on the transportation access, from which bridges play the most important role on land transportation. This dependence with the bridges increases the demand for safety and reliability of the structure.

Bridge failures can be catastrophic, both in terms of human life and economic loss. Variation of resistance to deterioration and damage between bridge elements makes the inspection and damage identification process challenging.

Reinforced concrete (RC) bridges often deteriorate due to ageing, materials, and construction defects, sever hazard due to exposure to fire, exposure to aggressive environments, lack of ductility, and excessive loads. Steel bridges, however, affected by sever hazard due to exposure to fire, exposure to aggressive environments, corrosion, fatigue, and material defects.

To achieve prolonged service life, the condition of the bridge should be inspected with a reliable bridge condition assessment (BCA) technique that can successfully identify defects in the bridge and recommend maintenance, rehabilitation, or replacement as needs.

Bridge management systems (BMSs) have been developed to assist decision makers in maximizing the safety, serviceability, and functionality of bridges within available budgets. Its system is mainly based on visual inspection, which is the traditional bridge condition assessment technique, to assess the bridges condition. The results of visual inspection are heavily dependent on the experience and judgment of bridge inspectors, yielding primarily qualitative and subjective results. Therefore, lack of identifying the posed risk during inspection led to missing the opportunity to save fatal bridge collapses.

As a result, a robust condition assessment technique is essential to eliminate the drawbacks of visual inspection and produce quantitative and systematic results, that doesn't depend on the experience or judgment of the inspector.

Structural health monitoring (SHM) is a non-destructive condition assessment technique. It uses sensors embedded in a structure to monitor and analyze the structure's response and detect abnormal behavior.

SHM shown successful application for short-term or long-term monitoring of a bridge's response to tracking change in previously identified damages. Once the damage is noticed on the structure, appropriate sensing equipment can be installed and the progress of damage will be tracked [1]. However, the area of damage identification by using SHM system is still in research stage. SHM system shown its effectiveness to detect and locate the damage in laboratory. Considering practical implementation on real structures, the result is not up to the desired level of damage detection. The field implementation is surrounded by noise, environmental effect, variation in

---

excitation mechanism of the structure from the laboratory model, the effectiveness of damage identification technique, and sensitivity of the installed sensor. Studies have been undertaken over the past few years for overcoming the effects of the uncertainty in SHM. [2] The lack of success in reducing the uncertainty in the field implementation hinders the utilization of SHM for damage detection in bridge condition assessment.

## 1.2 Motivation of the Thesis

Even though, the proportion of short to medium span bridge in the bridge stock of any country is large, the application of SHM system is centered on specific structures like long span bridges, tunnels, high-rise buildings, and dams. The utilization of SHM system on the inspection and decision making of short to medium span bridges in the bridge condition assessment is not given due concern. As a result, it is becoming an important social concern to develop and put to practical use of simple and efficient SHM system.

Furthermore, previously proposed SHM approaches adopt single technique to identify damages, this will have a limitation on the effectiveness of that specific SHM technique to address all possible damages occur on bridge components. Hence, it hinders the practicality of the approach for real time damage detection in practical bridge condition assessment.

In addition, the number and placement of the sensing devices play an important role to enhance the effectiveness of the SHM technique in damage detection. Yet, the optimization part of SHM system is not given enough share in the SHM related research.

Hence, in this PhD thesis, the integration of two damage identification methods, that utilize different approach but have a common objective, identifying damage location, are studied considering for reducing uncertainty and promoting practical implementation. The difference in susceptibility to the noise and disturbance between the two methods will complement each other to minimize the uncertainty and encourage practical utilization of SHM for damage detection. Furthermore, the optimal placement of sensing devices for the corresponding damage identification techniques to maximize the quality of measurement and minimize the number of sensors required will be explored.

## 1.3 Objectives of the Study

The main objectives of this research are:

- (i) Integrating multiple damage identification techniques, enhance the damage location identification in bridge structures condition assessment towards rational maintenance strategies.
- (ii) Improve the existing, displacement-based index, damage identification approaches for applicability in damage identification of dynamically excited bridges and

considering the possibility of transverse position shift to the moving load during the initial state and damaged state response measurement.

- (iii) Improve the existing, modal strain energy methods, damage identification approach towards practical implementation in bridge structures condition assessment with an elemental level damage representation from global bridge response.
- (iv) Improve damage identification efficiency by optimal placement of sensors and integrating them for detecting bridge damage for better accuracy level using Genetic Algorithm.

## 1.4 Research Contribution

The impact of this research is mainly on the improvement of practicability and utilization of SHM system for bridge condition assessment of vast majority of the stock in the bridge management system, which are small to medium span bridges.

The proposed multi-approach SHM technique increase the diversity of damage detection, user interactive approach and minimize environmental effect on the identification result. The integration of two approaches provides a reliable information about the bridge condition where the decision makers can rely on due to the conformity of damage location from the two systems.

The proposed approach will have a significant outcome towards enhancing the bridge management system in two areas. First, the information obtained from the SHM system prior to the inspection procedure can reduce the inspection time spent on undamaged structures or bridge members. Second, the SHM results provide consistent information so that miss interpretation, inexperience, or negligence from the inspectors will be noticed immediately and can be corrected.

The optimal placement of sensor's employed managed to minimize the number of sensors while acquiring significant information used in the damage identification. The optimization also ensures the integration of sensors used by multiple techniques.

## 1.5 Research Methodology

The initial stage of the methodology for the study is selection of target bridge. Due to the behavior of damage identification approach, i.e., comparison between healthy state response and damaged state response of a bridge, it is difficult to get the real bridge response data from record that will meet the objective of this study. Therefore, the response of the bridge is obtained from simulation by developing finite element model.

The target bridge is selected from the research by Amir Gheitani et.al.[3] where numerical simulation and validation at the system-level behavior of the composite steel girder bridges have been studied based on a scale laboratory investigation performed at the University of Nebraska. Therefore, the material properties and bridge integration have been modeled to meet the system-level behavior of the composite steel girder bridge validated by their research.



Following the validation of material properties and bridge element integration with the research conducted by Amir Gheitasi et.al.[3], the bridge is loaded with a moving axel load considering road roughness to generate a dynamic response. This dynamic repose is recorded throughout the vehicle movement crossing the bridge and used as a source data to optimize the placement of sensors corresponding to the studied damage identification technique.

A multi objective genetic algorithm is developed based on non-dominated sorting (NSGA - III) search platform introduced by Deb K. et.al. [4].

Based on multiple damage scenario, the response of the bridge is simulated for the damaged state. This response obtained from the optimized sensors at a damaged state is compared with the corresponding healthy state of the bridge for damage identification using the integrated approaches. The flow chart of methodology used in this study is presented in Figure 1 as follows.

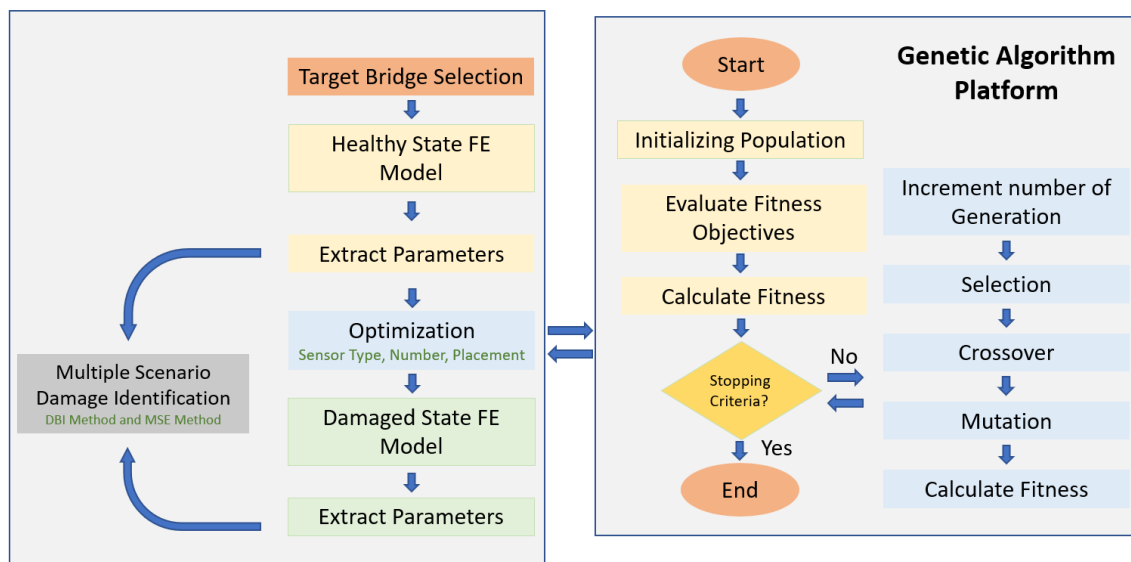


**Fig. 1** Research flow chart

## 1.6 Outline of the Thesis

This thesis is composed of eight chapters. This chapter provides the introduction and background of the thesis.

Second chapter provides review of the literature focusing on bridge condition assessment, structural health monitoring and optimization algorithm.

Chapter three is discussing about the integration of two damage identification techniques that are using different approach to identify the location. Hence, the application of both methods reduces the uncertainty in damage identification.

In chapter four, the selection of target bridge and its finite element modeling will be discussed. The effect of bridge-vehicle interaction on the bridge response is very important to consider when studying about bridge. In addition, the bridge response measurement is discussed.

Based on the measured response from the finite element method, the structural health monitoring sensors are optimized based on the methodology discussed in chapter five.

Once the optimized sensor locations are identified the damaged cases are measured. Hence, the analysis for damage identification by proposed methods will be evaluated. Thus, the damage modeling and scenarios are discussed in chapter six.

Chapter seven presents the figure and tables generated during damage identification and discusses in detail about the obtained results.

Finally, chapter eight summarizes and concludes the work done in this study.

# Chapter 2: Literature Review

## 2.1 Bridge Condition Assessment

Existing bridges and their elements are exposed to damage through aging, deterioration, and natural disasters during their operational life. This leads to structural and/or functional failure which can further lead to human life loss, economic loss, and limitation on social interaction. Evaluation of structural performance and damage of existing bridges is essential for rational and efficient stock management. Hence a proper condition assessment of the bridge shall be conducted.

The main objective in condition assessment for an existing bridge is to evaluate the safety and reliability over the remaining service life. Even though, several countries develop a guideline for assessment of existing bridges through bridge management system (BMS), the evaluation method is highly dependent on traditional visual inspection method. The challenge in this method is the difficulty for quantification of information on bridge condition.

Bases on their functionality several bridge condition assessment approaches exist. This includes visual inspection, load testing, structural health monitoring, non-destructive evaluation and finite element modeling.[5]

### 2.1.1 Visual Inspection

Visual inspection is the primary and traditional technique used in the inspection of bridge condition. Generally, it is conducted periodically. It's low cost and simplicity contribute to the broad adoption in bridge management. However, it is prone to inaccuracies. Visual inspection is often conducted within 24-months intervals depending on the condition of the bridge. [6] The fact that the inspection is conducted in the longer interval contribute to the unreliable result and difficulties in identifying the correct repair priority. In addition, Human factors greatly affect the result of the inspection. The same bridge once identified as a high-risk bridge could be reported good condition bridge without any maintenance. The experience of an inspector, perception, inspection condition, and environment greatly contribute to the consistency of the inspection.

Visual inspection commonly conducted as a routine inspection or in-depth inspection. The at which these inspections vary with in different countries. (US, Japan, Ethiopia). Due to the subjectivity of visual inspection the results of a bridge inspection vary depending on factors. As described by Tarek Omar [5] , the quality and consistency of visual inspection results greatly depend on the motivation and equipment of those conducting such inspections. Graybeal et.al [7] on their report that summarizes the results of the study by Federal Highway Administration conducted to investigate the reliability of visual inspection of highway bridges, it is found that significant variability in the assessment of condition rating is noticed. Some factors relate with the variation in results, including inspectors fear of traffic, near visual acuity, color vision, formal training in bridge inspection, accessibility, and complexity.

Moreover, accessing the damaged elements of the bridge is one of the challenges for visual inspection. Even though, there have been developed complicated machineries to avoid this challenge, they are mainly applied for specific types of bridges. The purchase and operation cost will inhibit it from practicality in wide variety of bridges.

In addition, the detectability of specific types of damages is compromised due to the visibility issue. Hence, the increased awareness of the visual inspection shortcomings has motivated advanced bridge condition assessment approaches. [8]

However, against the odds that visual inspection is subjective and have significant deficiency towards consistent condition assessment, unavailability of robust and reliable substitute for it, still makes visual inspection as a significant aid for bridge condition assessment.

### 2.1.2 Load Testing

Load testing is a procedure to determine the safe loading levels of a bridge, leading to a load rating which provides the capacity level of a bridge[6]. The maximum response can be detected using strain transducers placed at critical locations on the bridge. The load ratings can be determined through forced static and dynamic load testing of allowable stress, load factor, or load and resistance factor methods.

### 2.1.3 Non-Destructive Test

Non-destructive evaluation (NDE) are techniques that enable detection of deterioration processes at their early stages.[5] Non-destructive evaluation methods can be incorporated into the inspection process for example to evaluate stiffness and strength, moisture content, and hidden defects. Non-destructive evaluation is specified in some BMSs through periodical surveys or when visual inspection results indicate irregularities within the structure. Appropriate and effective use of NDE needs three requirements: (i) suitable understanding of the underlying phenomenon, (ii) deploying testing methods correctly, and (iii) applying appropriate and accurate models in the analysis to quantify the detected defects or variation of properties.

### 2.1.4 Structural Health Monitoring

Structural health monitoring (SHM) is a technique for bridge condition assessment using a sensing device embedded in a structure to monitor and analyze the structure's in-service performance through short-term or long-term evaluation. Using proper tools and techniques, changes to the material or geometric properties of structures are evaluated to identify potential harmful factors and provide assessment for maintenance decisions during its service life.

SHM is best suited for bridge condition assessment. These include, Low cost; ability to perform continuous assessment; sensitivity to low level of damage; Insensitivity to environmental condition changes. [8]

Based on the data accusation period SHM can be categorized as follows:

## **1. Long-term assessment**

Long-term assessment in SHM is a technique in which the performance of the structure is continuously evaluated through its response for relatively longer time. This technique is employed to ensure safety of an important structure and detect its performance deterioration during the long-time service. The application of SHM in long-term assessment often includes a group of variety of sensors to capture the condition of the environment that have effect on the target observation.

Long-term monitoring can provide detail information about the targeted performance of the bridge and additional information and the environmental factors related to change in the performance. This is crucial to detect any abnormality in very initial stage. Hence, it can be considered that the major advantage of this technique is providing information towards preventive action rather than corrective.

However, the amount of data collected is enormous, increasing the computation time for interpreting the responses. Furthermore, the overall budget of the SHM system for installation and running the system to acquire data without losing major information on structural daily behavior, will make it expensive. This can be considered as the disadvantage for long-term monitoring.

## **2. Short-term assessment**

Short-term assessment in SHM is a technique in which the performance of the structure is evaluated through its response gathered on a specific and extraordinary occasions. The reason to this approach is to reduce the data collection and evaluation of the structure performance on a normal condition.

This approach can greatly reduce the data generated from the sensing equipment, consequently, reduce the computational time. Even though, the progress of the structure's performance cannot be obtained, the information on critical condition will provide adequate evaluation. This will have elevated implication on the minimizing running cost of the system.

The condition assessment of bridge structures spanning from short to medium range are very crucial. These types of bridges constitute higher portion of the bridge stock in many countries. However, the initial implementation cost can be higher. Researchers have been trying to find a solution to these through sensor optimization and developing other techniques to gather SHM data. Taking the advantage of smartphone accelerometer development, Ozer E. et al. [9] proposed citizen sensors for SHM, where, citizens are enabled to measure the vibration of bridge structures and upload to the server. Later, modal parameters can be collected and evaluated for damage in the bridge. A related approach for this is a study by Miyamoto A. [10] where bus mounted accelerometers are used to measure the response of bridge structures along an in-service fixed-bus-routes. Measured bridge responses are used to detect a damage. These types of systems help bridge administrators to establish a rational maintenance strategy with low cost of investment on SHM system. However, the consistency of measurement locations has to be taken in to account as the users measurement points are varying between measuring each state of the bridge condition that will contribute greatly to the measurement noise.

## 2.2 Structural Health Monitoring (SHM) for Damage Identification

Recently, various structural condition assessment techniques have been proposed for damage detection. Among these, structural health monitoring is a highly applicable technique. Unlike the traditional visual inspection technique, structural health monitoring has improved the method to a level where the damage can be evaluated quantitatively.

Damage identification with SHM system can be conducted by comparing the response of the structure at healthy stage, where the bridge is new, and at damaged state. Unlike long-term or short-term assessment technique, the damage identification limited sensor and specific data to analyze a damage.

SHM uses several techniques for damage detection based on the proposed approach and sensing equipment. We can generalize the existing damage identification methods into two major categories: the dynamic identification methods using dynamic test data, and the static identification methods using static test data. The most common techniques followed by SHM system includes vibration-based monitoring,[11][12][13] strain-based monitoring,[14][15][16] displacement influence line-based monitoring [17][18][19], elastic waves-based monitoring,[20][21][22] electromechanical impedance-based monitoring[23] and comparative vacuum monitoring (CVM).[24][25] Most of these techniques are based on the correlation between two measured responses or comparison of the measured response of damaged structure to that of the healthy structure.

### 1. Vibration Monitoring

Vibration-based techniques focuses on the effects of damages on the dynamic behavior of a structure. They are one of the major fields of interest in SHM. Sensors are placed on the structure to obtain modal properties such as natural frequency, mode shape, mode shape curvature, and modal strain energy.

Basically, the vibration monitoring can be divided in to local and global monitoring. Local methods inspect the structure in a relatively small area. These methods are very sensitive and able to find small defects. In cases where the structures critical elements can be identified priorly from experience or analysis, the concerned location can be fit with appropriate sensors to inspects the predicted damage condition. Global methods on the other hand, use the fact that the local damage has an influence on the global behavior of the whole structure in terms of time and space. The characteristic vibration patterns from operational loads or natural vibrations can be used in global method. The stiffness loss due to local damage in the structure creates alteration in the system's physical properties like shifts in resonant frequencies, increases in damping or changes of vibration modes which can be used as indicator of damage affecting the structure's global behavior. Fewer sensor distribution can address the structure's response compared with the sensors used in local method. However, global methods are less sensitive, and they usually have lower spatial resolution.

Among the vibration methods, modal strain energy (MSE) method is becoming a focus of research area due to the sensitivity of MSE to change in structures due to damage rather than pure mode shapes, it is becoming of interest to gather detail information of damage with respect to damages the location and extent of damage.

Shi et al. [26] established an approach to detect the damage using the change in MSE. Shi's approach is simple and capable of detecting single or multiple structural damages. Identification technique is based on the Information of measured mode shapes and elemental stiffness matrix. Shi's result showed that the proposed approach can locate single and multiple damages that are contaminated with some percentage of noise effect. Dewangan et al. [27] used the MSE approach to identify damaged parts in wind turbine gearbox.

## **2. Strain Monitoring**

Strain monitoring measures the degree of strain imposed by the load on the structure. Strain measurement is one of the most reliable and available structural responses [28].

Jang et al. [28] used a strain damage locating vector (DLV) combined with static strain measurement for structural damage identification. Alaimo et al. [14] used strain sensing as a delamination cracks identification in composite structures. Garcia et al. [15] applied strain sensing to measure load and crack propagation in corrosion-fatigue. The use of fiber bragg grating optical sensors also improved the application of strain monitoring. Yeager et al. [16] used embedded and surface mounted fiber bragg grating on composite structures to study the effectiveness of embedding process, performance at different environment and performance of SHM result.

## **3. Displacement Influence Line Monitoring**

The displacement response of structures under static or dynamic loading will be used in structural damage detection from displacement its shape. Damage in the structure affects the flexural stiffness, as a result the displacement response of a structure in damaged state does not correspond with the measured displacement at the healthy state. Ono et al. [17] and Ha et al. [18] use the statical displacement of the structure at the healthy state and damaged state to locate the damage position in the longitudinal direction of the bridge structure. Stimac et al. [19] used the change in curvature to locate the damage location in beam and plate structures. Furthermore, Sun et al. [29] use a dynamic displacement response and separated in to quasistatic and dynamic components. Based on the curvature of the beam generated from quasi-static response, damage identification is conducted.

## **4. Elastic Waves Monitoring**

In thin plate-like structures, waves propagate as guided waves, also called Lamb waves. Information about the condition of materials was extracted from the analysis of the varying voltage recorded between the piezoelectric element electrodes. Kessler et al. [20] used optimal actuator and sensor configuration to provide procedure for easy and accurate determination of time-of-flight of lamb waves. Damages like delamination, transverse ply cracks and through-holes are used to investigate the effectiveness. Khalil et al. [21] used elastic wave monitoring in

detection of corrosion inspection. Giurgiutiu V. [22] used the embedded piezoelectric wafer active sensors to excite and detect lamb waves. Cracks are detected with the pulse echo technique.

## **5. Electromechanical Impedance Monitoring**

Electromechanical impedance monitoring is used for crack detection in metallic structures. It utilizes arrays of piezoelectric wafers attached to the surface of a metallic structures or inserted between the layers of a composite material. The piezoelectric wafers serve as active sensors that can act as both actuators and detectors of elastic waves in the structure. [23]

Electromechanical impedance assesses the local structural response at very high frequencies which is not affected by the global structural modes and environmental conditions. Local damages which produce only unnoticeable flaws in the large-scale dynamics of the structure. The local-area health monitoring identifies delamination and crack growth on composite structures.

## **6. Comparative Vacuum Monitoring**

Comparative vacuum monitoring is a pneumatic sensor technology developed to detect the initiation and propagation of cracks. CVM is a measure of the differential pressure between fine galleries containing a low vacuum alternating with galleries at atmosphere in a simple manifold. The small volume maintained at a low vacuum is sensitive to any ingress of air and leakage. Cracks on structure under monitoring will allow leakage in pressure resulting the measured pressure change. Hence cracked section can be detected.

CVM can monitor external surfaces of materials for crack initiation, propagation, and corrosion. Sensors are installed at critical regions of the structure. The vacuum level remains stable at health regions and the pressure rises for damaged section. When a crack develops, it forms a leakage path between the atmospheric and vacuum galleries, resulting in significant change in the pressure level. As a result, the flawed section can be identified.

In case of composite material, CVM sensors can also be embedded between components or within material compounds. Thus, problems related to cracking, fatigue and corrosion can be detected when and where they are initiated.

This type of sensors is effective for damage detection where we have the prior knowledge of the hotspot for crack initiation, the propagation of crack can be monitored using these devices. [24]

Most of the research conducted on the above mentioned SHM techniques are focusing on a specific approach for identifying damage. However, the damage or deterioration on the bridge structure or its elements are not known priory, in the structures healthy state. Therefore, implementing the damage detection technique prior to the occurrence of damage has been a great challenge. As a result, the full potential of SHM system for using as a bridge condition assessment technique in bridge management system is not yet explored. In this research, the integration of two damage identification techniques, vibration-based method, and displacement influence line-based method, is used to improve the damage identification and confirmability by the integrated approach. This is vital in reducing the uncertainty observed in decision making of Bridge Management System.



Furthermore, the damaged identification can be improved by optimal SHM sensor placement for the corresponding integrated approaches.

### 2.2.1 Displacement Influence Line Method

Damage detection technique uses displacement shape of the bridge to locate the existence of damage in the bridge. This technique is majorly based on static that depend on the stiffness matrix, because they can be obtained accurately and rapidly by inexpensive tools of measurement.

Recently, utilization of displacement response due to a moving load data attracted notable consideration, T M Ha et.al. [18] proposed a damage detection method to identify the occurrence of damage by evaluating correlations among measured displacement data. The difference in deflection when compared with the undamaged structure indicates its deterioration of flexural rigidity. Hence measuring the nodal displacement of the structure in undamaged state due to the applied static force vector is obtained by the static relation expressed in equation 1 below.

$$F = Ku \quad (1)$$

Where,  $K$  is a stiffness matrix,  $F$  is an applied static force vector, and  $u$  is displacement vector. Therefore, the damage in the structure affects the stiffness, as a result the displacement response of a structure in damaged state does not correspond with the measured displacement at the original state.

They introduced the Displacement-Based Index (DBI) as a damage localization method utilizing the change in displacement shape for detecting the structural damage of a prestressed concrete (PC) girder model. However, the DBI involved a technique based on static loads, and no consideration on the moving load was reported.

Ono R. et.al. [17] in their study present analytical study on damage detection method by improving the proposed approach by T M Ha et.al. [18]. They utilize the concept of displacement influence line of road bridge slab to incorporate the response of a bridge to a moving load. In their research they used Displacement Based Index (DBI) method for identifying damage in the bridge structure subjected to the statically moving load.

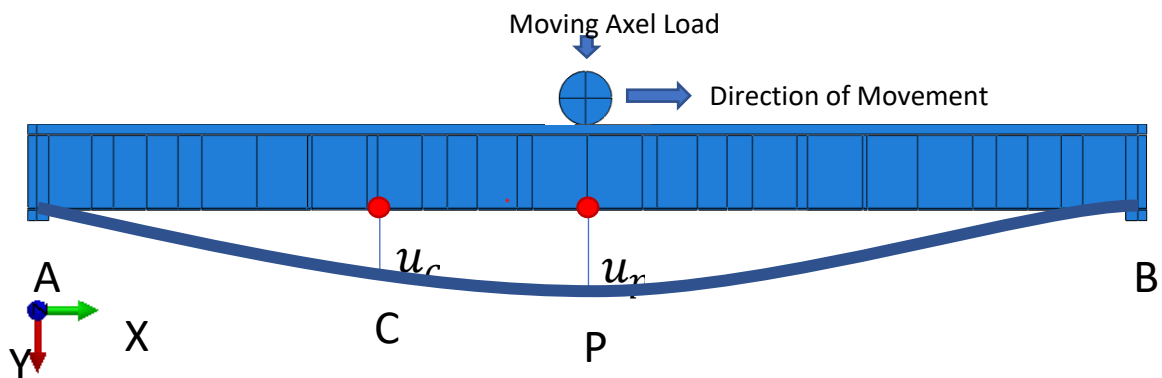


Fig. 2 Displacement influence line of a structure to a moving load

Basis of this approach can be summarized in to two hypotheses.

1. The Influence line of the displacement at point C in the elastic beam can be obtained by sequentially moving the unit load from support A to support B as shown in Figure 2.
2. Based on Maxwell-Betti reciprocity theorem, the deflection of point C due to a unit load at a certain point P is equal in magnitude to the deflection of point P produced by a unit load applied at point C.

Hence the nodal displacement at point C measured during a moving load crosses the bridge from support A to support B creates an influence line to the moving load with respect to point C. the mathematical express is presented on equation 2 for undamaged case and equation 3 for damaged case.

$$[x, u_i] = [(x_1, u_{i1}), \dots, (x_j, u_{ij}), \dots, (x_n, u_{in})] \quad (2)$$

$$[x, u_d] = [(x_1, u_{d1}), \dots, (x_j, u_{dj}), \dots, (x_n, u_{dn})] \quad (3)$$

$$\Delta u(j) = |u_d(j) - u_i(j)| \quad (4)$$

$$DBI(j) = \max \left[ 0, \frac{\Delta u(j) - \mu}{\sigma} \right] \quad (5)$$

Where;  $x$  is the loading position,  $u_i$  displacement influence line at the undamaged state,  $u_d$  displacement influence line at the damaged state,  $\Delta u$  is change in displacement influence line,  $\mu$  and  $\sigma$  are mean and standard deviation of  $\Delta u$ , and  $DBI$  is the displacement-based index for damage identification.  $DBI = 0$  indicates the undamaged section of the structure, whereas the  $DBI$  value reaches its highest at the location of the damage.

The approach has a potential to damage identification in bridge structures, however further studies shall be conducted to take into consideration the dynamic excitation generated due to the vehicle bridge interaction and the transversal position of the vehicle during measuring the undamaged state and damaged state responses.

Zhen Sun et.al [29] proposed a damage detection method which uses dynamic displacement of bridge structures under moving vehicle. Their method is based on curvature for damage detection, unlike the former methods this method does not require baseline of undamaged state of the bridge for detecting damage location and size. In the research by separating the displacement into quasi-static component and dynamic component, the proposed method focuses on the evaluation of quasi-static component for computing the curvature. Zhen Sun et.al [29] identified the quasi-static component of displacement of the bridge from the closed form solution expressed in equation 6.

$$y(x, t) = -\frac{2PL^3}{m\pi^2} \sum_{i=1}^{\infty} \frac{\sin\left(\frac{inx}{L}\right)}{i^2(i^2\pi^2a^2 - v^2L^2)} \sin\left(\frac{i\pi vt}{L}\right) + \frac{2PL^4v}{m\pi^3a} \sum_{i=1}^{\infty} \frac{\sin\left(\frac{inx}{L}\right)}{i^3(i^2\pi^2a^2 - \dot{u}^2L^2)} \sin(\omega_n t) \quad (6)$$

Where  $L$  is the length of the bridge,  $P$  is the amplitude of the moving load,  $m$  is the mass per unit length,  $EI$  is the flexural rigidity of the bridge,  $v$  is the velocity of the moving force,  $\omega_n$  is the natural frequency of the bridge.

The first part in equation 6 is related to the vehicle speed, which can be referred as the quasistatic component, whereas the second part that contain the bridge natural frequency is referred as the dynamic component that is resulted due to the vibration of the bridge.

The relation between bending moment and curvature of the beam, as expressed in equation 7, is used to identify damage from curvature.

$$M(x) = -EI(x) \frac{d^2w(x)}{dx^2} \quad (7)$$

Where E is the Young's modulus of the material, I denotes the second moment of area of the beam cross section,  $w(x)$  is deflection of the beam,  $x$  is the coordinate and  $M(x)$  is the bending moment.

The curvature is then calculated from the second derivative of deflection measurement expressed as follows

$$k(x) = \frac{d^2w(x)}{dx^2} = -\frac{M(x)}{EI(x)} \quad (8)$$

On the proposed approach, the damage in the structure is identified from the abrupt change in the curvature plot corresponding to the location where there is stiffness loss.

In this research, damage identification with displacement-based index method will be used with an improvement in considering dynamic vibration effect from vehicle bridge interaction. In addition, the effect of transverse position of the vehicle will be considered to minimize the uncertainty in measurement of bridge response at healthy and damaged state of bridge. Furthermore, the number and optimal placement of sensors will be conducted to locate best position with minimum noise effect.

## 2.2.2 Modal Strain Energy Method

Structural damage often causes changes in flexural moments and the flexural stiffness. In statically determinate structure, since flexural stiffness has no influence in flexural moment, change in flexural stiffness will affect the integrity of the structure. Whereas, in statically indeterminate structures, both change in flexural stiffness and flexural moment can affect the integrity of the structure. But the effect to change in flexural stiffness is intensify in a localized field compared to the flexural moment.

Therefore, in actual structures the damage often cause loss in stiffness in one or more elements of a structure, rather than a loss in the mass. [26] The effect of damage in stiffness matrix and modal parameters can be mathematically expresses based on equation of motion for a n-DOF system as:

$$\lambda M \Phi - K \Phi = 0 \quad (9)$$

$$K^d = K^i + \Delta K, \text{ where, } \Delta K = \sum_{j=1}^J \Delta K_j \quad (10)$$

$$\lambda^d = \lambda^i + \Delta \lambda \quad (11)$$

$$\Phi_j^d = \Phi_j^u + \Delta\Phi_j \quad (12)$$

Where,  $M \in R^{n \times n}$  and  $K \in R^{n \times n}$  are the system's mass matrix and stiffness matrix.  $\lambda$  and  $\Phi$  represent the eigenvalue and eigenvector of the system,  $J$  is the total number of elements, and superscript  $d$  and  $u$  are the damage and intact state indicators, respectively.

The elemental MSE is defined as the product of the elemental stiffness matrix and the second power of the mode shape component. The MSE in the healthy state and damaged state of a structure can be represented for the  $i^{\text{th}}$  mode and the  $j^{\text{th}}$  element as follows:

$$MSE_{ij}^u = \Phi_i^{uT} K_j \Phi_i^u \quad (13)$$

$$MSE_{ij}^d = \Phi_i^{dT} K_j \Phi_i^d \quad (14)$$

Where,  $MSE_{ij}^u$  and  $MSE_{ij}^d$  represent the modal strain energy values measured at bridge's healthy state and damaged state,  $\Phi_i^u$  and  $\Phi_i^d$  are mode shapes of the system at healthy and damaged state respectively and  $K_j$  is the elemental stiffness matrix at undamaged state.

The damage causes local stiffness reduction which affect the mode shapes of the structure in the localized region that can be measured from the structure's response. However, the elemental stiffness matrix change is difficult to determine prior identifying the location of damage. Hence the original stiffness matrix will be used in both healthy and damaged state.

The change in MSE between the healthy and damaged state of the structure can be obtained from the mode shapes as a difference of MSE of the  $i^{\text{th}}$  mode for the  $j^{\text{th}}$  element.

$$MSEC_{ij} = \Phi_i^{dT} K_j \Phi_i^d - \Phi_i^{uT} K_j \Phi_i^u \quad (15)$$

The normalized change in MSE is a potential indicator of the location of damage, and it can be represented as modal strain energy change ratio (MSECR)

$$MSECR_{ij} = \frac{|MSEC_{ij}|}{MSE_{ij}^u} \quad (16)$$

Where,  $j$  and  $i$  represent the element number and mode number, respectively. The  $MSECR_{ij}$  expressed in equation 16 computed for each available mode and its corresponding element. Therefore, the modal strain energy change for each element can be averaged from the normalized  $MSECR_{ij}$ , where  $m$  is the total number of available modes.

$$MSECR_j = \frac{1}{m} \sum_{i=1}^m \frac{MSECR_{ij}}{MSECR_{max}} \quad (17)$$

## 2.3 Multi-Objective Optimization with Genetic Algorithm

Multi-objective problems involve two or more conflicting objectives that should be considered simultaneously. The fact that multiple objective problems do not have a unique solution rather identifies a set of mathematically equally good solutions, providing diversified solutions for the decision-maker to choose from. These solutions are commonly described as nondominated, efficient, noninferior, or Pareto optimal solutions.

### 2.3.1 Non-dominated Sorting Genetic Algorithm (NSGA-III)

Non-dominated sorting genetic algorithm (NSGA) is one of the several variants of a multi-objective genetic algorithm. NSGA has been in improvement with different stage. NSGA-II [30][31][32], NSGA-III [4][33]. Based on the framework of previous version of the non-dominated sorting algorithm, Deb K. and Jain H [4] introduced NSGA-III with an improvement in the selection mechanism.

The proposed algorithm improves problems in multi objective optimization that are associated with; accommodation of adequate number of new solutions in a population encountered by elite-preserving evolutionary multi-objective optimization due to the occupation of population by non-dominated solution. Furthermore, improvements in the diversity preservation operator for reduced computational operation. NSGA-III emphasizes Pareto non-dominated population members close to the reference line of each reference point.

#### 2.3.1.1 NSGA-III Approach

The optimization procedure in NSGA-III starts with the definition of a set of reference points. The reference points are predefined taking in to account the required number of objective and the desired number of divisions along each objective. Therefore, the predefined reference points ensure diversity in acquired solutions. The total number of reference points are estimated using binomial coefficient in equation 18;

$$H = \binom{M + p - 1}{p} \quad (18)$$

Where;  $H$  is total number of points,  $M$  is number of objective and  $p$  is the desired number of divisions along each objective.

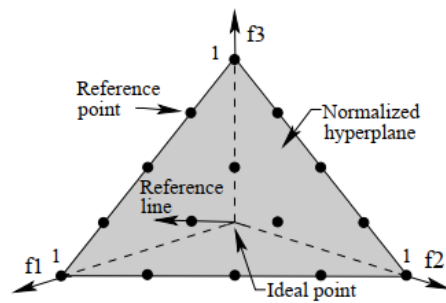


**Fig. 3** Reference points on a normalized reference plane [4]

The widely distributed reference points on the normalized hyper-plane can be useful in decision making and selection mechanism providing a diversified choice of solution.

The population size  $N$  is dependent on  $H$ , i.e.,  $N$  should be approximately equal to  $H$ . It is recommended [4] that the population size be a multiple of four of  $H$  which is slightly higher than  $H$ . Once the size of the population  $N$  is decided, an initial population with  $N$  members is randomly generated. For the rest of genetic algorithm parameters like; crossover rate, mutation rate, and termination parameter, NSGA-III follows same procedure.

Parent population  $P_t$  of size  $N$  is used in each generation to produce an offspring population  $Q_t$  of same size by using randomly selection. Later, the two populations  $P_t$  and  $Q_t$  are merged to form a new population  $R_t$  of size  $2N$ . Following the merge of population, a non-dominated sorting procedure is used to choose the best  $N$  members from  $R_t$  population. During this process, members of  $R_t$  population are classified into different non-domination levels ( $F1$ ,  $F2$ , and so on). The candidate population  $S_t$  for the next generation are constructed by filling members of different non-domination levels one at a time, starting from  $F1$ , until the size of  $S_t$  equals to  $N$  or for the first time becomes greater than  $N$ . Hence all solutions after  $N+1$  are rejected.

In the last front that may fulfil the population size to equal  $N$  is most probably accepted partially, the remaining population slots are chosen from the last front in such a way that a desired diversity is maintained in the population.

The selection mechanism in NSGA-III performs a careful elitist selection of solutions and attempted to maintain diversity among solutions by emphasizing solution closest to the reference line of each reference point. Hence, there is no need to employ any explicit selection operation; randomly picking parents for crossover and mutation is sufficient. To achieve good selection, objective values and supplied reference points are first normalized so that they have an identical range.

Furthermore, an ideal point is constructed by identifying the minimum values for each objective function. Hence the size of ideal point is equal to the number of objectives. Afterward, the ideal points are used to translate the objective to a zero-vector ideal point. Later, the perpendicular distance between a member in  $S_t$  and each of the reference lines (joining the ideal point with a reference point) is calculated. Member in  $S_t$  is then associated with a reference point having the minimum perpendicular distance.

A reference point may have none, one, or more population members associated with it. Therefore, niche preservation operation is conducted. The niche count  $\rho_j$  for the  $j$ -th reference point, defined as the number of members in  $S_t$  given the last front that are associated with the  $j$ -th reference point.

A niche-preservation operation is executed as follows. First, the reference point set  $J_{min}$  having the minimum  $\rho_j$  value is identified. In case of  $J_{min} > 1$ , one-member of  $J_{min}$  is randomly chosen. If  $\rho_j = 0$ , one member having the shortest perpendicular distance to the  $j$ -th reference line among members associated with the  $j$ -th reference point in last front is chosen. The count of  $\rho_j$  is then

increased by one. In the case of  $\rho_j \geq 1$ , a randomly chosen member from the last front that is associated with the  $j$ -th reference point is added to  $P_{t+1}$ , and the count of  $\rho_j$  also needs increasing by one. In both cases, once there exists no such member to be selected, the  $j$ -th reference point is excluded from further consideration for the current generation.

### 2.3.2 GA Operators

The effectiveness of genetic algorithm is mostly determined by the genetic operator's combination to achieve exploitation and exploration balance. NSGA-III employs the common genetic algorithm operators in the computation. Hence, careful selection of genetic operators like selection, crossover, and mutation appropriately for the posed problem is crucial.

#### 2.3.2.1 Crossover

The crossover operation is used a combination of one-point crossover, two-point crossover and uniform cross over.

**One-point crossover:** A randomly selected point on both parents' chromosomes is used to swap chromosomes. This results in two offspring, each carrying some genetic information from both parents.

**Two-point crossover:** A randomly selected two points on both parents' chromosomes is used to swap chromosomes. This results in two offspring, each carrying some genetic information from both parents.

**Uniform crossover:** the chromosome's information from the two parent is chosen with equal probability. This results in two offspring which inherit more genetic information from one parent than the other.

#### 2.3.2.2 Mutation

The mutation operator changes the value of nodes on each individual from one state to either of the four states depending on the mutation rate. i.e., if the value of a node is 3 (meaning the node is assigned as acceleration sensor location), during application of mutation the node might be either 0, 1, or 2. (no sensor assigned, longitudinal direction displacement sensor, or vertical direction displacement sensor, respectively.)

## Chapter 3: Multi-Approach Damage Identification

Bridge condition assessment is crucial to identify damages in the structures at very initial stage for conducting preventive maintenance rather than the damage distribute throughout the structure and needs lots of corrective maintenance or reconstruction, in which both options could be costly and needs longer time of public access closure. Furthermore, a damage that can be maintained with a minimal cost gets severe and requires more finance. However, the budget constraint inhibits all necessary maintenance work. As a result, the social, political, and economic interaction within a country can be significantly affected.

Several countries invest in the advancement of their bridge management system to handle the condition assessment of bridges in their stock, which usually be more tens of thousands. However, several country's still use visual inspection as the main data collection technique to assess their bridges condition. Even though, visual inspection is known to have unreliable results and lacks consistency, the limitation of practically suitable and reliable inspection technique as a replacement for visual inspection is not provided.

Currently, numerous researches are being conducted following various approaches. Though, these studies show promising improvement in damage identification, the fact that the methods are tested on the simplified bridge models raises concern in practicability, which will cause lots of uncertainty towards decision making.

Consequently, the authors perspective is that combining two different approach which have the same objective, to detect damage, significantly improve the practicability of the techniques by reducing the uncertainty and increasing confidence to the decision makers.

In this research, two techniques that follow different approach to identify damage have been presented with modification to improve practicability. The first approach is Displacement Based Index method which uses influence line-based damage identification technique. The second approach is Modal Strain Energy method, which uses vibration-based damage identification techniques. These methods show promising advancement towards damage identification. Both methods are capable of addressing all type of structural damages in global and local environment. In addition, they are compatible to any type of material type under consideration. Nevertheless, individually they have some difficulty towards avoiding a specific noise, like environmental condition, bridge element interaction, loading condition, boundary condition, etc., in the measurement that could potentially alter the result in their damage identification.

The fact that these two methods doesn't follow similar approach to identify damage hypothetically can be deduced that there will be mutual benefit regarding avoidance of uncertainty in the damage identification. If the damage cannot be identified by one approach it will be identified with the other, which may require further observation. Whereas, if both methods identify the damage, it will be a confirmation to the decision maker to act with confidence.



### 3.1 Modified Displacement Based Index Method

Ono R. et.al. [17] in their study present analytical study on damage detection method, presented in chapter 2.2, improving the proposed approach by T M Ha et.al. [18]. They utilize the concept of displacement influence line of road bridge slab to incorporate the response of a bridge to a static moving load. The proposed method is shown to be effective for displacement response measured in from static moving load.

Practically the measured displacement response has a static component generated from the vehicle's weight distribution to the axel loads and the dynamic component due to the vehicle characteristics, vehicle speed and surface roughness. Therefore, improvement considering the dynamic displacement response is necessary when considering practical application.

Furthermore, the road user's behavior with regard to driving on the road shall be taken into account. A driver using the same lane at different time of observation doesn't use the same position when measured from the reference point along the edge of the bridge. Hence, when using displacement measurement data recorded at the same point but in different times, not only the longitudinal position of the vehicle contributes to the damage identification but also the transverse position of the vehicle has contribution to accurately determine the damage.

Yu Y. et.al. [34], pointed out that each girder of the bridge is sensitive to the transverse position of the loading. Therefore, the common representation of a bridge as a beam for simplification of the proposed approach may not be effective in practical application due to lack of representing the torsional and other local effects due to the loading position and bridge elements integration. Therefore, the author, in this research propose the improvement on displacement-based index method based on considering the transverse position of the vehicle which the displacement response is measured at the healthy state and damaged state of the bridge. Furthermore, normalizing the dynamic displacement effect with the strain measurement is considered.

Maintaining the assumption taken by Ono R. et.al. [17], let's assume a unit load moves from support A to support B. The nodal displacement at point C can be expressed as a function of longitudinal position of load and displacement.

$$[x(t), u_i(t)] = [(x_1, u_{i1}), \dots, (x_j, u_{ij}), \dots, (x_n, u_{in})] \quad (19)$$

$$[x(t), u_d(t)] = [(x_1, u_{d1}), \dots, (x_j, u_{dj}), \dots, (x_n, u_{dn})] \quad (20)$$

$$\Delta u(j) = |u_d(j) - u_i(j)| \quad (21)$$

Hence, the change in displacement between the healthy state and the damaged state is considering only the position of the moving load along the longitudinal direction.

Noting the fact that the displacement measurements conducted at relatively longer time apart, when we consider comparing the difference of the healthy state and the damaged state of the bridge for the purpose of damage detection, not only the condition of the bridge change but also the vehicle characteristics, road surface roughness and transversal position of the vehicle.

Consequently, the nodal displacement record is no longer a function of longitudinal position of a load.

Assuming a unit load moves from support A to support B at a transverse position measured from a fixed reference edge of the bridge. Let's  $TP_i$  and  $TP_d$  be the position of the vehicle from the LHS edge of the bridge at the time displacement measurement during healthy state and damaged state measurement, respectively. The nodal displacement at point C is given by:

$$[x(t), u_i(t, TP_i)] = [(x_1, u_{i1}), \dots, (x_j, u_{ij}), \dots, (x_n, u_{in})] \quad (22)$$

$$[x(t), u_d(t, TP_d)] = [(x_1, u_{d1}), \dots, (x_j, u_{dj}), \dots, (x_n, u_{dn})] \quad (23)$$

Hence, before evaluating the change in displacement, the collinearity of measurement conditions used as comparison parameters should be similar for minimizing the measurement noise effect in identification for damage location. Practically, keeping every parameter to collinear with the original state requires great precaution and well-informed personnel. This will practicability of the proposed approach towards utilizing the any vehicles crossing the bridge as a means of ambient vibration inducer.

### 3.1.1 Transfer of displacement data

Yu Y. et.al [34], proposed an approach for bridge weigh-in-motion considering the transverse position of the vehicle from the fixed reference edge. They showed the use of influence surface to identify the transverse position from the strain sensor measurement. The general procedure of their approach is explained in the flow chart presented in Figure 4.

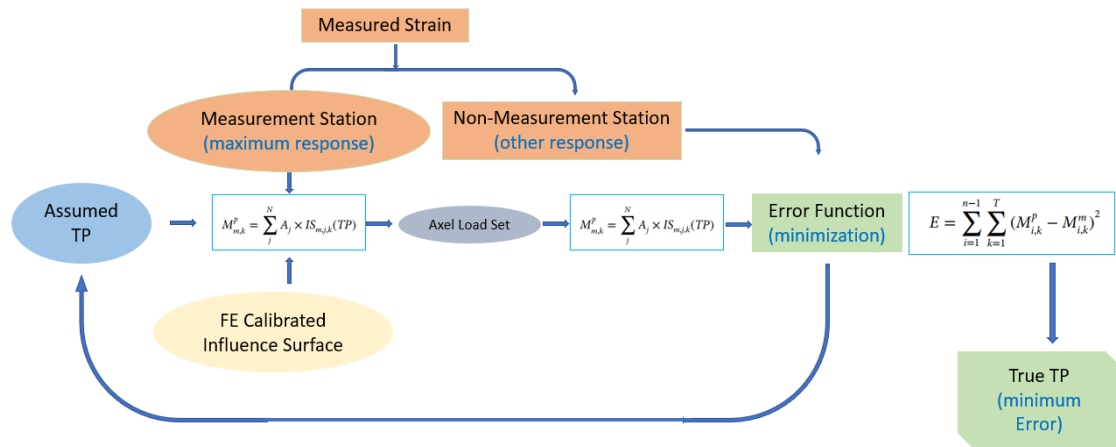


**Fig. 4** Flow chart for identification of true transverse position of the vehicle

In identifying the true transverse position of the vehicle from direct measurement data while it is crossing the bridge, Yu Y. et.al [34] used a calibrated influence surface is generated by shifting the vehicle in the transverse direction to cover all possible path of the vehicle. Once the strain

measurement is taken for all possible cases, the influence surface is generated from the measured strain data. During operation, when the vehicle crosses the bridge, the algorithm compares the measured response with the predicted response from the calibrated influence line to estimate the true transverse position of the vehicle and its axel load configuration.

Hence, using the TP identification approach proposed by Yu Y. et.al [34], the calibrated influence surface at the healthy state of the bridge will be used to transfer the displacement data measured at healthy state to collinear with the damaged case measurement data and it will be proposed as follows.

$$d_{SG}^i = S_{TP} - G_{TP}^i \quad (24)$$

$$d_T = \sum_{i=1}^N d_{SG}^i \quad (25)$$

$$r(IS) = \frac{1}{d_T} \sum_{i=1}^N d_{SGi} \frac{IS_i(TP_o)}{IS_i(TP_d)} \quad (26)$$

$$U_o(TP_d) = r(IS) * U_o(TP_o) \quad (27)$$

Where;  $S_{TP}$  is the transverse position of displacement sensor,  $G_{TP}^i$  is the transvers position of the  $i$ th girder with influence surface is associated,  $d_{SG}^i$  is the distance between the sensor and  $i$ th girder,  $N$  is the total number of Girders,  $IS_i(TP_o)$  is influence surface associated with  $i$ th girder at the time of measurement with original state transvers position,  $IS_i(TP_d)$  is influence surface associated with  $i$ th girder at the time of measurement with damaged state transvers position,  $r(IS)$  is the transfer ratio, and  $U_o(TP_o)$  is displacement response measured at the original state with  $TP_o$  from reference edge.

Consequently, the change in displacement influence line can be computed from equation ( ).

$$\Delta U_{TP} = | U_o(TP_d) - U_d(TP_d) | \quad (28)$$

Where;  $\Delta U_{TP}$  is the change in measured displacement response,  $U_o(TP_d)$  is displacement response measured at original state of the bridge but transferred to the TP at damaged state,  $U_d(TP_d)$  is displacement response measured at the damaged state with  $TP_d$  from reference edge.

Therefore, considering the vehicle characteristics, road surface roughness, longitudinal and transversal position of the vehicle, the modified displacement-based index method can be represented as follows:

$$DBI_{TP}(j) = \max \left[ 0, \frac{\Delta U_{TP}(j) - \mu}{\sigma} \right] \quad (29)$$

Where  $\mu$  and  $\sigma$  represent the mean and standard deviation of  $\Delta U_{TP}$ , respectively.  $DBI_{TP}(j)$  is the displacement-based index considering collinearity in the transverse position.

For more than one measurement point, the contribution of each measurement point to the total index estimation is factored, as shown in equation 30, by their position on the bridge with respect to the moving vehicle position.

$$r_{ds}^t = \frac{1}{d_{vs}^t} \left( \sum_{i=1}^S \frac{1}{d_{vsi}^t} \right)^{-1} \quad (30)$$

Where,  $r_{ds}^t$  is the location factor for sensor  $s$  at step time  $t$ ,  $d_{vs}^t$  and  $d_{vsi}^t$  are the Euclidean distance between the moving vehicle and the considered measurement point and group of measurement points respectively.

The effect of road roughness and change in vehicles contribution can be normalized by introducing the integration of strain response measured for transverse position identification.

$$r_{es} = w_s |\varepsilon_{TP_d}^d - \varepsilon_{TP_d}^i| \quad (31)$$

$$w_s = \frac{1}{d_{gs}} \left( \sum_{i=1}^G \frac{1}{d_{gis}} \right)^{-1} \quad (32)$$

Where,  $r_{es}$  is the strain-based normalizing factor,  $w_s$  is distribution factor of measured strain effect at each girder,  $d_{gs}$  the Euclidean distance between the strain measurement point and the displacement measurement point location,  $\varepsilon_{TP_d}^i, \varepsilon_{TP_d}^d$  are strain response measurement at each girder in the longitudinal direction at the time of healthy state and damaged state considering the transverse position corresponding to damages state measurement. The estimation of damage index with the modified displacement-based index can be expressed as:

$$MDBI = \sum_{s=1}^S \frac{DBI_{TP} * r_{ds}}{r_{es}} \quad (33)$$

Where,  $MDBI$  is the modified displacement-based index,  $S = \{s_1, s_2, \dots, s_n\}$  is displacement measurement points,  $DBI_{TP}$  is the estimated index by displacement sensor  $s$ ,  $r_{ds}$  is the location factor,  $r_{es}$  is strain-based factor.

### 3.2 Modified MSE Based Method

In this section the MSE based approach proposed by Shi et al. [26] is used jointly with FE modeling for improved damage detection considering the practical applicability of these approach. As most of the research related to the MSE are related to beam and 2D frame structures, as far as the authors' understanding, there is limitation in the study addressing damage identification in bridge structures using MSE.

The simplified 2D frames doesn't consider the torsional effects which are the dominant case in bridge like structures where the vehicle crossing a bridge cause unbalanced loading. Furthermore, considering the complexity of integration of bridge elements the following modification is proposed based on Shi et al. [26]

Let the bridge's equation of motion with nDoF system be expressed as:

$$\mathbf{M}\ddot{\mathbf{u}}(t) + \mathbf{C}\dot{\mathbf{u}}(t) + \mathbf{K}\mathbf{u}(t) = \mathbf{F}(t) \quad (34)$$

Where  $M, C$ , and  $K$  are the mass, damping and stiffness matrix in a  $\Phi \in R^{N \times M}$  be the mode shape will all  $N$  modal coordinates and  $M$  available modes.

Practically, the measured mode shapes are limited to  $s$  number of sensors, which will be represented as  $\Phi_s \in R^{n \times m}$ , are related to global coordinate. Where  $n$  is the product of number of sensors and direction of measurement and  $m$  is the identified modes. The limitation of mode shapes for all modal coordinates poses difficulty in identifying the elemental MSE index.

To address this issue, in this research the finite element-based estimation of modal strain energy from measured responses will be discussed.

Let  $\Phi_s \in R^{n \times m}$  be the identified mode shape from the acceleration measurement response of a bridge, and  $\delta_n$  be the nodal displacement estimated from measured response. The equivalent nodal force on the elements can be estimated from the finite element calibrated elemental stiffness matrix as follows:

$$F_n = K_e \delta_n \quad (35)$$

Hence, by substituting the calibrated equivalent force into equation 34 and numerically solve the bridge's equation of motion the mode shapes corresponding to  $N$  modal coordinates will be identified. After estimating the mode shapes corresponding to a full modal coordinate representing all elements under consideration, the identification of damage with modal strain energy follows the conventional method. The flow of damage identification procedure is illustrated by flow chart in Figure 5. The change in MSE will be as follows.

$$MSEC_{ij}^{fe} = \Phi_i^{dT} K_j^{fe} \Phi_i^d - \Phi_i^{uT} K_j^{fe} \Phi_i^u \quad (36)$$

Where  $MSEC_{ij}^{fe}$  is the change in MSE using finite element model calibrated mode shape estimation,  $K_j^{fe}$  is the FE calibrated elemental stiffness matrix, and  $\Phi_i^{dT}$  and  $\Phi_i^{uT}$  are estimated mode shapes from the measured acceleration responses of  $s$  number of sensors.

Similarly, the modal strain energy change ratio (MSECR) can be determined as follows:

$$MSECR_{ij}^{fe} = \frac{|MSEC_{ij}^{fe}|}{MSE_{ij}^{u-fe}} \quad (37)$$

Therefore, the modal strain energy change for each element can be averaged from the normalized  $MSECR_{ij}$ , where  $m$  is the total number of available modes.

$$MSECR_j^{fe} = \frac{1}{m} \sum_{i=1}^m \frac{MSECR_{ij}}{MSECR_{max}} \quad (38)$$

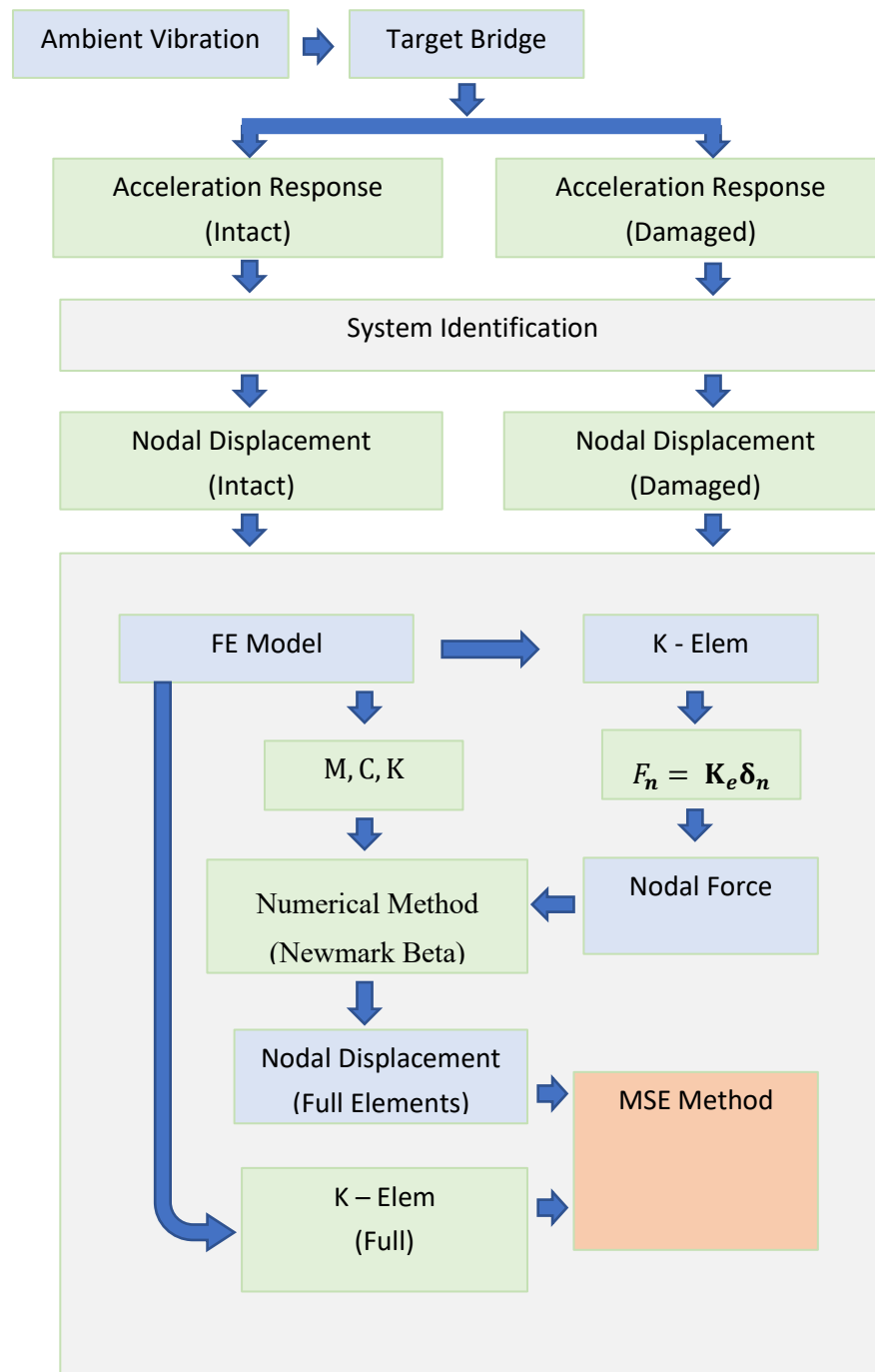


**Fig. 5** Flow chart of damage identification with FE based MSE

# Chapter 4: Numerical Analysis using FE Modeling

Limitation of sufficient data for the bridge that meets the objective of this study leads to the utilization of finite element modeling for generating the required information. Hence the choice of target bridge is focused on the modeling of the real bridge element integration, performance, and material properties calibration to represent the practical scenario.

## 4.1 Target Bridge Modeling

The selected target bridge is a 21-m single span concrete-steel composite bridge. The bridge is selected from the research by Amir Gheitasi et.al. , [3] where numerical simulation and validation at the system-level behavior of the composite steel girder bridges have been studied based on a scale laboratory investigation performed at the University of Nebraska. The Reinforced concrete deck is supported by three I-shaped steel girders. Total width of the bridge is 7.92m. The thickness of the reinforced concrete slab deck is 190.5 mm while the height of the steel girder is 1400mm. The bridges girders are simply supported on both ends. Cross beams are provided at the ends of the girders and intermediate sections. The three intermediate cross beams divide the slab in to four equal panels. Details of the bridge dimensions are expressed in the Figure 6 below.

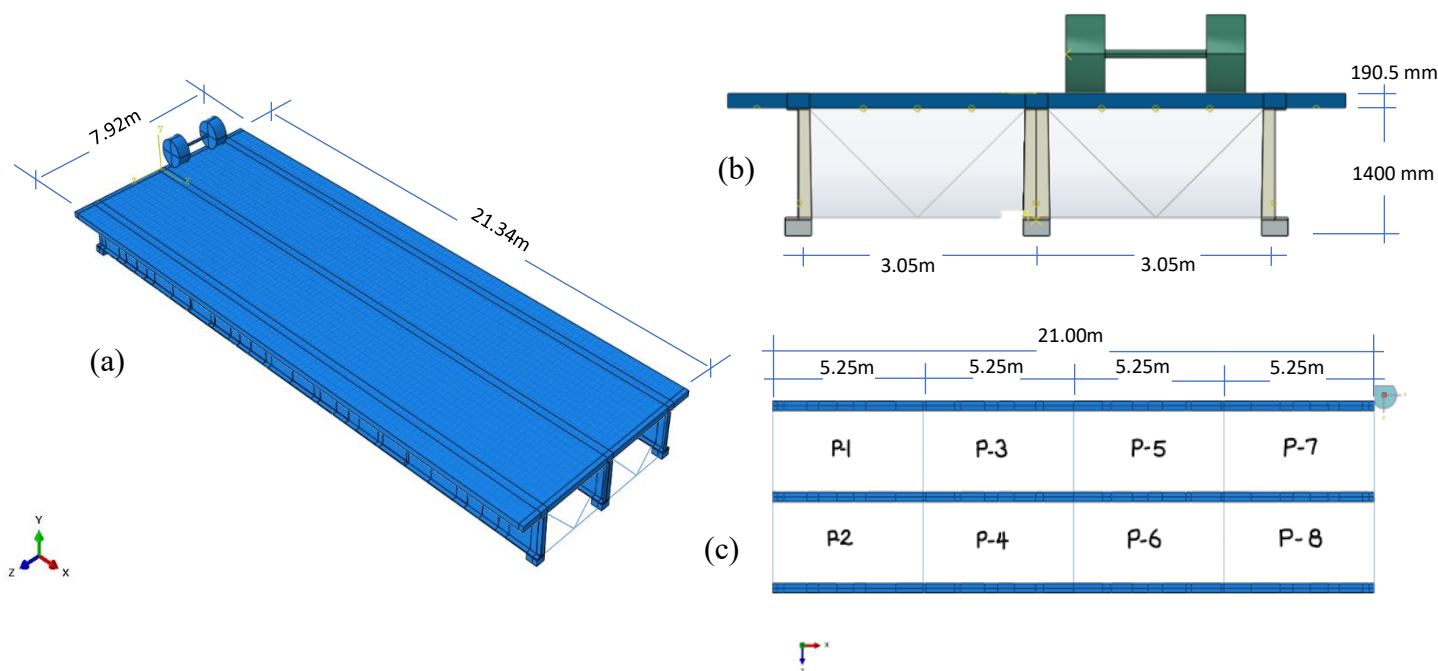


**Fig. 6** Target bridge information (a) Bridge dimensions (b) Bridge cross section (c) Panel arrangement

The referred research [3] primary objective was to numerically simulate and validate the system level behavior of the composite steel girder bridges. The test conducted was static ultimate loading

test to evaluate the load carrying capacity of the system. Hence, this model is selected to represent the full-scale bridge element's integration for analyzing for real case damage scenarios.

The initial study uses ANSYS finite element software, however, in this research Abaqus finite element software is used. Furthermore, due to the difference in the target objective of the studies the material representations are changed from the original research to meet the objective of this study. Consequently, prior to using the target bridge for this research purpose, the referred research's objective re-modeled with the new material model representation, and the results are compared for validating the material property. The model was loaded with a series of concentrated loads applied on the bridge deck to simulate two side-by-side HS20 trucks considering axle spacing as shown on Figure 7(a). The deflection at midspan of the bridge's interior girder was selected to validate the proposed numerical modeling approach. As shown in Figure 7(b), the result obtained from the simulation more correlates to the experimental result than the NLFEA simulation. Hence, the material representation and bridge element integration are representing well the bridge's elastic and inelastic behavior. Consequently, the verified material properties and bridge element integrations are utilized for the purpose of this research.

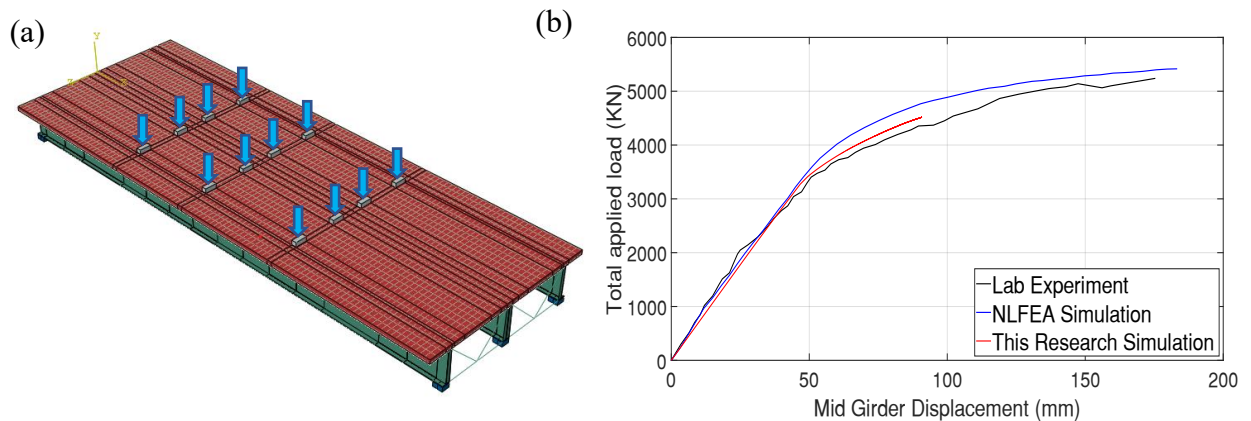


**Fig. 7** Bridge Loading. (a) Loading Arrangement (b) Material property Validation

The finite element model is executed by Abaqus software. 3D solid elements are used to model the concrete deck slab and I-shaped steel girder structures. The reinforcement bars and the bracings are modeled with beam elements. The bridge model contains a total of 39,189 elements and 56,412 nodes. This results a total number of 363669 Degree of freedom problem. Modal dynamic analysis is conducted with ABAQUS, the result of the first six modes is illustrated in the Figure 8.



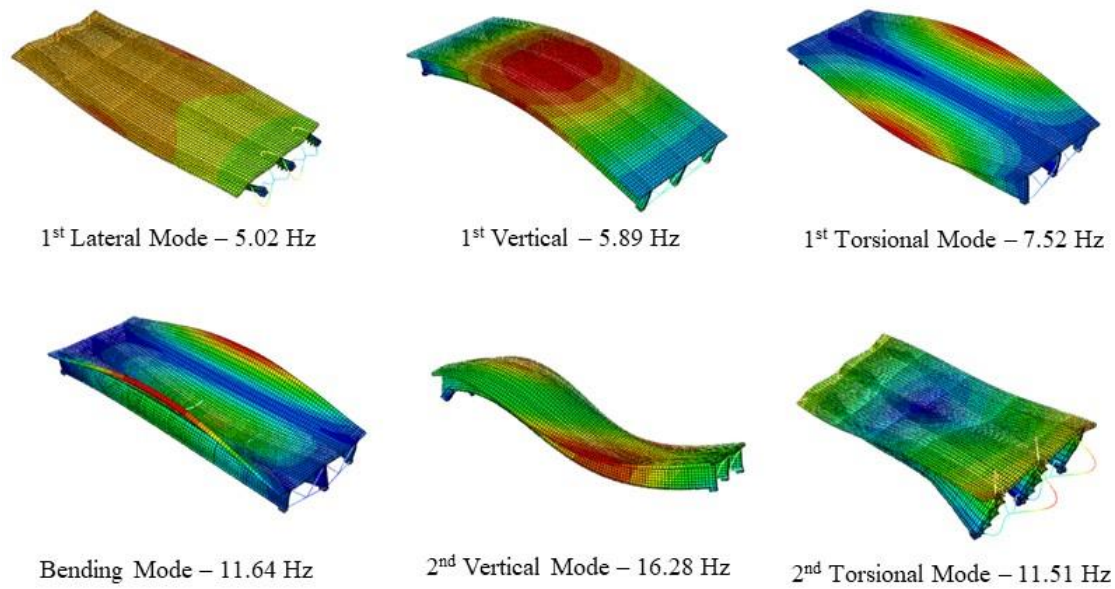


**Fig. 8** Mode shapes of the target bridge

## 4.2 Bridge Vehicle Interaction

Bridge subjected to a moving load will be affected by the dynamic load generated from the interaction between wheels and road surface. The variation load transferred to the road surface is a function of static component and dynamic component. The static component is generated from the vehicle weigh distribution over the vehicle axles, whereas the dynamic component is caused by factors like vehicle characteristics, speed, and roughness of the road surface.

Understanding the effect of road roughness on the dynamic excitation is useful to implement the ambient vibration as a tool for structural health monitoring. This will reduce the requirement of closing the bridge while inspection of the bridge and data collection. Furthermore, the cost of utilizing very expensive type of techniques to generate vibration on the structure will be omitted by implementing the ambient vibration generated from traffic.

### 4.2.1 Road Surface Profile

Road roughness can be defined as the profile representing the variations in height of the road surface measured along one track on, and parallel with, the road. It is continuously distributed in a random trend, which affects dynamic behavior of both vehicle and bridge. Hence, at the interaction point, the deterioration of the road will have higher impact in altering the dynamics of the vehicle body and the bridge [29],[35], [36].

The ISO 8608 [37] describes the methodologies to be used for the generation of the road surface profile from data measured on site. The road roughness profile can be calculated through the use of the PSD (Power Spectral Density) of vertical displacements  $G_d$ , as a function of spatial frequency  $n$  ( $n = 0.1$  cycles/m). Eight classes of roads profiles, from class A to class H, are

proposed by the ISO 8608. Class A being the best condition road profile and class H being the poorest road profile condition.

**Table 1** ISO 8608  $G_d(n_0)$  values

Road Class	$G_d(n_0) (10^{-6} \text{ m}^3)$		
	Lower Limit	Geometric Mean	Upper Limit
A	-	16	32
B	32	64	128
C	128	256	512
D	512	1024	2048
E	2048	4094	8192
F	8192	16384	32768
G	32768	65536	121072
H	121072	262144	-
$n_0 = 0.1 \text{ cycles/m}$			

ISO 8608 provides that the road roughness profile can be defined using the equation:

$$G_d(n) = G_d(n_0) \left( \frac{n}{n_0} \right)^{-2} \quad (39)$$

Agostinacchio M. et. al. [35], presented the estimation of road roughness from the PSD for practical application, describing the road profile as a simple harmonic function.

$$h(x) = A_i \cdot \cos(2\pi \cdot n_i \cdot x + \varphi_i) = A_i \cdot \cos(2\pi \cdot i \cdot \Delta n \cdot x + \varphi_i) \quad (40)$$

where  $A_i$  is the amplitude,  $n_i$  is the spatial frequency and  $\varphi_i$  is the phase angle. Therefore, the artificial road profile can be described as.

$$h(x) = \sum_{i=0}^N \sqrt{2 \cdot \Delta n \cdot G_d(i \cdot \Delta n)} \cdot \cos(2\pi \cdot i \cdot \Delta n \cdot x + \varphi_i) \quad (41)$$

substituting equation (9) to equation (11) we can produce the artificial profile from ISO classification by using:

$$h(x) = \sum_{i=0}^N \sqrt{\Delta n} \cdot 2^k \cdot 10^{-3} \cdot \left( \frac{n_0}{i \cdot \Delta n} \right) \cdot \cos(2\pi \cdot i \cdot \Delta n \cdot x + \varphi_i) \quad (42)$$

Where:  $x$  is arbitrary position along the bridge length.  $\Delta n = (n_{max} - n_{min})/N$ ,  $n_{max}$  and  $n_{min}$  are the upper and lower cut-off frequencies, respectively.  $k$  is the road profile classification;  $n_0 = 0.1 \text{ cycle/m}$ ;  $\varphi_i$  is the random phase angle uniformly distributed from 0 to  $2\pi$ .

In this research, the effect of road roughness is introduced by assuming the condition of the road is good. Hence, we can further assume that the roughness effect in the right wheel and left wheel are identical. The artificial road profile is then generated from a stochastic representation as a function of Power Spectral Density. The following parameters from ISO 8608 is used to generate the artificial road profile  $n_{max} = 5\text{Hz}$  and  $n_{min} = 0.1\text{Hz}$  ar.  $k = 3$  is the road profile

classification;  $n_0 = 0.1$  cycle/m;  $\varphi_i$  is the random phase angle uniformly distributed from 0 to  $2\pi$ . The generated road roughness is presented in the Figure 9 below.

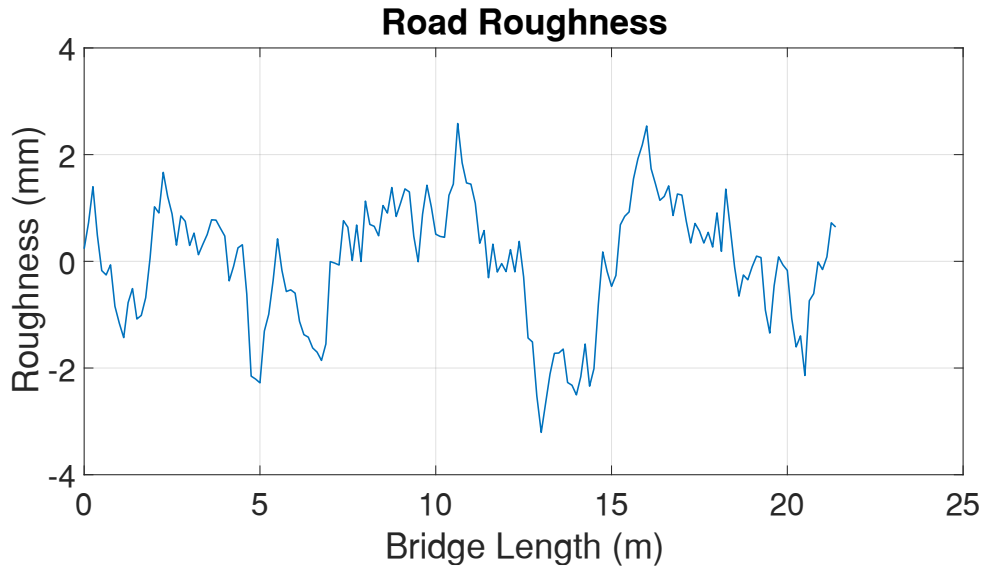


**Fig. 9** Road surface profile

#### 4.2.2 Vehicle's Dynamic Load

Irregularities on the surface of the bridge's pavement create the vibration on the vehicle mass, which intern respond with more applied load to the bridge. These phenomena create a special and temporal varying force application to the bridge. Thus, the excitation of the bridge will be dependent on the mass of the vehicle, the speed, vehicle's suspension characteristics and the roughness of the road.

Equation of motion for the vehicle is obtained using the Lagrange's equation. For practical purposes, the quarter car model (QCM)[35] shown in Figure 10 is used to effectively model the dynamic interaction between vehicle and road roughness profile. The parameters used in the model are listed in Table 2. Considering the mass of tire is much smaller than the vehicle body, it is neglected in the calculation.

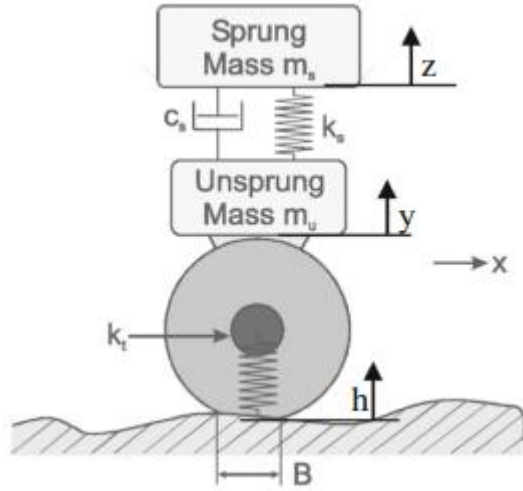


**Table 2** Vehicle's dynamic characteristics

Parameters	Unit	Amount
Speed	m/s	12.5
Sprung mass ( $m_s$ )	Kg	1109
Unsprung mass ( $m_u$ )	Kg	679
Suspension stiffness ( $k_s$ )	N/m	570000
Suspension damping ( $c_s$ )	N.s/m	21000
Tire stiffness ( $k_t$ )	N/m	3000000

**Fig. 10** Quarter car model

The vertical force at the contact point due to the road roughness is computed from the equation of motion for the vehicle:

$$M_v \ddot{x} + C_v \dot{x} + K_v x = f_v \quad (43)$$

Where  $M_v = \begin{bmatrix} m_s & 0 \\ 0 & m_u \end{bmatrix}$ ,  $C_v = \begin{bmatrix} c_s & -c_s \\ -c_s & c_s \end{bmatrix}$ ,  $K_v = \begin{bmatrix} k_s & -k_s \\ -k_s & k_s + k_t \end{bmatrix}$ ,  $x = \begin{pmatrix} z \\ y \end{pmatrix}$ , and  $f_v = \begin{pmatrix} 0 \\ k_t \cdot h \end{pmatrix}$

are the mass matrix, damping matrix, stiffness matrix, vehicles response and vertical force on the vehicle, respectively. The equation is solved with Newmark's method using the Matlab software application. Thus, the contact force on the bridge will be obtained from:

$$f = f_v + M_v g - C_v \dot{x} - K_v x \quad (44)$$

The generated contact force is applied one second before the start of the bridge and after the exit, as shown in Figure 11, that the approach road will provide smooth entrance and exit from the bridge section.

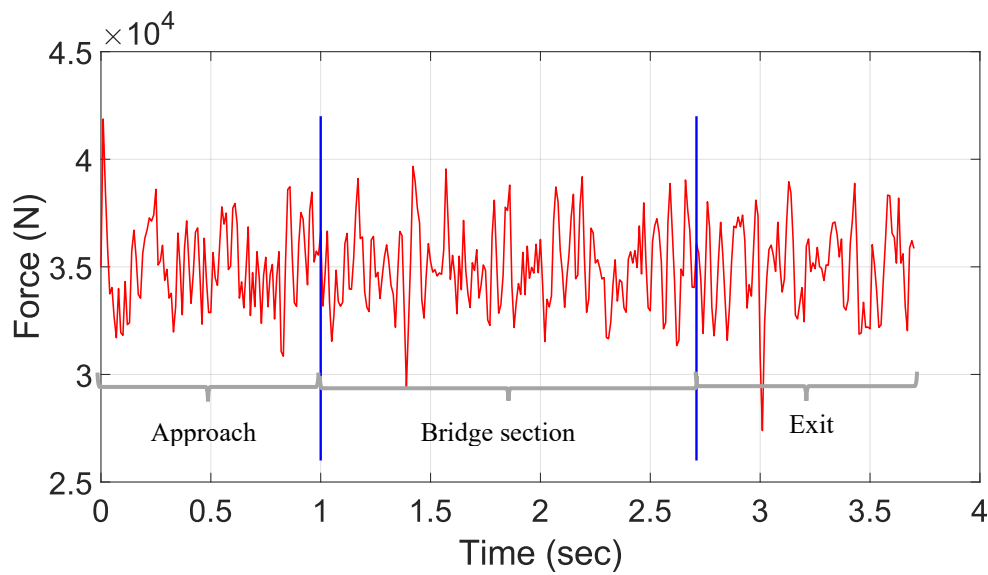


**Fig. 11** Dynamic loading generated by the vehicle on the bridge

The bridge is assumed to be at rest as the initial condition. The contact force is applied on the center of left lane of the bridge with the movement of direction is from left to right out of the plane. The assumption that both the wheels experience the same road roughness is considered to generated force from the vehicle that act only vertical direction. The driving velocity of vehicle is 12.5 m/s. The analysis is conducted with Abaqus software with a time step of 15 seconds. An extended time is provided to simulate the vehicle induced ambient vibration after the moving axel load exits the bridge.

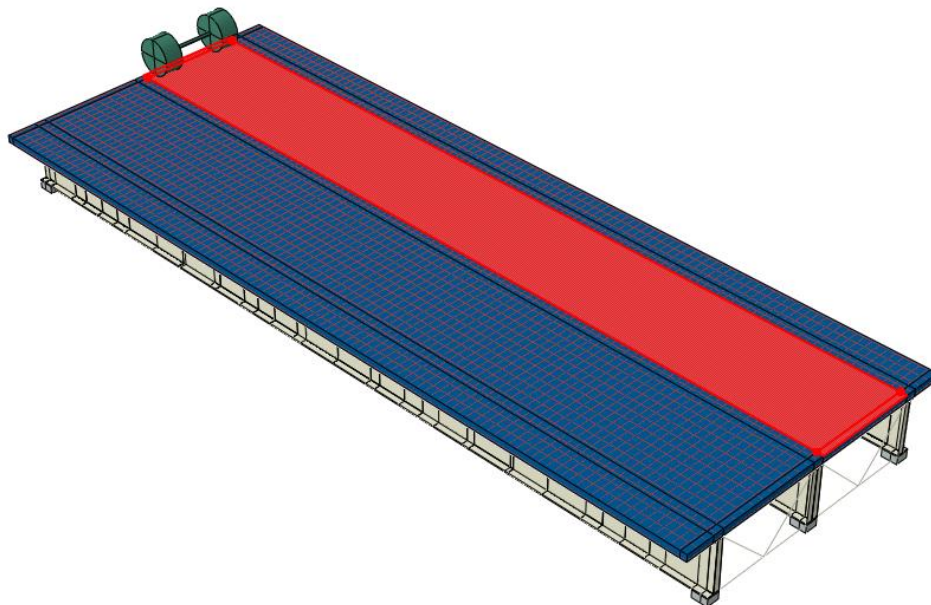


**Fig. 12** Bridge loading with moving axel load

### 4.3 Bridge Response Measurement

Response of the bridge to the moving axel load is recorded at the predefined node points to simulate the candidate structural health monitoring sensors. The simulation generates a displacement response history and acceleration response history at 231 candidate sensor points illustrated in Figure 13. The distribution includes 21 node points spaced with 1.0m interval in longitudinal direction and 11 node points distributed in the transversal directions. A candidate strain sensor located at the midspan of each girder record the strain response of the elements.

The displacement sensors considered are unidirectional, i.e., at each node a possible candidate position for one direction displacement response. Therefore, the response of displacement response in each direction is recorded as input to the placement optimization. Similarly, the acceleration response of the bridge is recoded at these nodes, while the tri-directional acceleration sensor is simulated.

The strain response in the longitudinal direction of the bridge is recorded at the midspan of each girder. At predefined position where the maximum strain occurred. The objective of collecting strain response data is as input to the identification of transverse position using bridge weigh in motion approach rather than for optimization.

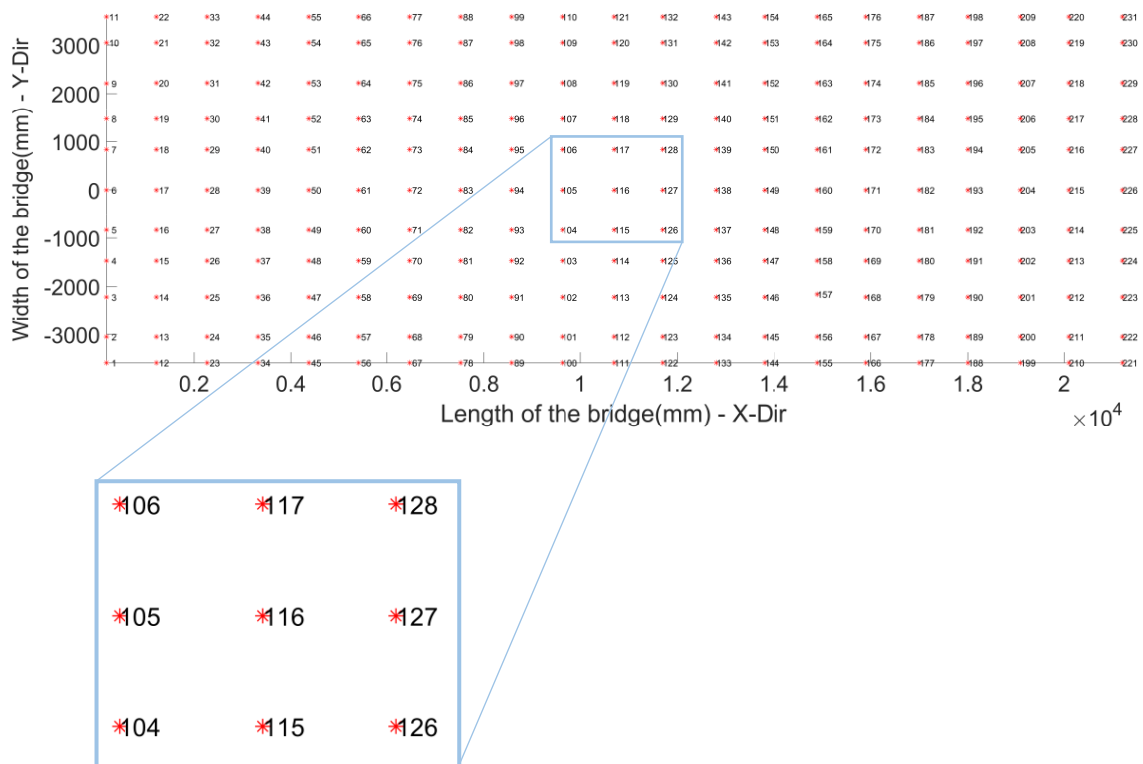


**Fig. 13** Candidate node distribution under the slab and girder

## Chapter 5: SHM Sensors Optimization with NSGA-III

The performance of the SHM system for condition assessment depends on three factors, advancement in the sensor's technology, improvement in damage identification technique and optimal placement of the sensors for collecting quality information. The placement optimization for sensors has more additional benefit in addition to improving SHM performance. The cost of instrumentation of the structure, the data management effort, sensor maintenance cost, and energy requirement can be reduced by optimizing the number of sensors. Hence, there will be huge economic incentive by conducting sensor placement optimization for SHM system.

Non-dominated Sorting Genetic Algorithm (NSGA-III)[4] is used to optimize the network integration and placement optimization of the sensors for damage identification purpose. Displacement sensor and acceleration sensors are required to be installed in the way that could result best quality of measurement with a minimum number of sensors.

### 5.1 Problem Representation

Integration of different kinds of sensors used in SHM techniques following distinct approach for identifying damage requires finding the best distribution of sensor that could meet the highest quality output that works well for all techniques employed. In this research, finding appropriate integration between displacement sensors and acceleration sensors is critically important to maximize the quality of data generated for damage identification based on influence line-based method and vibration-based method.

To address the two methods, displacement sensors are assigned for influence line-based method and acceleration sensors are assigned for vibration-based method. Therefore, the integration of these sensors in identifying the damage and minimizing the uncertainty for decision making is investigated in conjunction with the placement optimization.

The possible installation location of the sensors are assigned to a candidate sensor locations distributed under the slab and the girders with a 1m x 1m grid, which makes a total of 231 candidate sensor locations. There are some assumptions considered in the placement of sensors at the candidate locations as follows.

1. Any two types of sensors cannot be installed at the same candidate position.
2. The preference of one sensor to the other is equal, where there is a need to place two sensor types at one point. Hence, one of the sensors is randomly selected to be installed at the point.
3. The displacement sensor is considered uni directional. Therefore, each direction will have sensors positioned in different positions.
4. The acceleration sensor is considered tri directional.

At each node, only one candidate sensor can be installed as a sensor. Hence, the optimization will have a three-objective optimization problem, longitudinal direction displacement sensors, vertical

direction displacement sensors, and acceleration sensors. The transversal direction sensors are not considered here because the effect of lateral load is not considered in this research.

## 5.2 Optimization Objective Functions

The objective functions for placement of the sensors are in-line with the considered damage identification technique to get the most probable configuration and placement of sensors required for both techniques. The optimization is considering improvement in the sensors' sensing ability by searching good placement location and minimizing the number of sensors up to the sufficient level and maximize the quality of identification of the desired parameters. The objective function for each sensor types is discussed as follows.

### 5.2.1 Displacement Sensors

The objective of displacement sensor optimization is to find the best stable position in which the measurement records have good correlation with other nodes for a better estimation of change in displacement. Displacement response records to a moving axel load at a candidate sensor location are evaluated based on the Grey relational analysis[38] to find the strong correlation between the reference point and the comparison points. The reference point is described as a candidate sensor location and the comparison points are other locations on the span which are not set as a sensor location. The optimization is aiming to obtain a strong relationship that covers the bridge surface using the least possible number of sensors.

Consider that the displacement influence line is measured at the candidate node position is reference data, and the displacement influence line is measured at other node positions are comparison data. Consequently, the correlation of candidate sensor position with other nodal positions can be estimated from the Grey relational analysis.

Let  $u_s$  be the displacement influence line measured at candidate sensor position and  $u_{ni}$  ( $i = 1, 2, \dots, m$ ) be the displacement influence line measurement at other nodes position, where  $m$  is the total number of candidate nodes under consideration for sensor placement; The grey relational coefficient will be estimated from equation 48:

$$u_s = [u_{s1}, \dots, u_{sj}, \dots, u_{sk}] \quad (45)$$

$$u_{ni} = [u_{ni1}, \dots, u_{nij}, \dots, u_{nik}] \quad (46)$$

$$\Delta u_j = |u_{sj} - u_{nij}| \quad (47)$$

$$GRC_i(j) = \frac{\min_i \min_j \{\Delta u_i(j)\} + \alpha \max_i \max_j \{\Delta u_i(j)\}}{\Delta u_i(j) + \alpha \max_i \max_j \{\Delta u_i(j)\}} \quad (48)$$

Where  $\Delta u_j$  is the absolute difference between the reference data and the comparison data.  $\alpha = 0.5$  is the GRC coefficient, and  $GRC_i(j)$  is the correlation coefficient between reference and  $i^{th}$  comparison data.



The strength of correlation between the evaluated data can be expressed from GRC analysis as:

- $GRC > 0.9$ : the reference data and comparison data have strong relationship
- $0.8 < GRC < 0.9$ : the reference and comparison data have relationship.
- $0.6 < GRC < 0.8$ : the reference and comparison data have weak relationship
- $GRC < 0.6$ : the reference and comparison data have not relationship

The optimization of displacement sensor is aimed to maximize the measurement relationship throughout the bridge while keeping the required sensors to a minimum. As there are two directions of measurement – longitudinal direction and vertical direction – while one location is dedicated only to one sensor, the fitness equation is set to select the best directional sensor positioning for a specific node. Hence, the optimization objective of displacement sensors is aiming to achieve three criteria's; maximizing strength of relationship, maximize the full coverage of the span and minimize the number of sensors by controlling overlap of sensors at a specific point. The three criteria's will be discussed accordingly.

1. **Maximizing the GRC relationship strength:** the node having a strong correlation with most of other nodes is considered to be the candidate sensor position. It signifies the possibility of minimizing the required sensors to cover the whole bridge. Therefore, evaluating the scale of relationship each node has with other position other positions can be evaluated as follows:

Let  $C_i = \{g_1, g_2, g_3, \dots, g_n\}$  be the  $i^{th}$  individual in the population, where  $g_n$  is the position of  $n$  candidate sensor selected from the total available  $N$  positions.

The relationship counts for each candidate sensor based on GRC evaluation will be

$$g_n = \begin{cases} r_s, & \text{number of nodes with } GRC > 0.9 \\ r_n, & \text{number of nodes with } 0.8 < GRC < 0.9 \\ r_w, & \text{number of nodes with } 0.6 < GRC < 0.8 \\ r_0, & \text{number of nodes with } 0.6 \end{cases} \quad (49)$$

Maximized  $r_s$  will indicate that the candidate sensor position has a strong correlation with most of the nodes. Therefore, the candidate sensor position's fitness to GRC is evaluated from equation 50.

$$f_{gr} = \begin{cases} 1, & \text{if } g_n \geq \frac{N_{nd}}{2} \\ 0, & \text{if } g_n < \frac{N_{nd}}{2} \end{cases} \quad (50)$$

Where  $f_{gr}$  is the fitness of candidate sensor  $g_n$  correlation with other nodes,  $N_{nd}$  is the total available nodes.

While identifying the candidate sensors having maximized correlation with other nodes, their presence in a set of sensor with in the individual should be minimized to achieve a maximized coverage with minimum number of sensors. Finally, the fitness of the set of

candidate sensors towards achieving correlation with all available nodes can be estimated based on:

$$f_{dr} = -\frac{100}{\sqrt{N_{nodes}}} \times \sqrt{\frac{N_{nodes}}{\sum_{n=1}^j f_{gr}}} \quad (51)$$

Where  $f_{dr}$  is the fitness evaluation with respect to strong correlation for the set of candidate sensors in the individual,  $N_{nd}$  is the total available nodes,  $f_{gr}$  fitness value of each sensors in the set of sensors, and  $n = \{1, 2, \dots, j\}$  is the number of candidate sensor with in the set.

2. **Maximizing the span coverage:** the proposed distribution of candidate sensors position within the individual should satisfy full correlation with the available nodes in the span. Therefore, this criterion ensures that the proposed set have a capacity of having strong relationship with all nodal positions. The evaluation of the fitness corresponding to maximizing span coverage is discussed here:

Let  $C_i = \{g_1, g_2, g_3, \dots, g_n\}$  be the  $i^{th}$  individual in the population, where  $n_c$  is the count of candidate sensors strong relation with node  $n$ . Considering, the operational failure and malfunction of sensor in practical implementation, the distribution of sensors is conducted in order to achieve each nodal positions on the span to be covered by at least three sensors.

$$f_{cg} = \begin{cases} 1, & \text{if } n_{ci} \geq 3 \\ 0, & \text{if } n_{ci} < 3 \end{cases} \quad (52)$$

Where  $f_{cg}$  is the fitness of the each node identified by at least three sensors from a set of candidate sensor  $C_i$  evaluated with respect to span coverage, and  $n_{ci} = \{n_{c1}, n_{c2}, n_{c3}, \dots, n_{cN}\}$  is the number of sensors identifying the nodes where  $N$  is the total available nodal positions. The fitness of the set of candidate sensor towards achieving full span coverage is evaluated as:

$$f_{dc} = -\frac{100}{N_{nd}} (\sum_{n=1}^N f_{cg}) \quad (53)$$

Where,  $f_{dc}$  the fitness evaluation of a set of candidate sensor  $C_i$  evaluated with respect to span coverage,  $N_{nd}$  is the total available nodes, and  $f_{cg}$  is fitness value for each node.

3. **Overlap Control:** considering the possibility of sensor malfunction and operational failure, the minimum overlap of sensors at each node in the span is set to three. However, the maximum limit of overlap shall also be minimized to three to avoid the unwanted redundancy and minimize the number of sensors as much as possible while keeping the objective of having three sensors overlap.

Let  $C_i = \{g_1, g_2, g_3, \dots, g_n\}$  be the  $i^{th}$  individual in the population, where  $n_c$  is the count of candidate sensors strong relation with node  $n$ . The fitness equation evaluating the overlap control can be expresses as:

$$f_{do} = \begin{cases} -100 * \frac{(\frac{3}{max_c} + \frac{min_c}{3})}{2}, & \text{for } min_c < 3 \\ -100 * \frac{(\frac{3}{max_c} + \frac{3}{min_c})}{2}, & \text{for } min_c \geq 3 \end{cases} \quad (54)$$

Where  $f_{do}$  is the fitness evaluation with respect to controlling overlap for the set of candidate sensors in the individual,  $max_c = \max(\forall n_{ci})$  is the maximum number of sensors strongly related with node  $n_{ci}$ , and  $min_c = \min(\forall n_{ci})$  is the minimum number of sensors strongly related with node  $n_{ci}$ .

Based on the above mentioned three criteria the fitness function for evaluating each directional sensor sets will be:

$$f_{di} = (f_{dr} * f_{dc} * f_{do}) \quad (55)$$

Where  $f_{di}$  is the directional sensor set fitness evaluation function,  $i = x$  for longitudinal direction sensor sets and  $i = y$  for vertical direction sensor sets.

### 5.2.2 Acceleration Sensors

Acceleration sensors are widely used in the vibration base system analysis. They are best candidate for damage identification by utilizing vibration-based approach. The acceleration history record of a sensor on the bridge subjected to an ambient vibration due to a moving load crossing a bridge will be used for determination of damage existence. Hence, the quantity of sensors and their placement position greatly matter on the quality of system parameter identification.

The optimization for acceleration sensors placement adopted in this research focuses on the use of a method associated to modal strain energy for damage detection. Hence, the placement of the sensors is set to enhance the system identifiability by improving the observability of the system.

A discrete structural system under applied force  $f(t)$  can be expressed in the first-order form of a state space equation as follows:

$$\dot{z}(t) = \mathbf{A}z(t) + \mathbf{B}f(t) \quad (56)$$

$$y = \mathbf{C}^*z(t) \quad (57)$$

Where,  $\dot{z}$  is the first order state form,  $\mathbf{A}$ ,  $\mathbf{B}$  and  $\mathbf{C}^*$  are matrices,  $f(t)$  is the applied force. The matrices are defined as follows:

$$\mathbf{A} = \begin{bmatrix} \mathbf{I} & \mathbf{0} \\ -\mathbf{M}^{-1}\mathbf{K} & -\mathbf{M}^{-1}\mathbf{C} \end{bmatrix}, \mathbf{B} = \begin{bmatrix} \mathbf{0} \\ \mathbf{M}^{-1} \end{bmatrix}, \mathbf{C}^* = [-\mathbf{M}^{-1}\mathbf{K} \quad -\mathbf{M}^{-1}\mathbf{C}] \text{ and } z(t) = \begin{bmatrix} \dot{x}(t) \\ x(t) \end{bmatrix} \quad (58)$$

$\mathbf{M}$ ,  $\mathbf{C}$  and  $\mathbf{K}$  are mass, damping and stiffness matrices of the system.

The observability matrix  $\mathbf{O}_p \in R^{pm \times 2N}$  is composed by the output influence matrix  $\mathbf{C}$  and the system matrix  $\mathbf{A}$ . The generalize form can be expressed by:

$$[O_p] = [C \ CA \ CA^2 \ CA^3 \ \dots \ CA^{p-1}]^T \quad (59)$$

The minimum size of full rank observability matrix in modal coordinate given by

$$[O_{pm}] = [R_m \ R_m A_m]^T \quad (60)$$

Where  $R_m = [-\Phi_s \omega^2 \ -\Phi_s C_m]$  is the output influence modal coordinate and  $A_m = \begin{bmatrix} 0 & I \\ -\omega^2 & -C_m \end{bmatrix}$  is the system matrix in modal coordinates, Hence the observability matrix will be:

$$O_{pm} = \begin{bmatrix} -\Phi_s \omega^2 & -\Phi_s C_m \\ -\Phi_s C_m \omega^2 & -\Phi_s \omega^2 + \Phi_s C_m^2 \end{bmatrix} \quad (61)$$

Rearranging the matrix into a multiplication of two matrices  $\Gamma \in R^{2S \times 2N}$  and  $Z \in R^{2N \times 2N}$

$$\Gamma = \begin{bmatrix} \Phi_s & \mathbf{0} \\ \mathbf{0} & \Phi_s \end{bmatrix} \text{ and } Z = \begin{bmatrix} -\omega^2 & -C_m \\ C_m \omega^2 & \omega^2 + C_m \end{bmatrix} \quad (62)$$

The observability matrix will have full rank if matrix  $\Gamma$  is full column rank and matrix  $Z$  is nonsingular. The matrix  $\Gamma$  will be full rank if and only if the output sensor is configured in such a way that makes the mode shape partition full rank.

Hence, the desired observability of the system is influenced by the optimal configuration of sensors on the structure. The configuration should achieve a minimum size of observability matrix  $O_p$  that maintain full rank. This implies that at least  $S$  sensors must be placed to identify  $M$  target mode partitions that are linearly independent.

In this research, the acceleration data are considered responses of the ambient vibration created by the moving vehicle on the bridge. As researchers [39] suggested, the response data recorded should be pretreated with Natural Excitation Technique (NExT).

Natural excitation technique uses principle that states the cross-correlation function between two responses made on an ambient-excited structure has the same analytical form as the impulse function of the structure [39], The full derivation of the method can be referred from Farrar and James III [40]).

The equation for the cross-correlation function [40] is expressed as follows:

$$R_{ijk}(T) = \sum_{r=1}^n \frac{\alpha_k \phi_i^r \phi_k^r \phi_j^s \phi_k^s}{m^r \omega_d^r m^s \omega_d^s} \int_0^\infty G^r_{ijk} [e^{-r\zeta^r \omega_n^r T} \cos(\omega_d^r T)] + H^r_{ijk} [e^{\zeta^r \omega_n^r T} \sin(\omega_d^r T)] \quad (63)$$

Where:

$$G^r_{ijk} = \sum_{s=1}^n \frac{\alpha_k \phi_i^r \phi_k^r \phi_j^s \phi_k^s}{m^r \omega_d^r m^s \omega_d^s} \int_0^\infty e^{(-\zeta^r \omega_n^r - \zeta^s \omega_n^s) \lambda} \sin(\omega_d^r \lambda) \sin(\omega_d^s \lambda) d\lambda \quad (64)$$

$$H^r_{ijk} = \sum_{s=1}^n \frac{\alpha_k \phi_i^r \phi_k^r \phi_j^s \phi_k^s}{m^r \omega_d^r m^s \omega_d^s} \int_0^\infty e^{(-\zeta^r \omega_n^r - \zeta^s \omega_n^s) \lambda} \sin(\omega_d^r \lambda) \cos(\omega_d^s \lambda) d\lambda \quad (65)$$

It is obvious from the above equations that, cross-correlation functions between two response measurements have a form of decaying sinusoids which have the same characteristics as the system's impulse response function. An IRF has been shown on [39] to be equivalent and contain the same information, and can be derived from cross-correlation functions of random response.

The information in the IRF is used to generate a Hankel matrix, which is essential parameter in the Eigensystem Realization Algorithm (ERA) for system identification[39]. Later, the singular value decomposition (SVD) of the Hankel matrix is performed.

$$H_0 = \begin{bmatrix} Y_0 & Y_1 & \cdots & Y_r \\ Y_1 & Y_2 & \cdots & Y_{r+1} \\ \vdots & \vdots & \ddots & \vdots \\ Y_s & Y_{s+1} & \cdots & Y_{r+s+2} \end{bmatrix} \quad (66)$$

$$U\Sigma V^T = SVD[H_0] \quad (67)$$

The data matrix  $H_0 \in R^{n \times m}$  and its reduced order representation are expressed as follows:

$$H_0 = U\Sigma V^T \quad (68)$$

$$= [U_{1:r} \ U_{(r+1):m}] \begin{bmatrix} \Sigma_{1:r} & 0 \\ 0 & \Sigma_{(r+1):m} \end{bmatrix} \begin{bmatrix} V_{1:r} \\ V_{(r+1):m} \end{bmatrix} \quad (69)$$

$$= U_{1:r} \Sigma_{1:r} V_{1:r} + U_{(r+1):m} \Sigma_{(r+1):m} V_{(r+1):m} \quad (70)$$

The truncating parameter  $r$  is determined from the singular values where the consecutive singular values have higher difference. i.e., there will be a sudden drop in the plot for singular value. Figure 14(a) shows the sudden drop in the singular value plot and Figure14(b) plots the ratio of consecutive singular value, where it will be maximum for location of sudden drop in singular value.

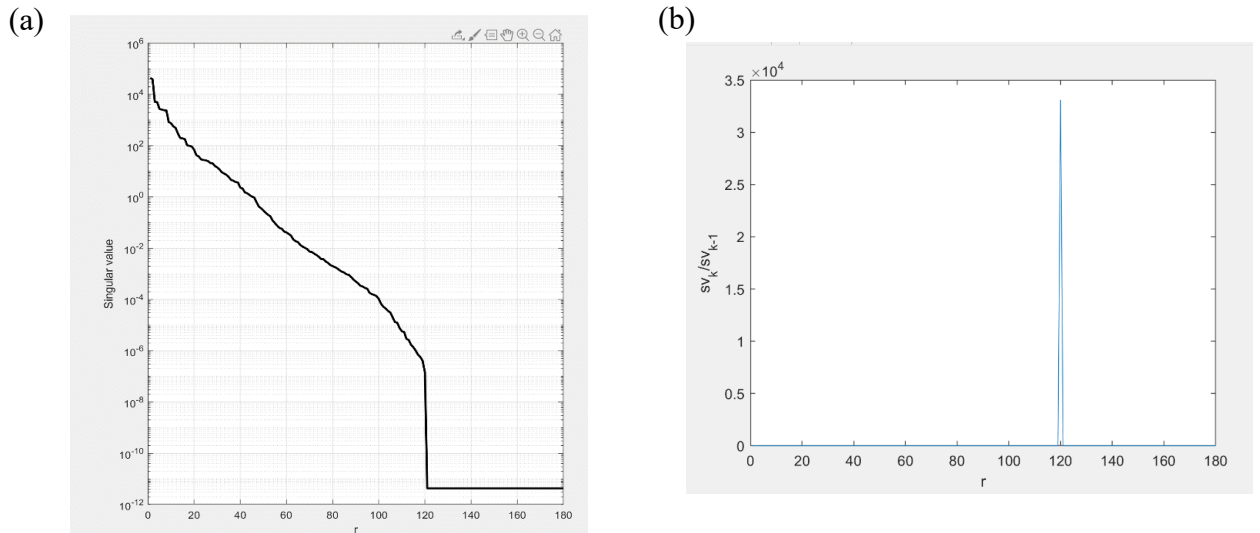


**Fig. 14** (a) Singular value plot. (b) location of sudden drop in singular value

Assuming  $S$  number of acceleration sensors measure a response data as vector  $y_s$ . Hence, the placement of these sensor can be optimized by decomposing the measurement vector,  $y_s$ , into the components of designated modes  $\phi$ .

$$y_s = S\phi q + w \quad (71)$$

Where;  $S = \{s_1, s_2, s_3, \dots, s_n\}$  is a set of sensors,  $s_i \in R^{(1 \times n)}$  refers to the  $i$ th sensor location that has unity in the  $i$ th component and zero otherwise, extracts the  $i$ th row vector from modes  $\phi$  to create a reduced order measurement matrix  $\phi_s$ ,  $w$  is the uncorrelated measurement noise assumed to have the same variance and zero mean for every observation point., and  $q$  is mode amplitude.

The placement of sensors can be considered as optimized if the covariance matrix of the estimated error is minimized while maintaining full rank observability. Considering the uniform independent Gaussian noises are assumed, the estimated parameter can be obtained as:

$$\hat{q} = (\phi_s^T \phi_s)^{-1} \phi_s^T (y + Sw) = q + (\phi_s^T \phi_s)^{-1} \phi_s^T Sw \quad (72)$$

Hence, the covariance matrix of the estimation error is expressed as follows:

$$E[(q - \hat{q})(q - \hat{q})^T] \quad (73)$$

$$= E[(\phi_s^T \phi_s)^{-1} \phi_s^T Sw w^T S^T \phi_s (\phi_s^T \phi_s)^{-1}] \quad (74)$$

$$= \sigma^2 E[(\phi_s^T \phi_s)^{-1} \phi_s^T \phi_s (\phi_s^T \phi_s)^{-1}] \quad (75)$$

$$= \sigma^2 (\phi_s^T \phi_s)^{-1} \quad (76)$$

Where;  $E[\ ]$  represents the expected value,  $E[ww^T] = \sigma^2 I$  is the covariance matrix and  $SS^T = I$ . Hence maximizing the determinant of  $\phi_s^T \phi_s$ , both the special independence and signal strength of the mode shapes are maximized.

$$R^* \equiv E(ww^T) \quad (77)$$

$$= (U\Sigma V^T - U_r \Sigma_r V_r^T)(U\Sigma V^T - U_r \Sigma_r V_r^T)^T \quad (78)$$

$$= (U_{r+1:m} \Sigma_{r+1:m} V_{r+1:m}^T)(U_{r+1:m} \Sigma_{r+1:m} V_{r+1:m}^T)^T \quad (79)$$

$$= (U_{r+1:m} \Sigma_{r+1:m}^2 U_{r+1:m}^T) \quad (80)$$

The noise covariance matrix corresponding to the sensor location will be:

$$E(Sww^T S^T) \equiv SE(ww^T)S^T \quad (81)$$

$$= S R^* S^T$$

$$= R$$

Where  $R$  represents a covariance matrix of the noise that  $S$  sensors make. Hence, the selected sensor set are evaluated step by step increasing wise, aiming to maximize the logarithm of the determinant of the fisher information matrix, which realize the covariance matrix of the estimate error will be minimum. As a result, both the special independence and signal strength of the targeted mode shapes are maximized. The fitness function for fast greedy optimization of sensors expressed by Keigo Yamada et.al [41] can be express as follows:

$$f_{Ais} = \operatorname{argmax} \log \det(C^T R^{-1} C + Q^{-1}) \quad (82)$$

Here,  $Q$  is the normalization term. The normalization term makes the inverse operation regular for  $S > r$  or  $S < r$ . The normalization term  $Q$  is expressed as follows:

$$Q \equiv E(zz^T) \quad (83)$$

$$\begin{aligned} &\approx \frac{1}{m} \Sigma_r V_r^T V_r \Sigma_r \\ &\approx \Sigma_r^2 \end{aligned}$$

Let the  $I_i$  be the  $i$ th member in the  $P$ th population, and  $S$  acceleration sensors are included in  $I_i$ th individual integrated along with other sensor types. Since the optimization is conducted at the same time instant with other sensor, we consider  $A_s = \{a_j, a_k, a_l, \dots, a_s\}$  be a set containing the information about the acceleration sensors only and  $(j, k, l, \dots, s)$  be the position of acceleration sensor in the  $I_i$ th individual out of the possible sensor candidate positions.

For a set of  $S$  acceleration sensors in the  $I_i^{\text{th}}$  individual in the  $P$  populations. The evaluation criteria for the objective problem focuses maximizing the number of independent information as much as possible while minimizing the number of sensors on that specific set. The fitness of the sensors set will be computed based on Algorithm 1 as Keigo Yamada et.al [41] demonstrated in their determinant calculation considering correlation between sensors.

**Table 3** Fast Greedy optimization algorithm

---

Algorithm 1: Detailed accelerated determinant-based greedy algorithm considering correlation between sensors.

---

Set amplitudes variance matrix

$$Q = \Sigma_r^2 \quad (84)$$

Set noise variance vector

$$d(\text{s.t. } d(j) = \mathbf{s}_j \mathbf{R}^* \mathbf{s}_j^T) \quad (85)$$

$$\mathbf{t}_1^i = \mathbf{s}_i \mathbf{d}^T \quad (86)$$

Fitness function of 1<sup>st</sup> sensor

$$f_{A1s} = \operatorname{argmax} \det(\mathbf{u}_i^T \mathbf{t}_1^i \mathbf{u}_i + Q^{-1}) \quad (87)$$

Set sensor location and observation matrix

$$\mathbf{S}_1 = \mathbf{s}_{i1} \quad (88)$$

$$\mathbf{C}_1 = \mathbf{u}_{i1} \quad (89)$$

Set sensor-covariance matrix

$$\mathbf{R}_1 = \mathbf{s}_{i1} \mathbf{d}^T \quad (90)$$

For  $n = 2, \dots, j, \dots, s$  do

$$f_{Ajs} = \text{argmax} \det (\mathbf{C}_j^T (\mathbf{R}_j^i)^{-1} \mathbf{C}_j + \mathbf{Q}^{-1}) \quad (91)$$

$$= \text{argmax} \det \left( \frac{(h_j^i (\mathbf{R}_{j-1})^{-1} \mathbf{C}_{j-1} - \mathbf{u}_i) \left( (\mathbf{C}_{j-1}^T (\mathbf{R}_{j-1}^i)^{-1} \mathbf{C}_{j-1} + \mathbf{Q}^{-1}) \right)^{-1} (\mathbf{C}_{j-1}^T (\mathbf{R}_{j-1})^{-1} \mathbf{h}_j^T - \mathbf{u}_j^T)}{(t_j^i - s_j^i (\mathbf{R}_{j-1}^i)^{-1} \mathbf{h}_j^T)} \right) \quad (92)$$

$$\mathbf{h}_j^i = \mathbf{s}_i \mathbf{U}_{r2-r1} \Sigma_{r2-r1}^2 \mathbf{U}_{r2-r1}^T \mathbf{S}_{j-1}^T \quad (93)$$

Set sensor location and observation matrix

$$\mathbf{S}_j = \begin{bmatrix} \mathbf{S}_{j-1} \\ \mathbf{s}_j \end{bmatrix} \quad (94)$$

$$\mathbf{C}_j = \begin{bmatrix} \mathbf{C}_{j-1} \\ \mathbf{u}_j \end{bmatrix} \quad (95)$$

Set noise covariance matrix

$$\mathbf{h}_j^i = \mathbf{s}_i \mathbf{U}_{r2-r1} \Sigma_{r2-r1}^2 \mathbf{U}_{r2-r1}^T \mathbf{S}_{j-1}^T \quad (96)$$

$$\mathbf{t}_j = \mathbf{h}_j^i \mathbf{d}^T \quad (97)$$

$$\mathbf{R}_j = \begin{pmatrix} \mathbf{R}_{j-1} & \mathbf{h}_j^T \\ \mathbf{h}_j & \mathbf{t}_j \end{pmatrix} \quad (98)$$

End for

---

The total cost function for evaluating the  $A_i^{\text{th}}$  acceleration sensor set to minimize the number of sensors by setting a ratio of identified modes with the number of sensors in the set. Hence the cost function will be

$$f_{Ai} = \frac{1.15^{N_m}}{6^{3.5/N_s} \times N_s^{1.5}} * f_{Ais}^{0.1} \quad (99)$$

Where  $N_m$  is the number of modes identified,  $N_s$  is the number of acceleration sensors in the set, and  $f_{Ain}$  is the fitness identified by the fast algorithm presented in Algorithm 1.



The number of identified modes  $N_m$  corresponding to the selected sensor set are extracted from the eigenvectors of state matrix  $A$  obtained from NExT-ERA identification [40][42]. By retaining the  $R$  sub vectors, the eigenvalues containing natural frequencies and damping ratio are identified by solving the eigenvalue problem of state matrix  $A$  [39].

$$A = \Sigma_R^{-1/2} U_R^T H_1 V_R \Sigma_R^{-1/2} \quad (100)$$

As the ERA method generates imperfect modes, to distinguish the real modes from the flawed modes, Dionysius M.S. et.al. [39] suggested filtering with a post process after performing ERA. To conduct the post processing, the set of identification criteria like MAC, EMAC, MPC, and CPI, suggested by Pappa R.S. et.al. [43], are set to be 80% or higher. Hence the post processing procedure follows extracting and removing all modes with MAC, EMAC, MPC, and CPI less than 80%, or having negative damping ratio, or having uncharacteristically large damping.

### 5.3 Genetic Algorithm Coding

Individual members in a population is encoded by real number representing the status of each candidate sensor locations. There are a total of 231 nodes exist as a candidate sensor position per individual. A candidate node can only be assigned to one sensor at a time. Hence, considering the displacement sensor is one dimensional and the acceleration sensor is three dimensional a total of three candidate sensor types are available. The representation of sensor's type assignment follows numbering from 0 – 3, 0 – means no sensor assigned to the candidate sensor location, 1 – longitudinal direction displacement sensor, 2 – vertical direction displacement sensor, and 3 – tri-directional acceleration sensor.

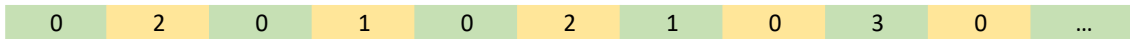


**Fig. 15** Genetic coding representation of individual in a population

In the above example node Nd-4 and Nd-7 are assigned as longitudinal direction displacement sensor, node Nd-2 & Nd-6 are assigned as vertical direction displacement sensors, and Nd-9 is assigned as tri-directional acceleration sensor. The other nodes are not assigned as a sensor location to any type.

## 5.4 Optimization Flow

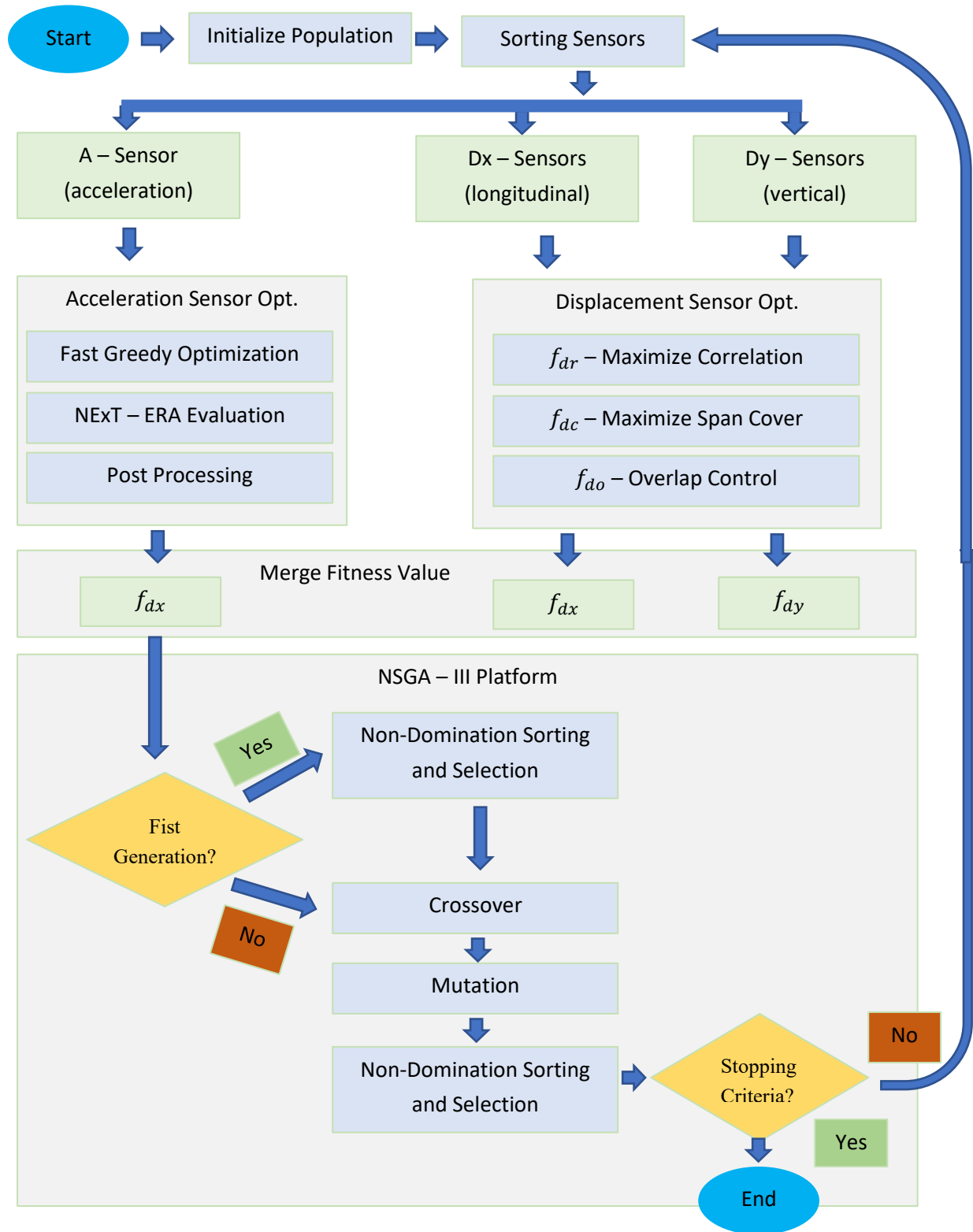


**Fig. 16** Flow diagram of the optimization process

## 5.5 Optimality curve

The performance of SHM system is enhanced by increasing the number of sensors deployed on the structure to collect as much system information as possible. However, due to the economical, computational, and data management difficulties, the search will focus on getting a specific information with minimum possible number of sensors.

On the other hand, an optimization aiming at obtaining a specific modal parameter doesn't prioritize minimizing the number of sensors, however the primary focus is obtaining the required system information no matter how much the sensor is and search for the best configuration that can give the specified modal parameters.

Hence, we can say that the objectives for optimal sensor placement problems can be drawn from two perspectives. The first one is to systematically place a limited quantity of sensors to best estimate system parameters. Given the available  $s$  sensors out of  $p$  possible locations, placing the sensors in optimal arrangement to get as much independent information as possible will have an enormous computational time  $\left(\frac{p!}{(p-s)!s!}\right) \sim O(p)^s$ .

The second perspective is setting the required estimate of system parameters, optimizing the number of sensors to minimum quantity. To address this issue simultaneously in one optimization, the concept of optimality curve is introduced.

The optimality curve constantly updates during the search process of a non-dominated sorting genetic algorithm. The main purpose of this application is to tack the best-found solutions in the specific objective that can be lost due to the restriction of one sensor per node installation rule and the combined fitness evaluation. Hence, the optimality curve provides tradeoff information between deploying minimum sensor and obtaining maximum modal parameters.

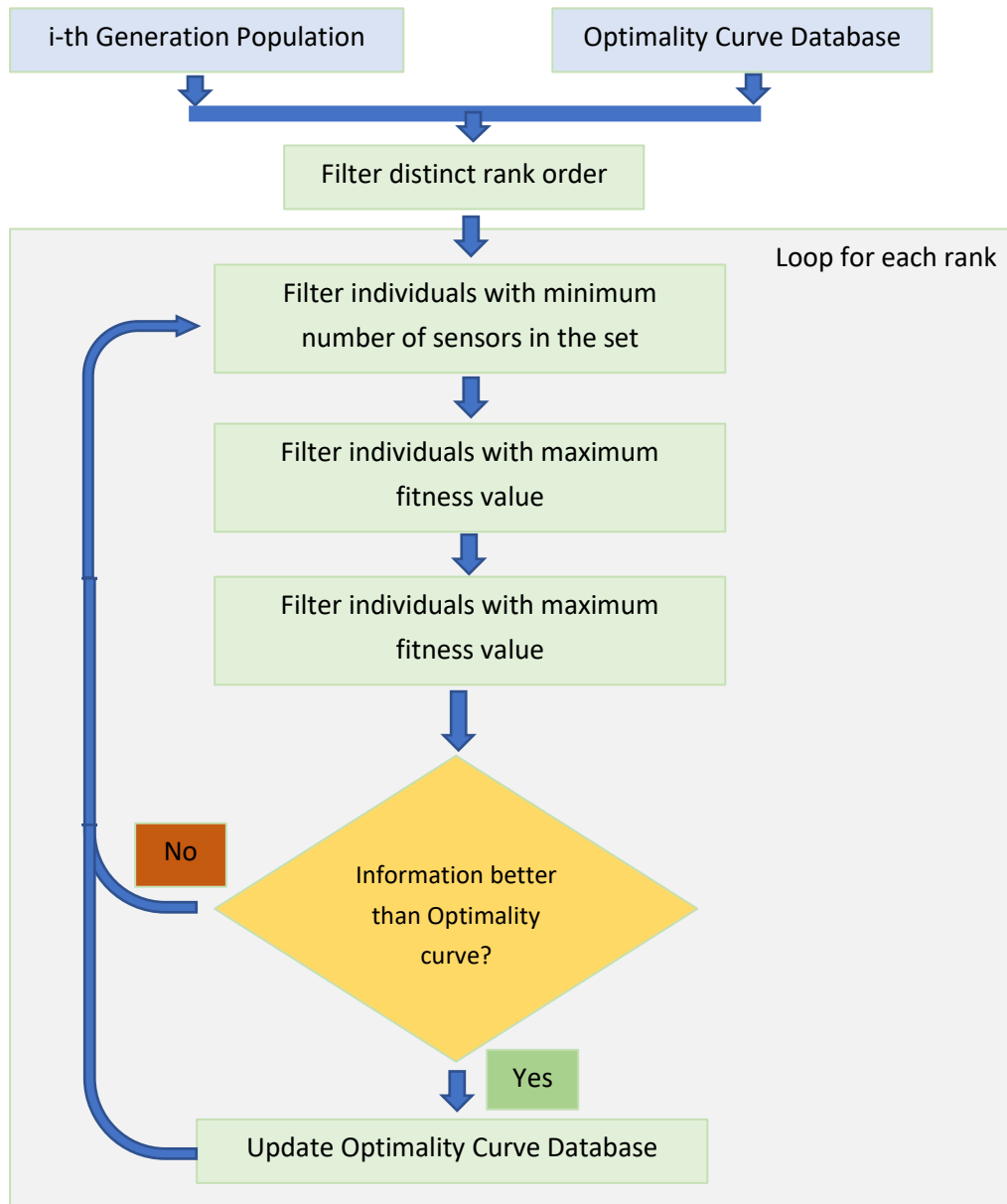


**Fig. 17** Flow diagram for the optimality curve updating

# Chapter 6: Damage Identification

## 6.1 Damage Modeling

Bridge consists of several components that have variable resistance to the damage and deterioration during their service life. The damage may rise from either the loss in mass, chemical interaction, or mechanical interaction between structural members. Cracks, spalling off, delamination, corrosion, fire, fatigue, rebar-concrete bond failure are some of the common damages encountered in the reinforced concrete and steel members of a structure.

Most of structural damages usually affect the flexural stiffness of a member. The loss in the stiffness at a localized part of the bridge members affects the global behavior of the structure. Hence, this change in response can be used as an indicator of damage location.

Bridge condition inspection manuals express the maximum allowable crack width with respect to the condition of the environment. However, the crack depth has direct relation on the assumption of flexural stiffness reduction for the corresponding damage encountered due to the occurrence of crack on the structure. Li Y. et. al. [44] conducted an experimental study on the correlation between crack width and crack depth of RC Beams. The developed curve from the experiment shows that the curve of depth/ width shows steep linear increase until the reinforcement yielded, and the crack depth remain stable even with large increase in crack width. Hence, taking a crack width of 0.02mm, which is the minimum value that can be noticed with bare eye, the crack depth grew beyond half the beam depth. As a result, the estimation of 50% flexural stiffness reduction proofs to be logical in modeling damage due to very small crack on the structure

In this research, damage has been defined as any type of deterioration on the parts of the bridge which can potentially affect the structural integrity by undermining the flexural stiffness of the bridge. The identification these damages are performed using the integration of MDBI method and FE-MSE method. The damage scenario is conducted by assuming two types of damages in modeling the variable deterioration mechanisms.

Damages in steel girder are modeled by reducing the flexural stiffness of the damaged elements by 25%. Deterioration in reinforced concrete slab is modeled for local bond-slip failure.

Bond slip failure occurs when the reinforcing bar is subjected to pull out and crack develops at the interface between the steel bars and the surrounding concrete. It affects the interaction by reducing surface friction and rebar anchorage in to concrete. Local bond failure is critical because the damage is unnoticeable since the surrounding concrete are unaffected. As a result, there will be no sign of crack on the surface of the concrete.

This phenomenon is a potential risk in reinforced concrete structures, where it can create both increased deflections and reduced strengths, and subsequently leading to catastrophic failure. However, it can be unnoticed by visual inspection while the damage is posing potential danger to the users and the surroundings of the bridge.

Damage cases with variable area, position and number of local bond slip failure is considered. The reinforcement-concrete bond failure within the slab deck is modeled in the simulation by releasing the reinforcement bar – concrete embedment interaction with in the considered damaged sections. Three damage sizes are considered in the damage scenarios. The first size is D-1 type damage, where 2.81 square meter (19.1%) of the total panel area is affected by local bond slip failure and the second size is D-2, where 0.67 square meter (4.5%) of the panel area. And the third size is D-3, where 0.34 square meter (2.3%) of the panel area is used. The location of damage and panel arrangement of the slab is presented in Figure 18 and the information about the considered damage area is listed in Table 4.

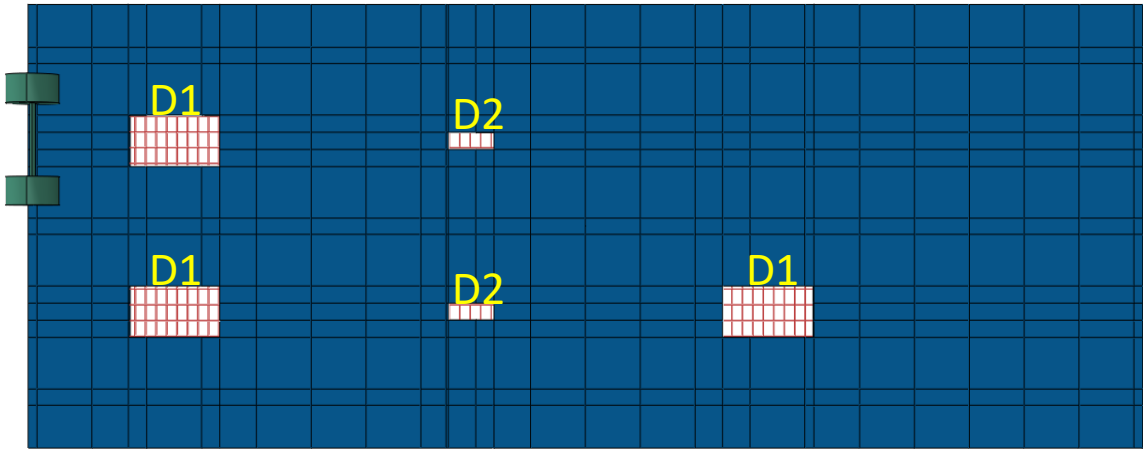


**Fig. 18** Damage locations considered in the scenarios

P-1	P-3	P-5	P-7
P-2	P-4	P-6	P-8

**Fig. 19** Panel arrangement of the slab

**Table 4** Damage types general information

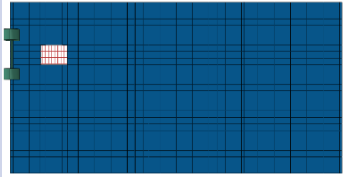
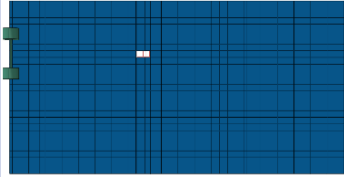
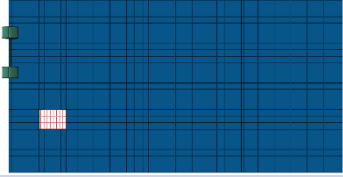
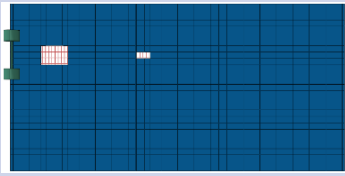
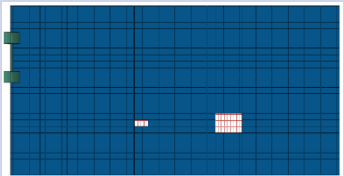
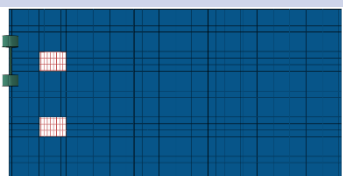
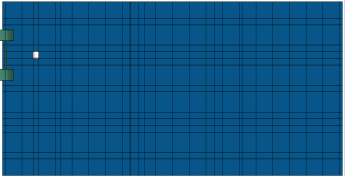
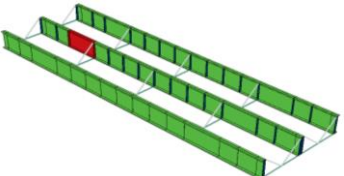
Damage Type	Damage Size	Damage Area	% Panel Area
None	5.33m x 2.76m	14.71 m <sup>2</sup>	
D1	2.01m x 1.40m	2.81 m <sup>2</sup>	19.1 %
D2	1.20m x 0.56m	0.67 m <sup>2</sup>	4.5 %
D3	0.60m x 0.56m	0.34 m <sup>2</sup>	2.3 %

## 6.2 Damage Scenarios

Several cases have been simulated, as shown in the Table 5, for investigating the effectiveness of the proposed approach in damage location identification. The cases are developed based on the possibilities of structural damage occurring on different parts of the bridge, different position within the part, location of damage with respect to the moving load, size of damaged area, number of damages at a time.

- In the first case, damage type D1 is investigated where the moving axel load directly passes over the damaged slab.
- The second case, damage type D2, is also considering damage located in the same path of the axel load but the damage area is reduced.
- The third case, damage type D1, where the moving axel load crosses the bridge while the damaged area is on the opposite lane.
- The fourth and the fifth cases are considering multiple damage with variable damage area, where the former case is multiple damage in the same path with axel load while the latter case is multiple damage in opposite path with the axel load.
- The sixth case, double D1 type damage, is considered as the damage of equal size occur in both lanes, Hence the effect of damage overlap at the same location is investigated.
- The seventh case, damage type D3, is the replication of first case with smallest damage extent.
- In the last case, girder damage with 25% in stiffness reduction is located at the middle girder near the first quarter of the span.

**Table 5** Damage analysis scenarios

<p>Case 1</p> <p>Single Damage (D-1)</p> <p>On the same lane of Axel pass</p>	<p>Case 2</p> <p>Single Damage (D-2)</p> <p>On the same lane of Axel pass</p>	<p>Case 3</p> <p>Single Damage (D-1)</p> <p>On the opposite lane of Axel pass</p>
		
<p>Case 4</p> <p>Multiple Damage (D-1&amp;D-2)</p> <p>On the same lane of Axel pass</p>	<p>Case 5</p> <p>Multiple Damage (D-2&amp;D-1)</p> <p>On the opposite lane of Axel pass</p>	<p>Case 6</p> <p>Multiple Damage (D-1 x2)</p> <p>On both lanes of the bridge</p>
		
<p>Case 7</p> <p>Smaller Damage (D-3)</p>	<p>Case 8</p> <p>Girder Damage (25% Stiffness)</p>	
		



## Chapter 7: Results and Discussion

### 7.1 Data collection and processing

The bridge deck is divided in to approximately 1m along the longitudinal direction and the transverse direction division considers the position of girders and evenly distribution between girders. Totally, the slab area is divided at 21 nodal points in the longitudinal direction and 11 nodal points in the transvers direction totally 231 nodes which are assigned as candidate sensor positions are obtained as shown in the Figure 20.

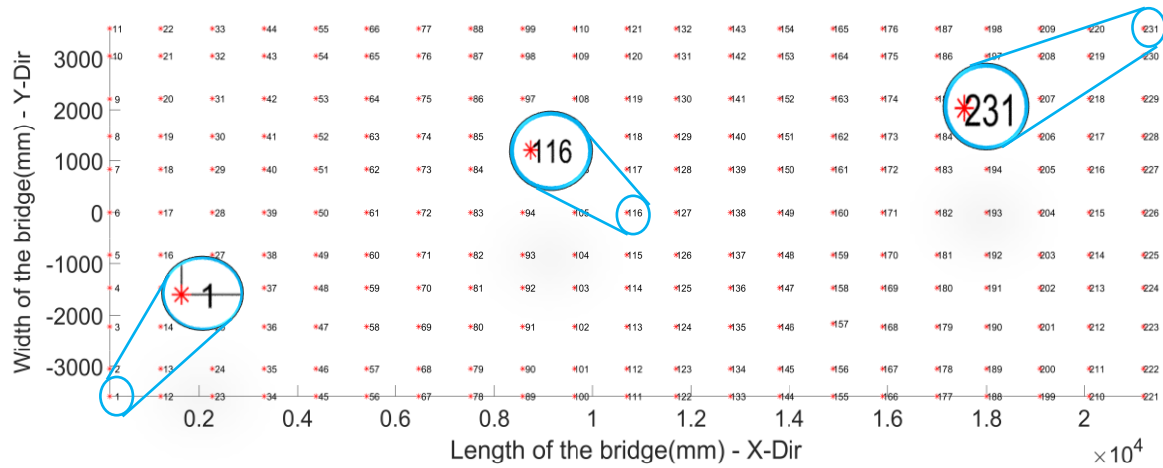


**Fig. 20** Candidate sensor position and assigned notation

In the Figure 20, the view of the slab is from bottom; therefore, the position of the nodes will be inverted when viewed from the top. In this case, the left side edge of bridge will be the bottom edge of the figure and the right-side edge of bridge will be the top edge of the figure, for the vehicle movement from left to right. Accordingly, the numbering of nodes start from the left bottom and ends at the right top of the assigned node distribution.

The bridge is loaded with the moving axel load considering the road roughness. The bridge responses – acceleration, and displacement – are recoded at each nodes assigned candidate as a candidate sensor location. Each node will have acceleration record response in the three directions – longitudinal, vertical, and transversal – representing the tri-directional acceleration sensor. Furthermore, the displacement responses in the two – longitudinal and vertical – directions will be used representing the uni-directional displacement sensor, that can be installed either in the longitudinal direction or vertical direction at a specific node.

After obtaining the measured responses at all assigned nodal positions, the data preparation for utilizing in the optimization process is presented on Figure 21 to 27.

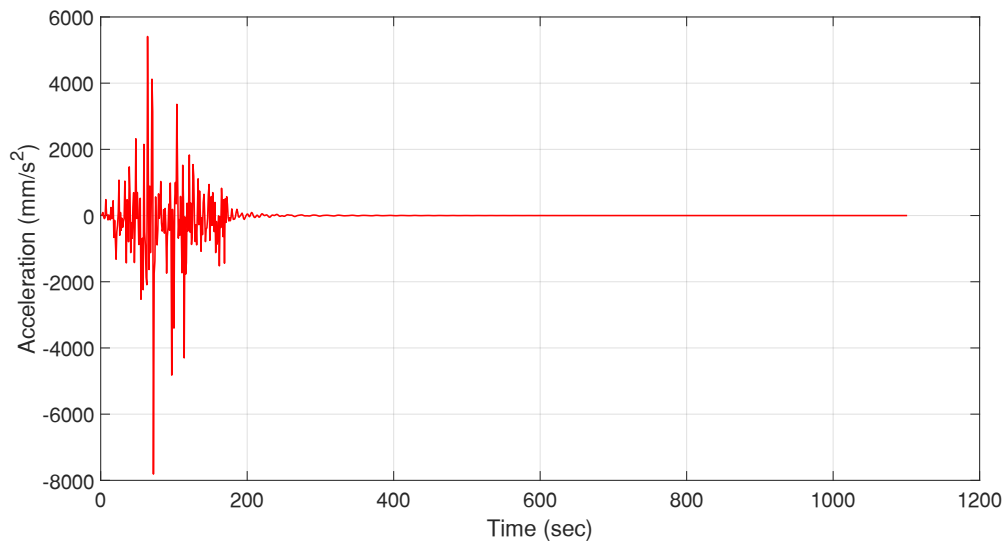


**Fig. 21** Vertical acceleration response at node 116 (mid span) measured for full length of simulation

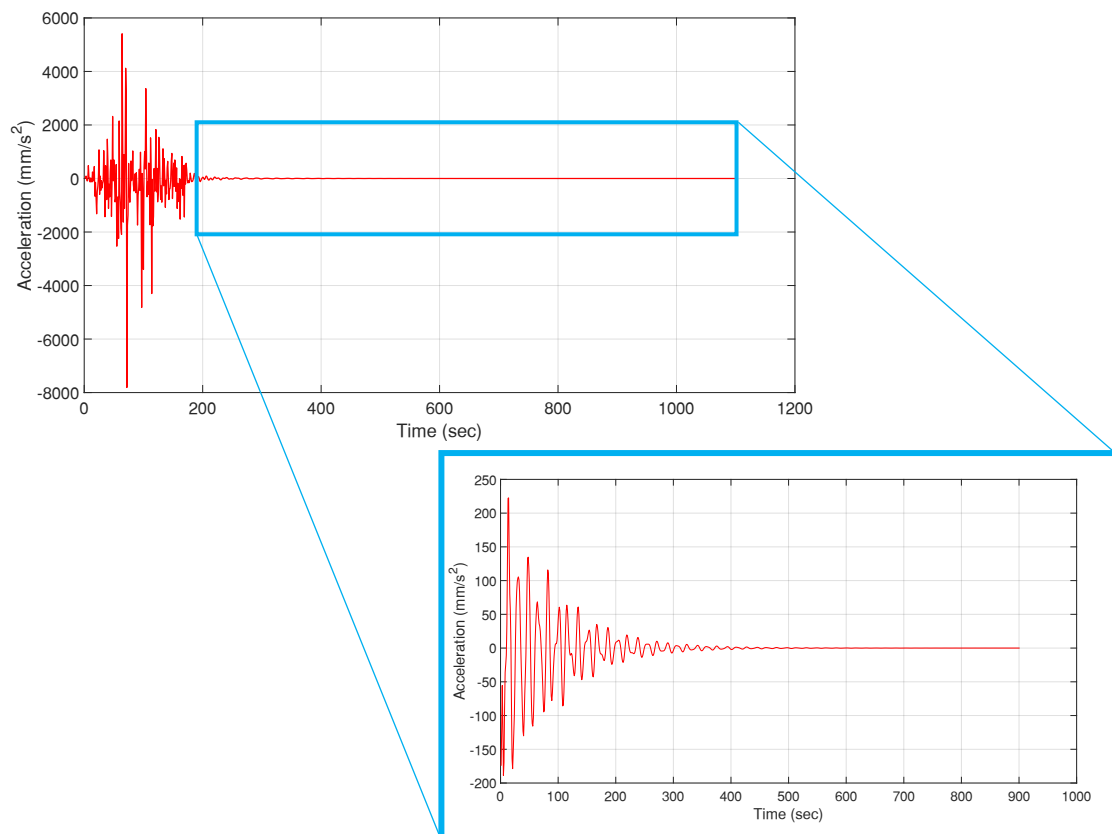


**Fig. 22** Vertical acceleration response at node 116 after removing the section when the load is on bridge

The vehicle load applied at the bridge will create a random vibration varying in time and space. This phenomenon creates nonlinearity on the measured response. To avoid the nonlinearity and comply with the requirement of eigensystem realization algorithm ERA, the section of the measured response after the vehicle exits the bridge is used. Hence the measured response will be the ambient vibration data excited by the moving load. Similarly, the longitudinal and transversal directions of the measured acceleration responses are treated as presented in Figure 23 and 24 respectively.

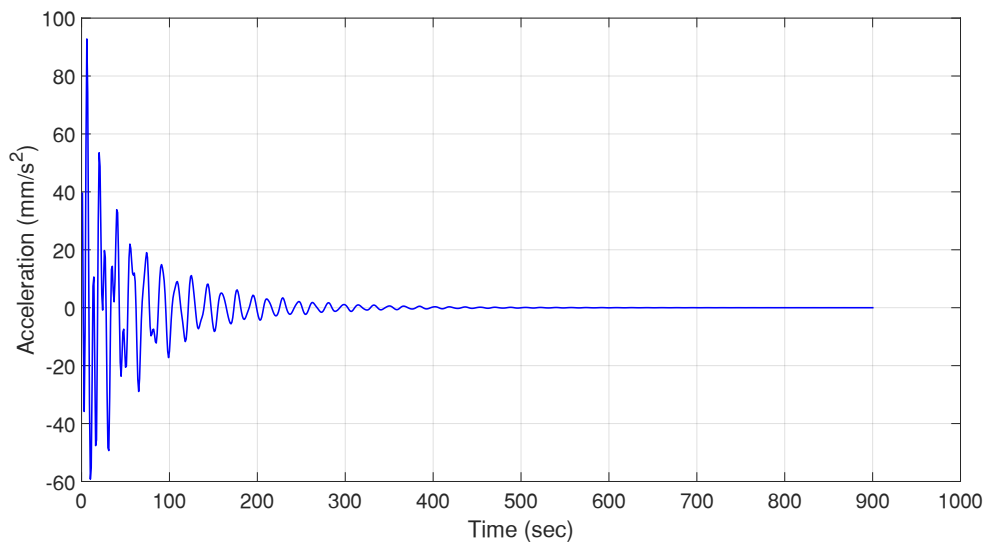


**Fig. 23** Longitudinal acceleration measured at node 116 after the vehicle leaves the bridge.

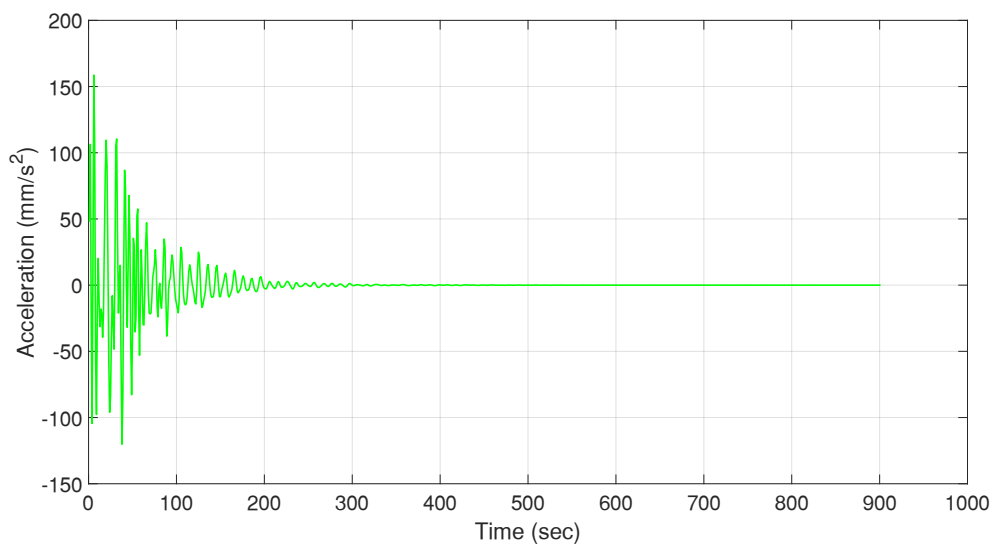


**Fig. 24** Transversal acceleration measured at node 116 after the vehicle leaves the bridge

For the case of the measure displacement response, the response corresponding to the time where the vehicle is moving on the bridge is required. Consequently, the displacement responses are treated to meet the required data sampling for the corresponding evaluation method adopted in the optimization process. Figure 25 shows the full length of measured displacement response at the mid span node. The treated measurement data and location of trimming is shown in Figure 26. Similarly, the longitudinal direction measurement is trimmed as shown in Figure 27.

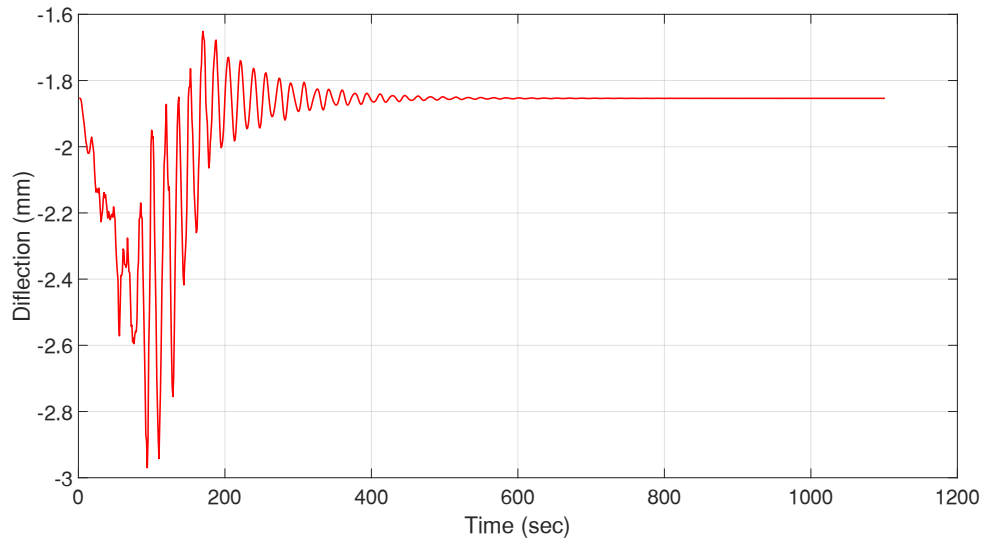


**Fig. 25** Vertical displacement response measured at node 116

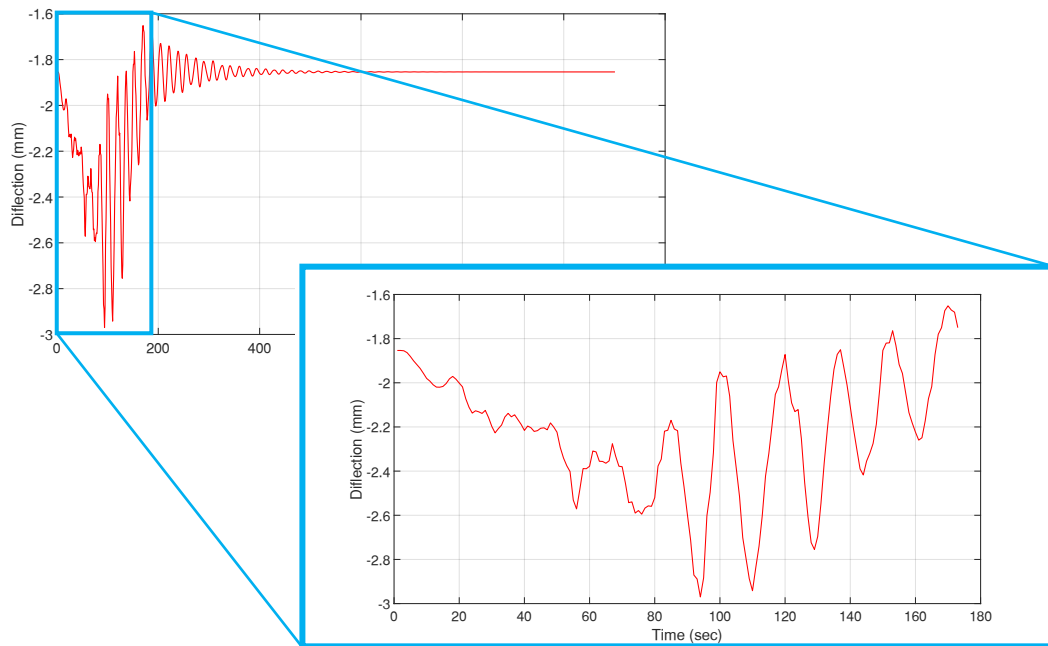


**Fig. 26** Extracting vertical displacement response for section where the vehicle is on bridge

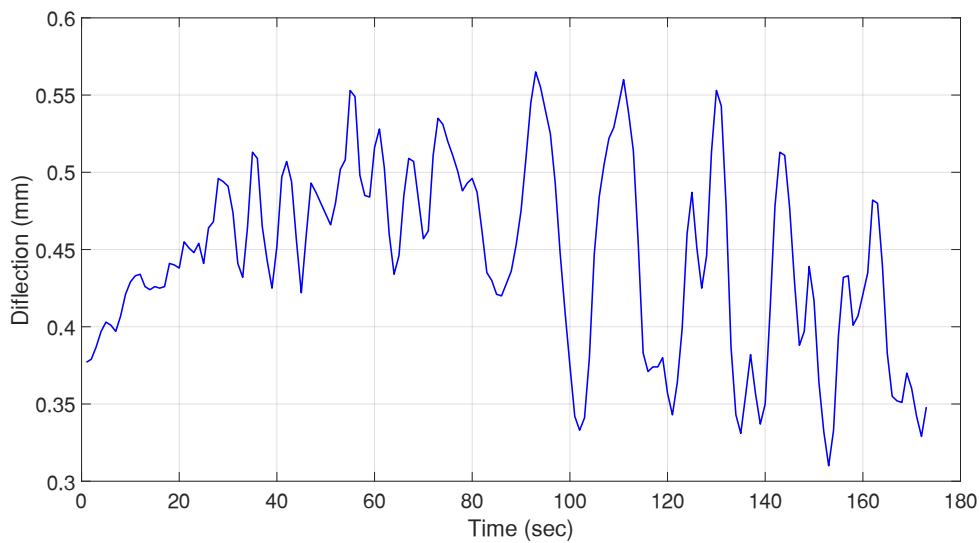


**Fig. 27** Longitudinal displacement response for section where the vehicle is on bridge

## 7.2 Sensor Placement Optimization

The optimization process is based on the non-dominated sorting algorithm NSGA-III [4] platform. The genetic algorithm parameters are evaluated for conformity with the fitness evaluation method followed by this research. Hence prior to commencing optimization, the genetic algorithm parameters are checked and adopted throughout the optimization process. Selection of crossover type, generation size and mutation rate are compared between different values as shown in the Figure 28 to 30.

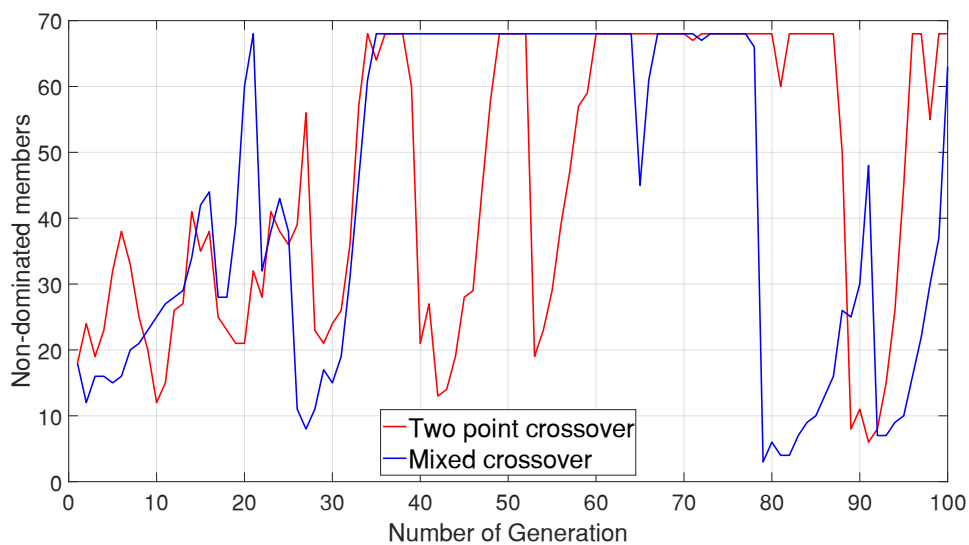


**Fig. 28** GA parameters comparison: two-point crossover vs mixed crossover

Suitability check for crossover type between two-point crossover and mixed crossover is conducted. The size of non-dominated members throughout the search process is taken into consideration for evaluating the performance of the crossover type. As shown in the Figure 28 the mixed crossover is relatively stable for most of the generation than the two-point crossover. Hence, mixed crossover type is selected as suitable crossover choice for this research objective.



**Fig. 29** GA parameters comparison: 1% mutation rate vs 2% mutation rate

The 1% mutation rate is observed to be stabler than 2% mutation rate towards keeping the non-dominated members for most of the generation. However, in both GA parameters comparison plots there is a sudden loss of non-dominated members from the population. Thus, the comparison towards the fixing the maximum generation size is conducted as illustrated in the Figure 30. It showed that the selection of generation size of 150 is better to get a stable non-dominated population.

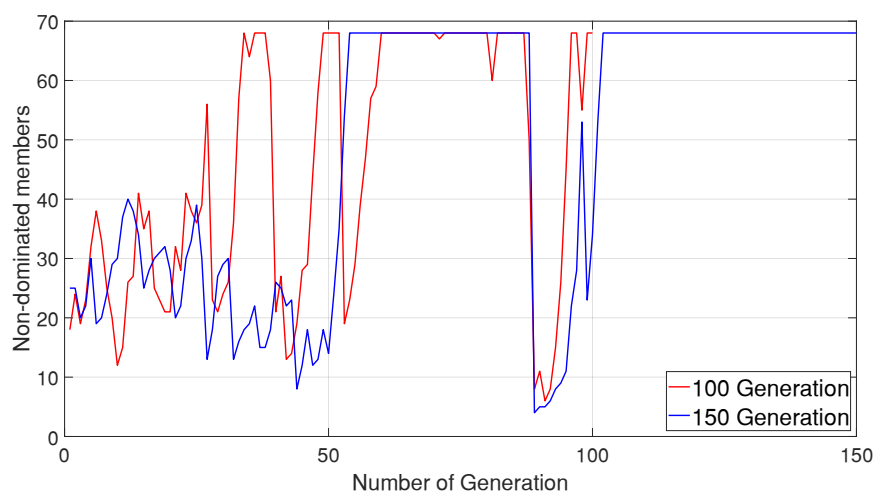


**Fig. 30** GA parameters comparison: 100 Generation vs 150 Generation

Even though, the maximum generation size of 150 is proved to be sufficient in keeping consistency in non-dominated members as illustrated in Figure 30, the size is increased to 250 considering the capacity of the computer. Finally, the genetic algorithm parameters listed in the Table 6 below is adopted for the rest of optimization process.

**Table 6** Genetic algorithm parameters adopted for optimization

Genetic Algorithm Parameters	
Objectives (M)	3
Number of division (p)	12
Population Size	91
Maximum Generation	250
Cross-over Type	Mixed
Cross-over Rate	0.5
Mutation Rate	0.01

The optimization process is conducted several times varying the initial population at each search process. Hence the following optimized values are extracted from one of the optimization results.

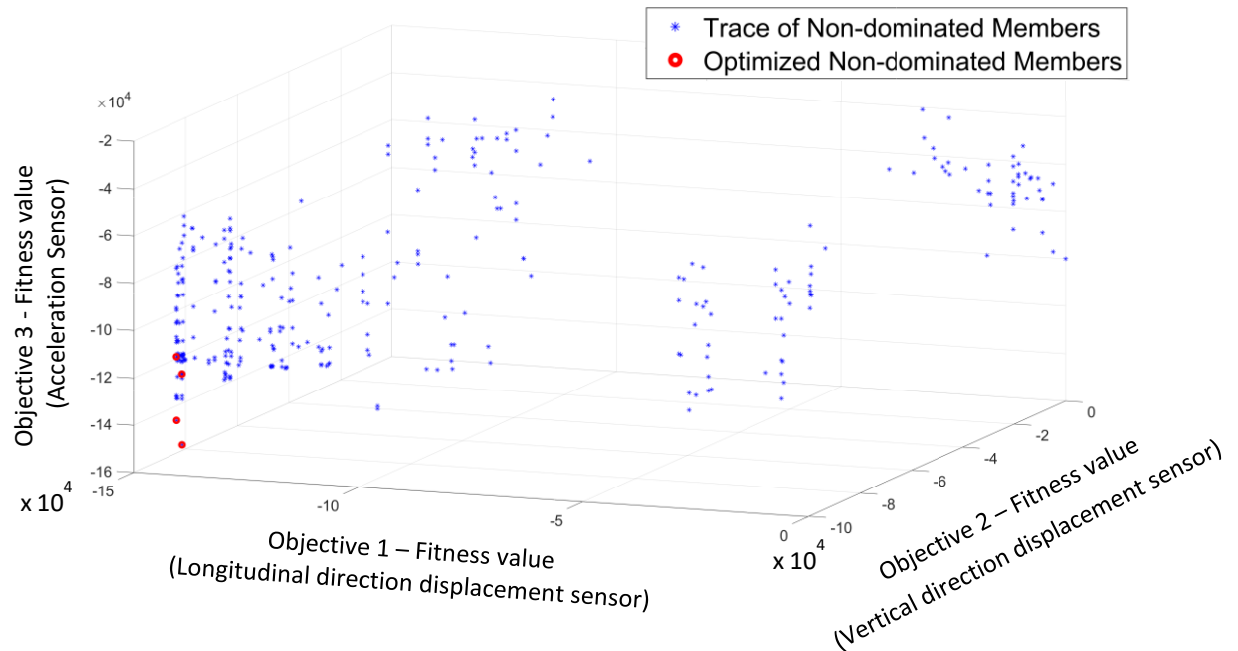


**Fig. 31** Optimized non-dominate members through the search progress

As shown in the Figure 31, during the search process, non-dominated members of the population progress minimizing the objective function each time. The final F1 members are shown with red dots in the left bottom edge of the figure.

### 7.2.1 Longitudinal direction displacement sensor optimization result

The optimization for the longitudinal direction sensor positioning resulted with a few set of sensors. In most cases, the optimized sensors are able to achieve a set of three sensors. The result of overlap control and strong relationship plot for the case of set number 1 in the Table 7 is shown on the Figure 32 to 35.

**Table 7** Optimized longitudinal sensor locations

No	Optimized Sensor Positions
1	[10, 43, 54]
2	[21, 43, 54]
3	[10, 83,178,204]
4	[24, 215, 226]
5	[28, 193, 204]
6	[13, 215, 226]
7	[6, 13, 94,178,211]
8	[24, 193, 215]

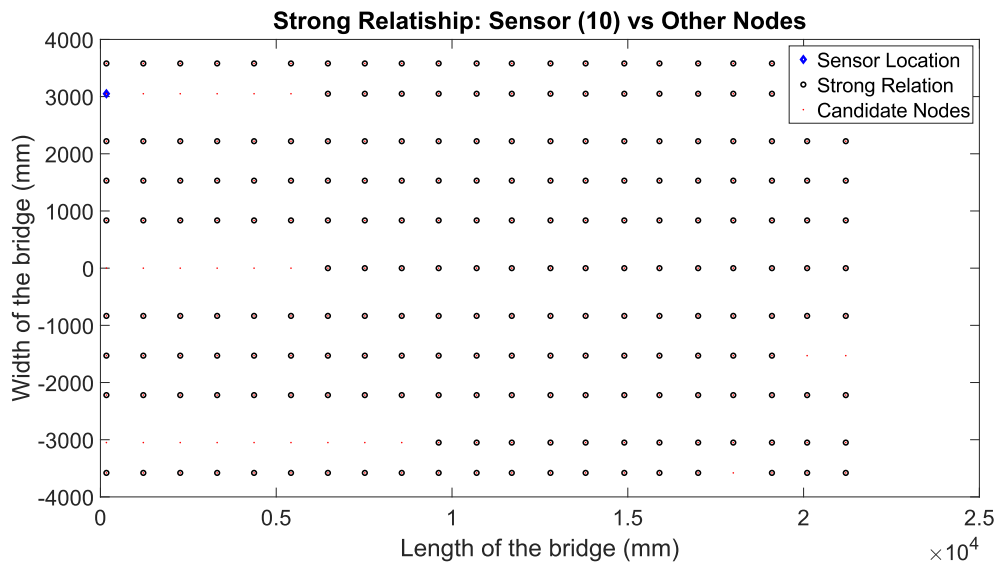


**Fig. 32** Strong relationship plot for sensor 10 with other candidate nodes



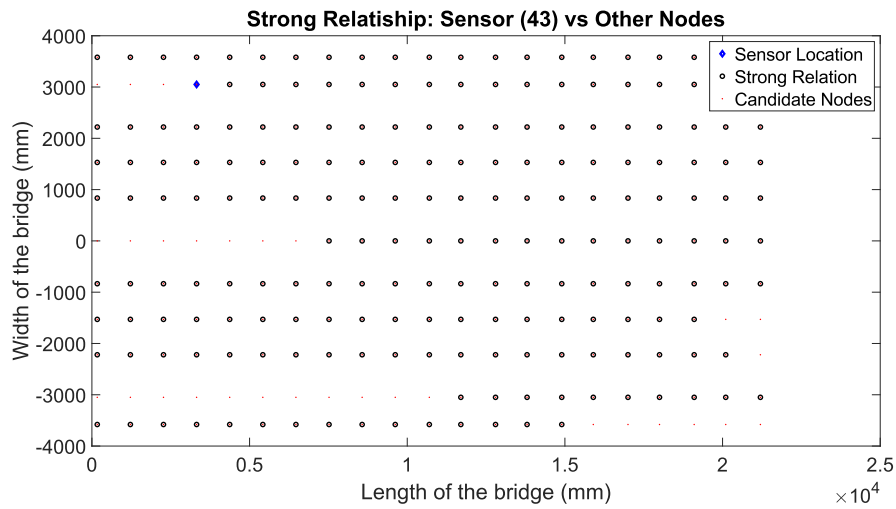


**Fig. 33** Strong relationship plot for sensor 43 with other candidate nodes

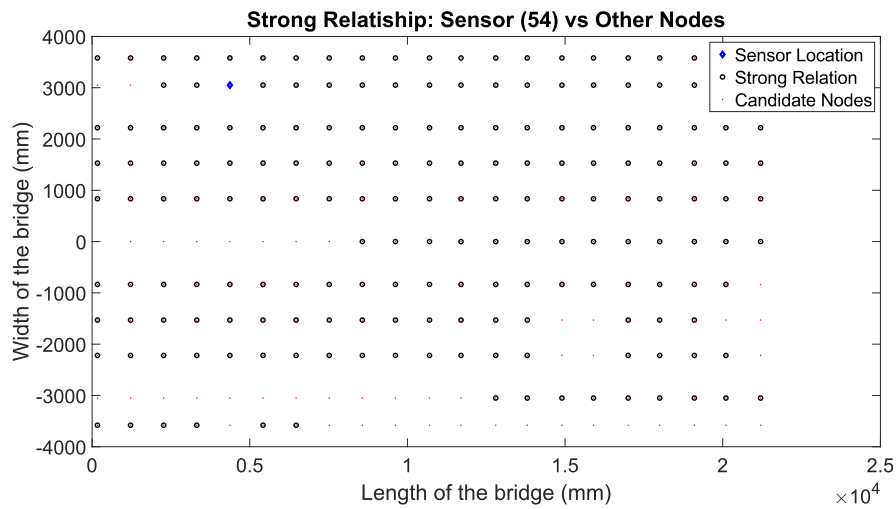


**Fig. 34** Strong relationship plot for sensor 54 with other candidate nodes

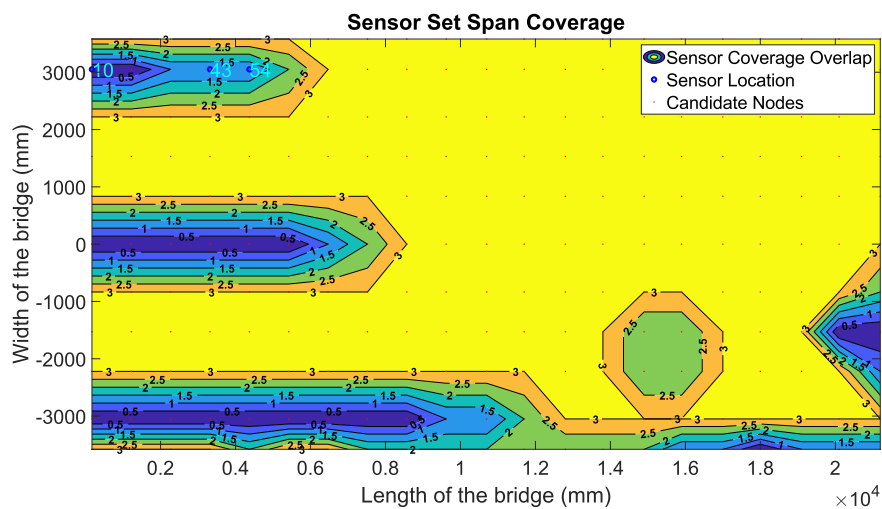


**Fig. 35** Contour plot of sensor overlap

### 7.2.2 Vertical direction displacement sensor optimization result

Similarly, the optimization for the vertical direction sensor positioning resulted with a set of sensors listed in Tabel 8. In all of the cases, the optimized sensors are able to achieve a set of three sensors. The result of overlap control and strong relationship plot for the case of set number 1 in the Tabel 8 is shown on the Figure 36 to 39.

**Table 8** Optimized vertical sensor locations

No	Optimized Sensor Positions
1	[2, 6, 230]
2	[1, 120, 227]
3	[10, 219, 222]
4	[2, 10, 222]
5	[1, 120, 227]
6	[2, 222, 230]
7	[1, 2, 230]
8	[2, 22, 222]

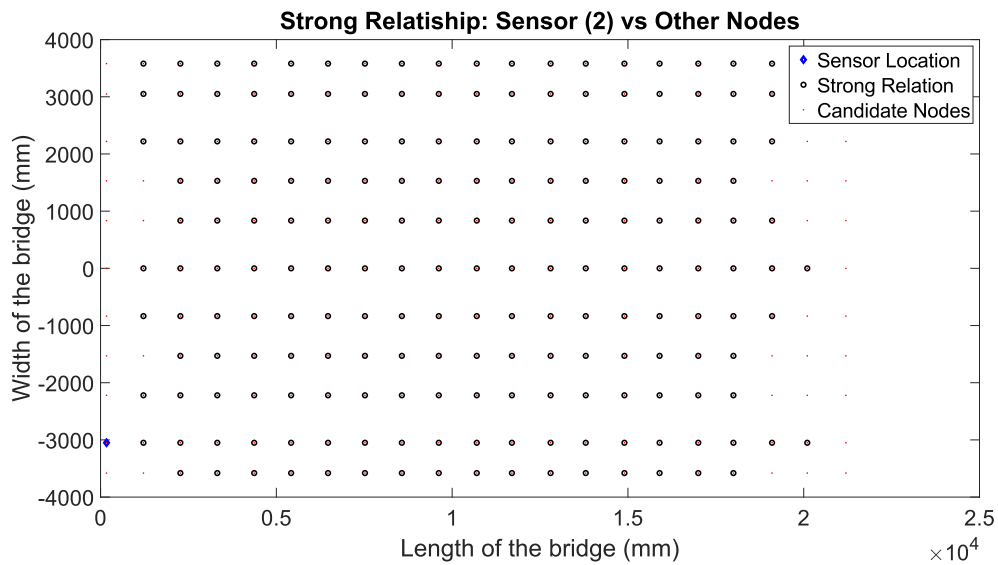


**Fig. 36** Strong relationship plot for sensor 2 with other candidate nodes

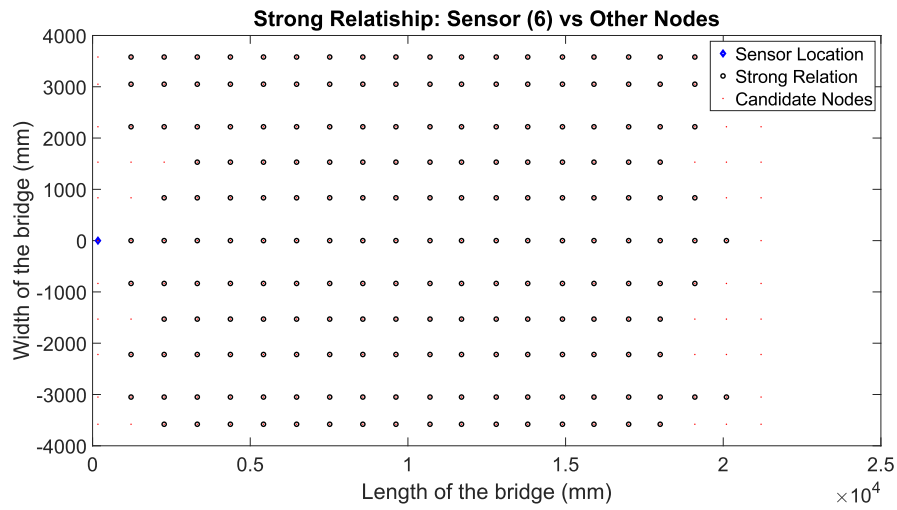


**Fig. 37** Strong relationship plot for sensor 6 with other candidate nodes

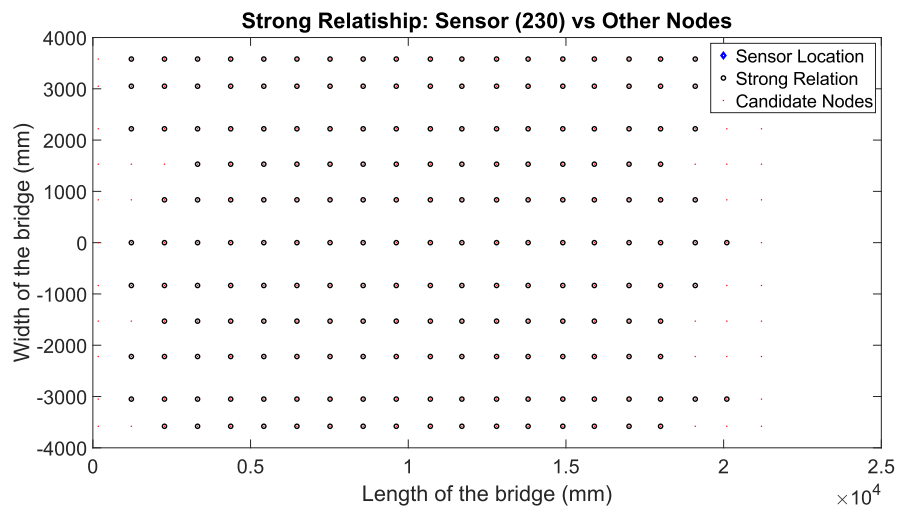


**Fig. 38** Strong relationship plot for sensor 230 with other candidate nodes

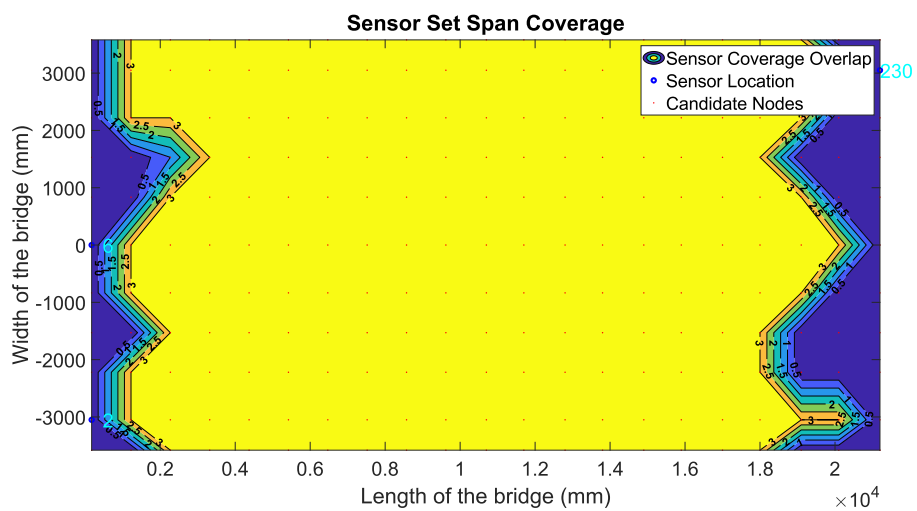


**Fig. 39** Contour plot of sensor overlap

### 7.2.3 Acceleration sensor optimization result

The search for optimized acceleration sensor position is conducted without any restriction on maximum number of sensors in the set. However, the effect of additional number of sensors in the set is observed to minimize at some point inhibiting further addition of sensor do not identify additional mode. This phenomenon is observed on the optimality curve plot, shown in Figure 40 and 41, updated during the search process. Table 9 lists the identified modes frequency and the corresponding FEM extracted frequency.

**Table 9** Identified and FEM frequencies corresponding to the mode shapes

Mode		Error	
Identified	FEM	err	%
1.93	1.16	0.77	66.4%
4.8	4.87	0.07	1.4%
5.3927	5.02	0.3727	7.4%
5.7941	5.9	0.1059	1.8%
7.44	7.53	0.09	1.2%
8.64	9.66	1.02	10.6%
24.54	24.76	0.22	0.9%
25.68	25.76	0.08	0.3%
27.87	27.82	0.05	0.2%
30.62	30.86	0.24	0.8%
31.4	31	0.4	1.3%
36.03	36.38	0.35	1.0%
39.15	39.01	0.14	0.4%
40.81	41.01	0.2	0.5%

7.2.3.1 Optimality Curve

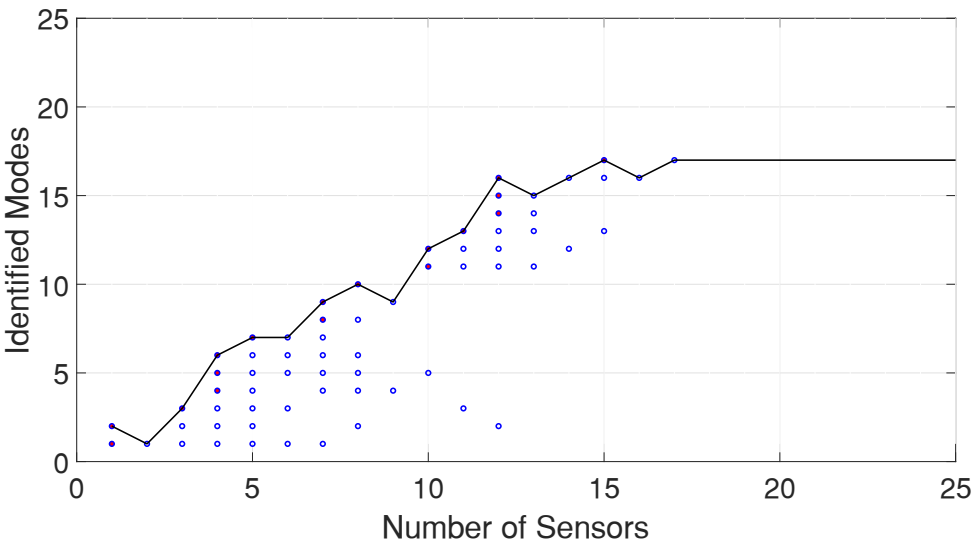


Fig. 40 Optimality curve sample 1

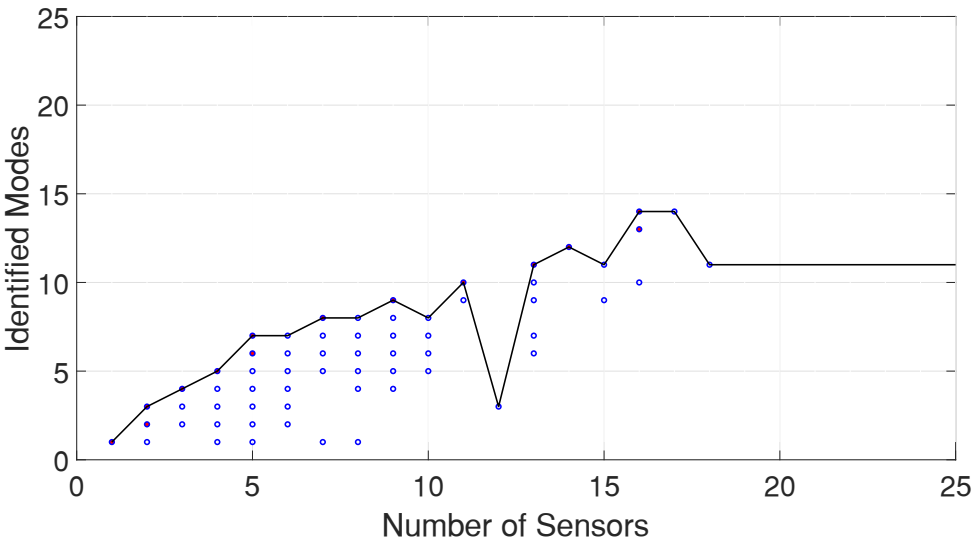
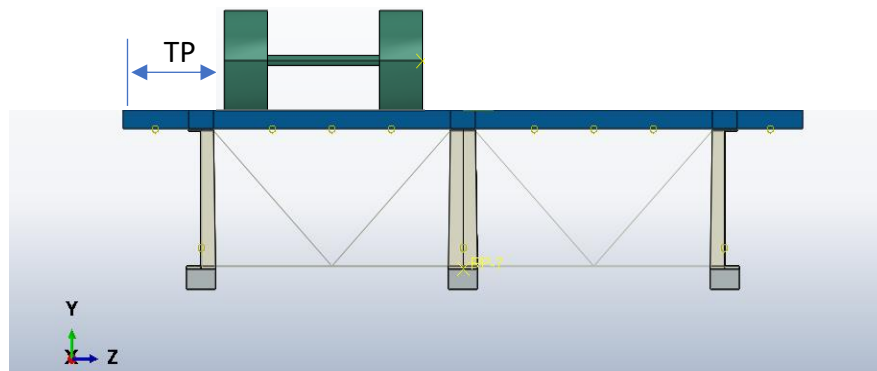


Fig. 41 Optimality curve sample 2

### 7.3 Vehicle's Transverse Position Identification

The transverse position of the vehicle is measured from the left edge of the bridge as shown in Figure 42. The methodology proposed by Yu Y. et.al.[34] is adopted to identify the position of the vehicle in the transverse direction. To cover all possible path of the vehicle on transverse direction of the bridge, repeated simulation is conducted with the shift of 201mm, width of the wheel, to the right side until the right wheel reaches the edge of the second lane. The considered shift to the transverse position is presented in table 10.



**Fig. 42** Transverse position measurement reference

**Table 10** Shift in transverse position of vehicle from the reference point

Transverse position of the axel load considered in the analysis										
TP-1	TP-2	TP-3	TP-4	TP-5	TP-6	TP-7	TP-8	TP-9	TP-10	TP-11
800	1001	1202	1403	1604	1805	2006	2207	2408	2609	2810
TP-12	TP-13	TP-14	TP-15	TP-16	TP-17	TP-18	TP-19	TP-20	TP-21	
3011	3212	3413	3614	3815	4016	4217	4418	4619	4820	

Strain measurements at the mid span of each girder is taken as shown in the Figure 43. Later, the influence surface is generated from the measured strain responses as shown in the Figure 44 and 45.

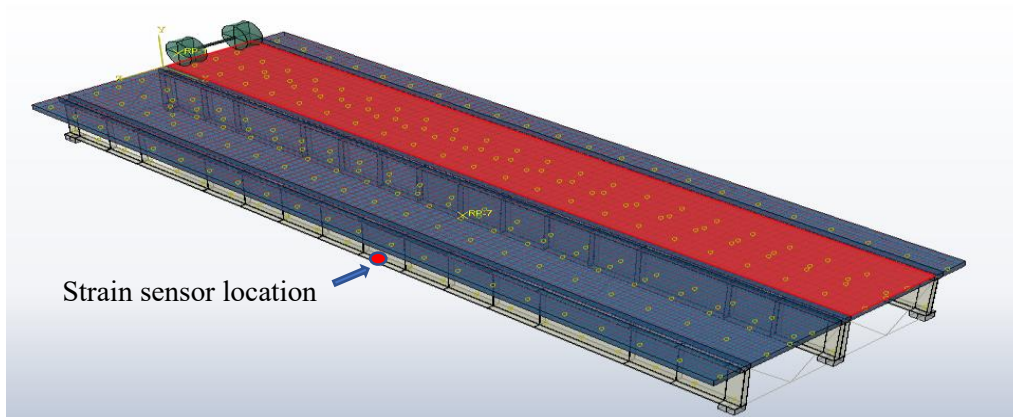


**Fig. 43** Strain response measurement location

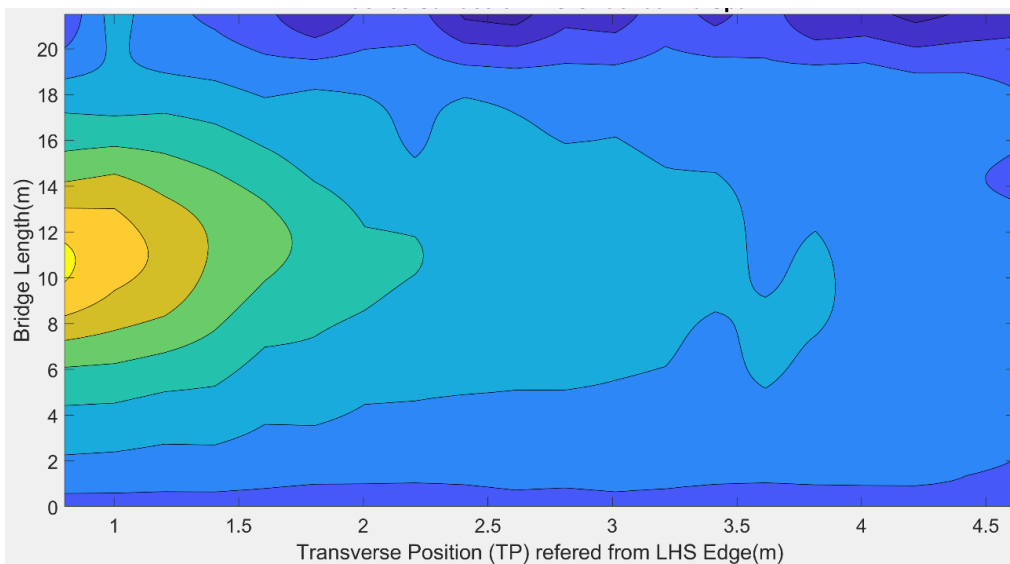


**Fig. 44** Influence surface calibrated for the left-side outer girder.

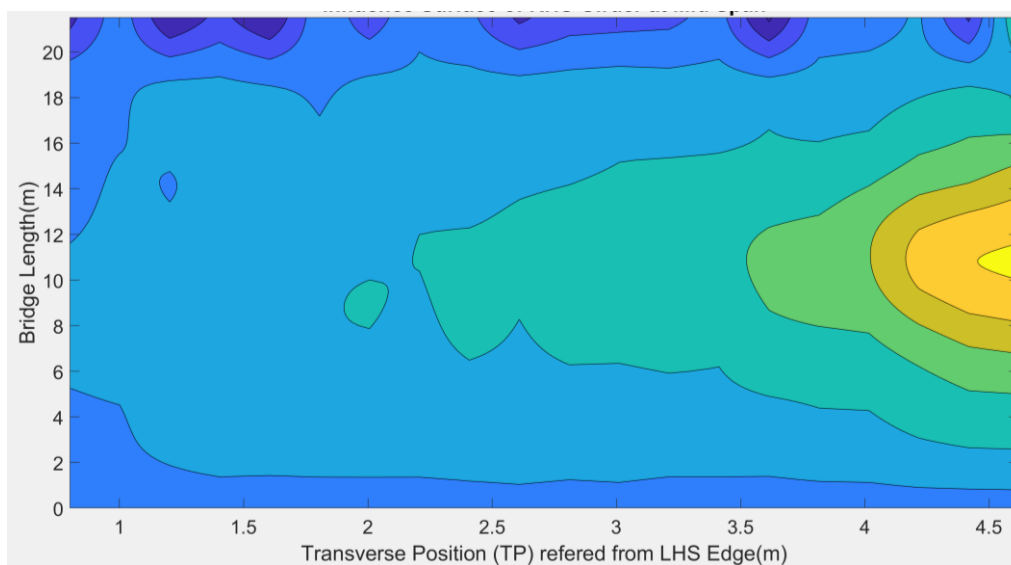


**Fig. 45** Influence surface calibrated for the right-side outer girder.

From Figure 44 and Figure 45, we can observe that the maximum value of the influence line occurs when the load passes exactly at the top of the measuring point. Therefore, when comparing the displacement responses measured at different times, the transverse position must be taken in to consideration.

To evaluate the transverse position identification algorithm, three random positions from the available measurements is chosen. TP-5 with 1.604m shift, TP-12 with 3.011m shift, and TP-18 with 4.217m shift. Accordingly, the error function versus transverse position plot for each shift cases are presented in Figure 46 to 48.

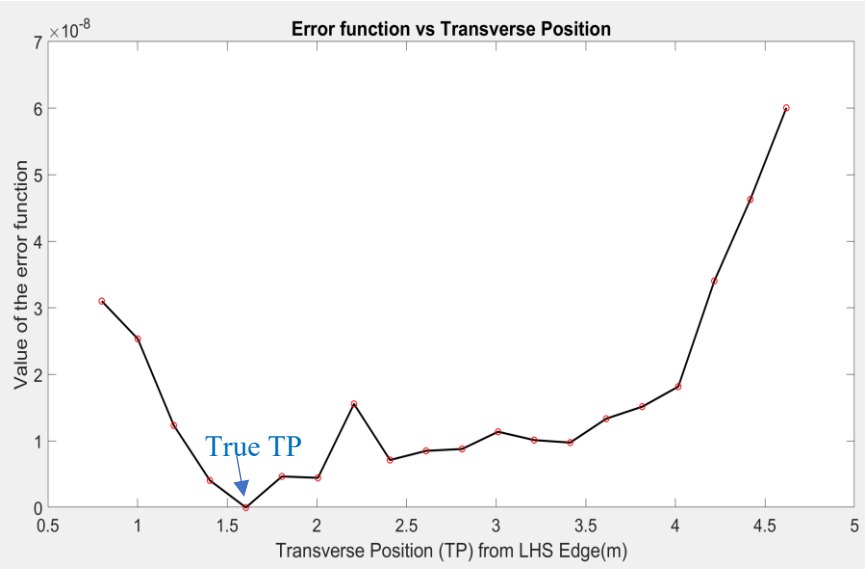


**Fig. 46** True transverse position identified at 1.604m shifted from reference point

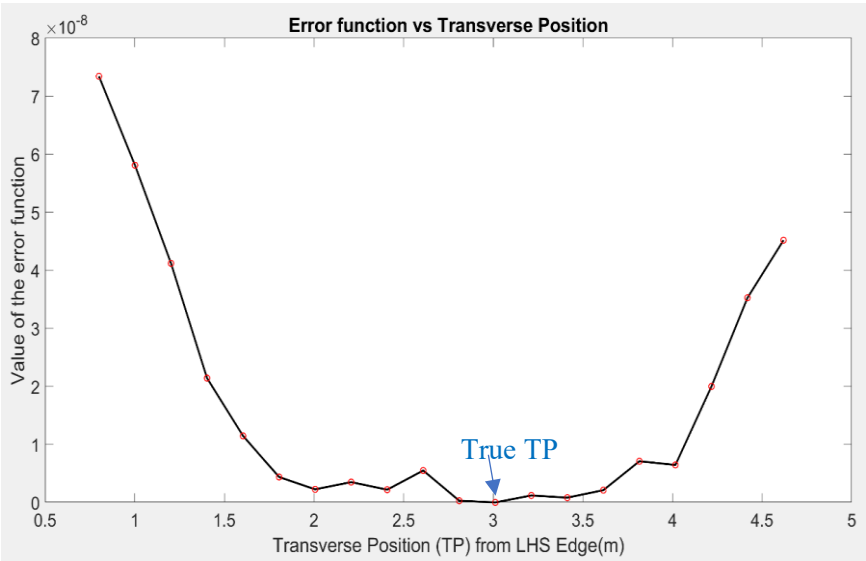


**Fig. 47** True transverse position identified at 3.011m shifted from reference point



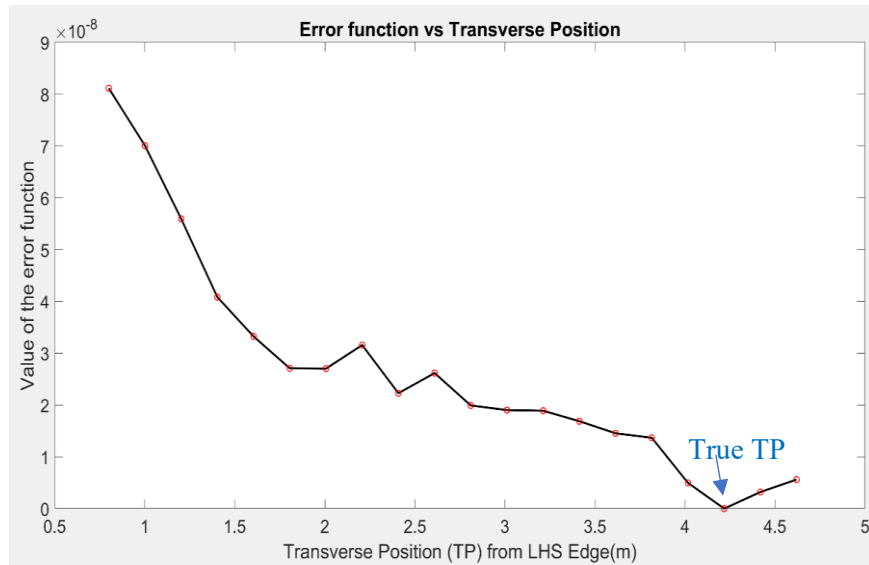


**Fig. 48** True transverse position identified at 4.217m shifted from reference point

## 7.4 Damage Identification

Damage location identification is conducted considering the sensor distribution presented in Figure 49. The result of analyzed scenarios with the M-DBI method, FE-MSE method and their integration is discussed here.

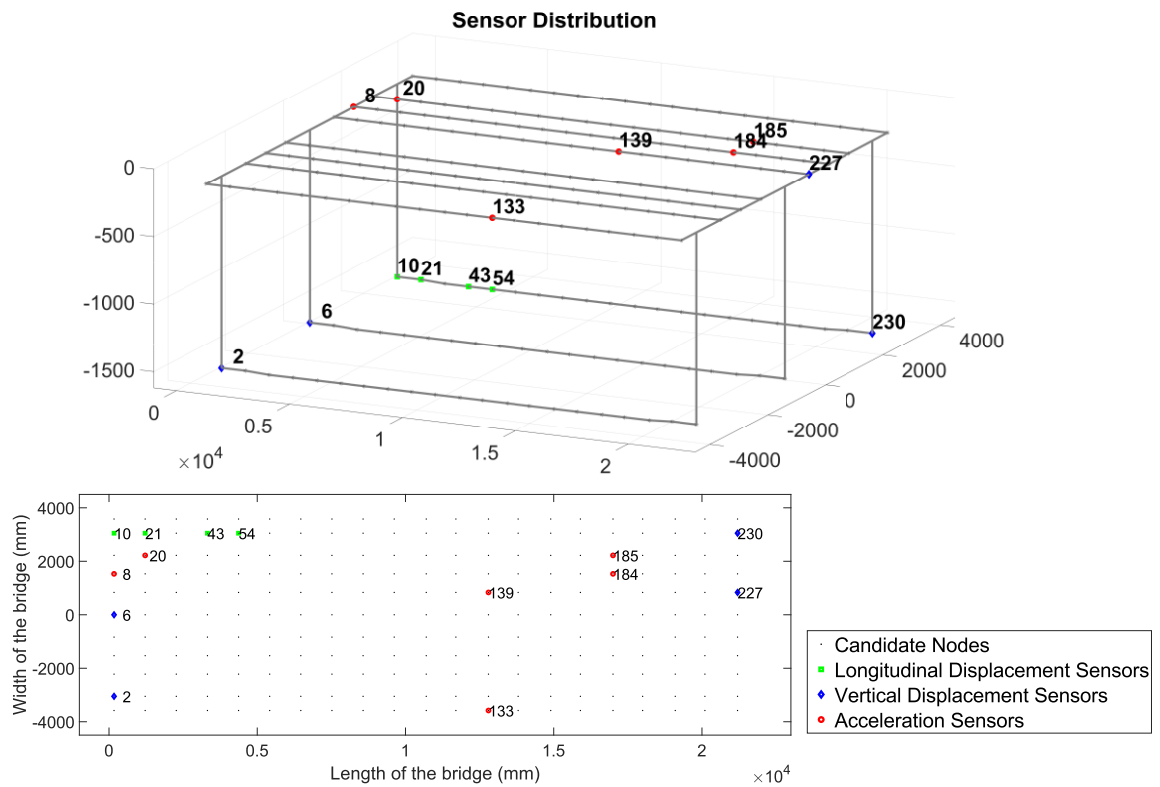


**Fig. 49** Sensor distribution under the target bridge a) 3D view b) Top view

#### 7.4.1 Case-1

In the first case, damage in the first panel of the slab with the damage type of D1 is considered. The damage occurs on the same lane of the moving axel load close to the bridge entrance point. In the Figure 50, the damage index cumulated from each sensor's estimated result is shown for both the DBI method and the modified M-DBI method. In both methods, the actual position of the simulated damage is illustrated with the vertical dashed lines. The horizontal dashed line represents a 10% threshold of the maximum value as a base for identifying the damaged location. In the DBI method the damage location identification has been affected by the displacement response behavior changes due to dynamic excitation of the bridge. Even though, the actual damaged section is identified, the higher DBI amplitude observed on other positions of the bridge created a flawed damage locations beyond the actual damaged region. On the other hand, the modified DBI method minimized the effect of measurement noise due to the displacement response behavior change beyond the damaged section by introducing the strain-based normalizer and considering the transverse position of the vehicle. As a result, the actual damage location is clearly identified.

The individual sensor's damage index estimation with both methods is shown in Figure 51 and 52. Similarly, 10% of the maximum cumulative value is used as a threshold to keep consistency on evaluating the individual sensors.

The DBI method identifies the damage location with some noise still appearing outside of the damage range when sensors only at the bridge entrance are evaluated individually. But the sensors at the bridge exit side show an equal magnitude of damage index which might mislead the identification process.

For the case of modified DBI method, the identification accuracy increases when the sensor individual evaluation is conducted. For the sensors located at the bridge exit side, even though the true position of damage is not identified, unlike the DBI method the magnitude of damage index is lower than the threshold value providing no misleading information on the identification of the actual damage position. As a result, the uncertainty with the damage location can be reduced.

Furthermore, we can observe from Figure 51 and 52 that the sensors located in the bridge entrance side have good identification than the sensors on the bridge exit side. Hence using measurement data from sensors at the bridge entrance side is sufficient for the proposed technique.

Bridge condition assessment with M-DBI alone does not provide full information about the actual damaged part and location. The information we get is generally along the longitudinal section of the bridge in the direction of the moving load crossing the bridge. Information regarding the trasversal location, especially the actual damage component is crucial.

The modal strain energy-based damage identification technique provides elemental level damage identification which will be a suitable technique to integrate with displacement influence line-based method. Figure 53 shows the damage position estimation using finite element based modal strain energy method (FE-MSE).

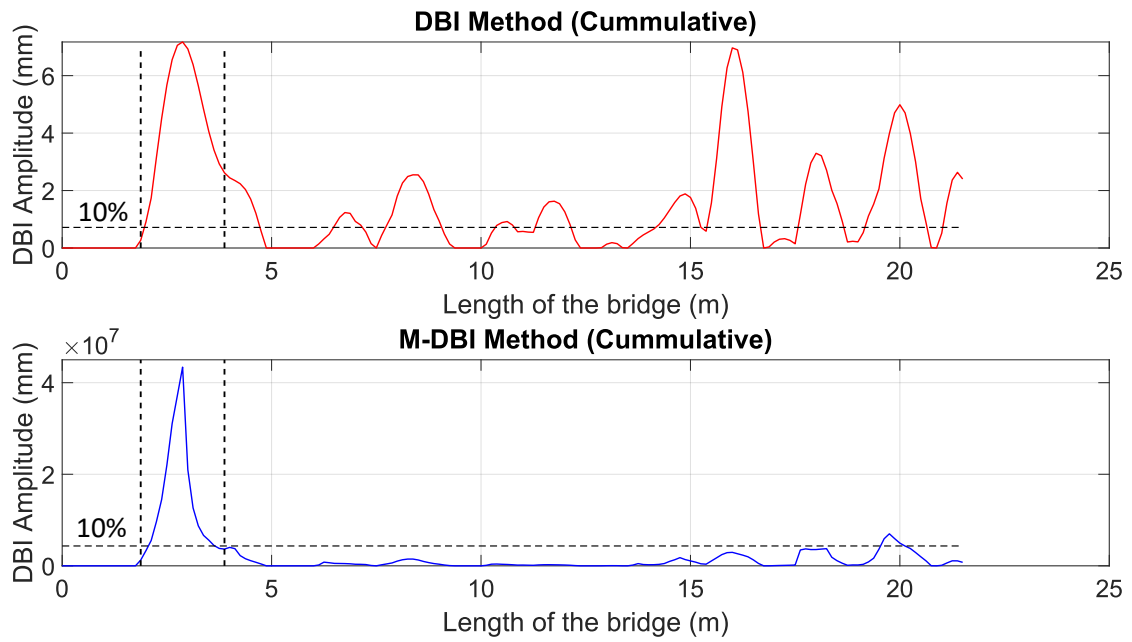


**Fig. 50** Case 1 damage location identification with DBI and M-DBI methods.

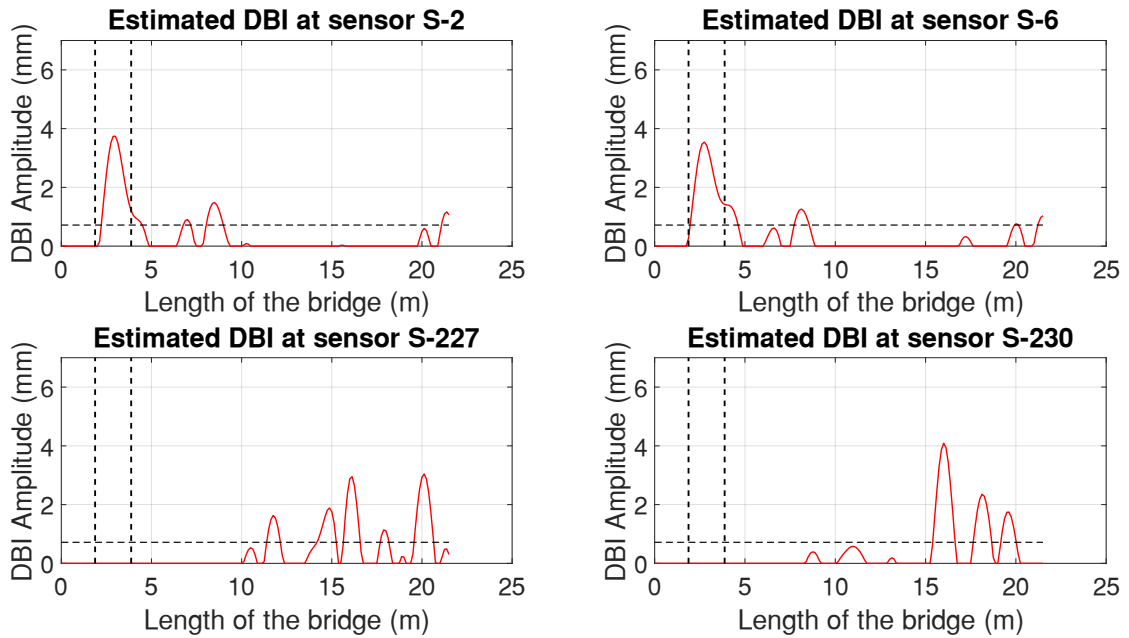


**Fig. 51** Case 1 individual sensors estimation of the damage index with DBI method.

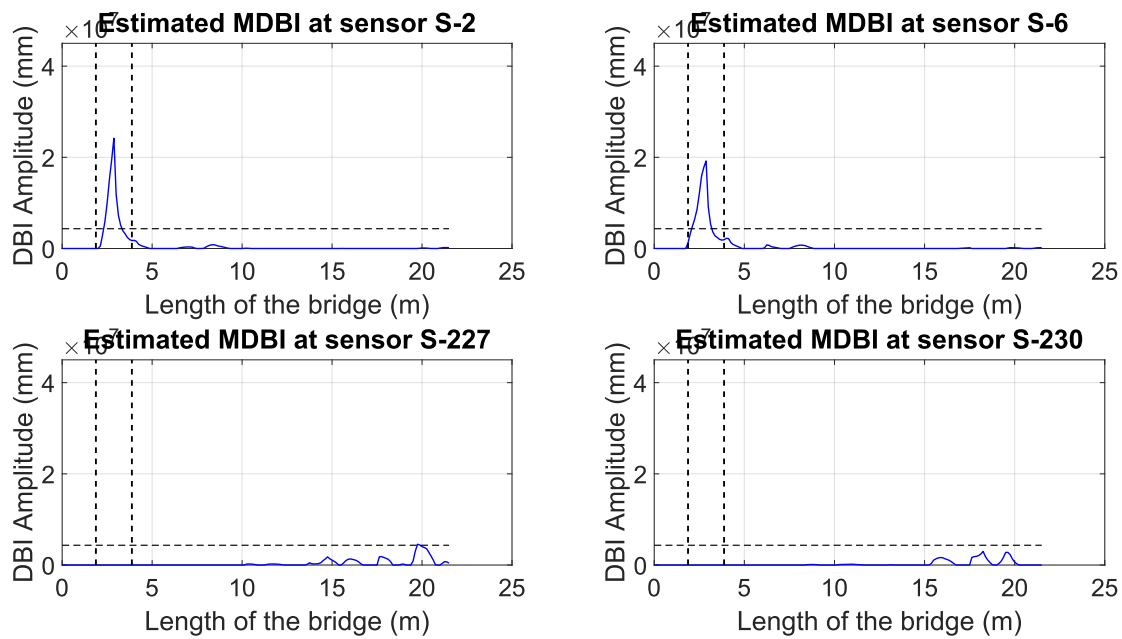


**Fig. 52** Case 1 individual sensors estimation of the damage index with modified DBI method

Elements in the FE-MSE estimation are designated in the global bases starting from bracing components up to the slab as shown in Figure 53. Each element is represented with a bar line in the graph. Lines at 60, 212, 343 and 474 are indicators of borders separating elements of one part from other. Hence, the actual elements in the part can be identified by subtracting the immediate border value from the global number of the required element.

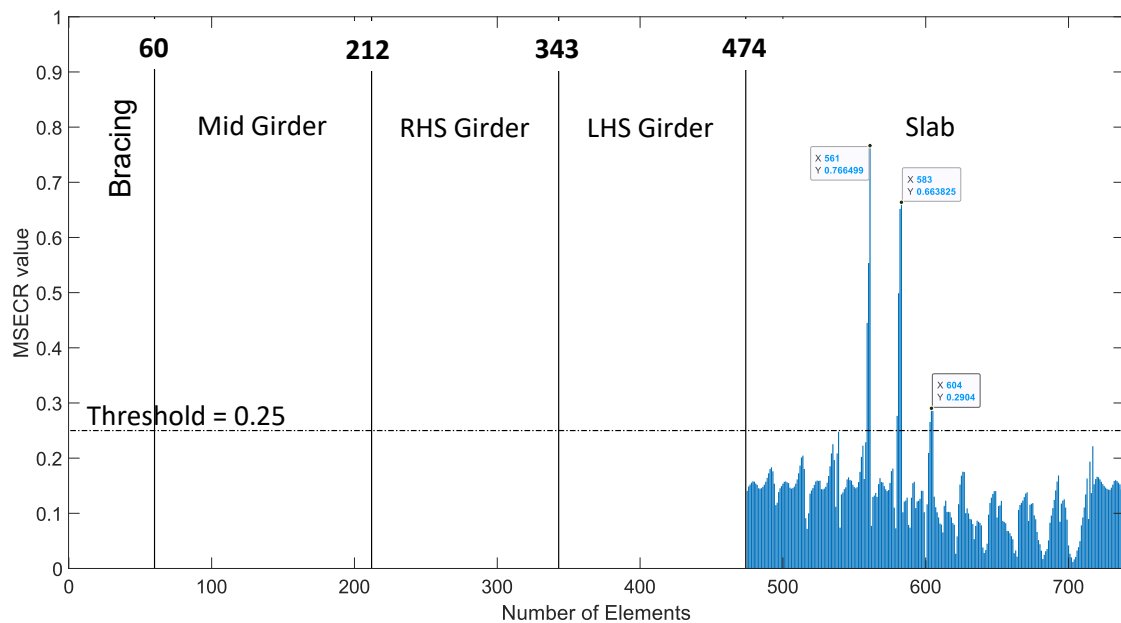


**Fig. 53** Case 1 identified damaged elements using FE-MSE method

Result from FE-MSE analysis indicate that elements in the slab part are estimated as damaged elements. Three cluster elements with global numbering of 561, 583, and 604 are estimated as damage. The actual element numbers in the slab part can be found by subtracting 474, the border line between LHS girder and Slab. Hence the actual damaged elements in the slab part will be 87, 109 and 130. Since the identified elements are a cluster of two to three elements.

The FE-MSE estimation as shown on Figure 54 c) have located the actual damaged part of the bridge and furthermore it approximated the location of damaged elements. However, due to the use of simplified FE model of the real bridge, this approach provides the approximated condition assessment.

Integration of M-DBI method and FE-MSE method further narrow the uncertainty encountered in the damage location estimation. In addition user interactive condition assessment can be achieved with better visualization of the damage location.

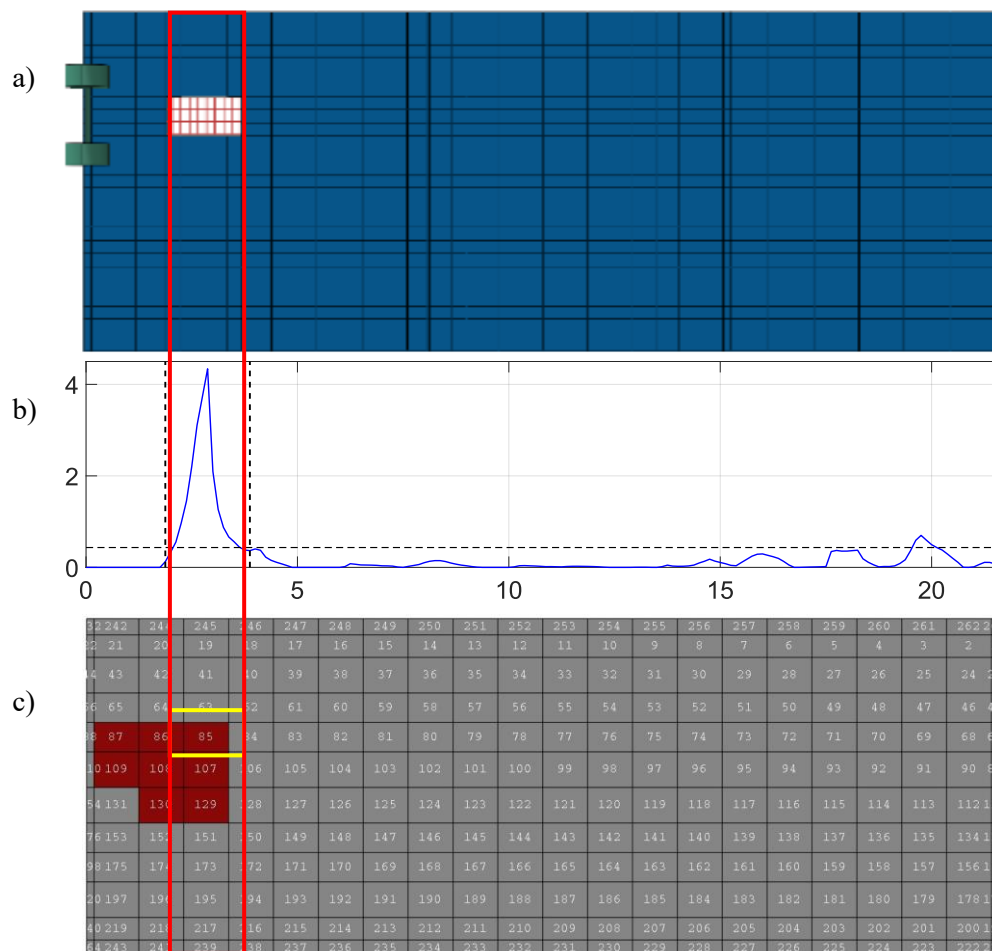


**Fig. 54:** Integrated damage location identification for case 1. a) actual simulated damage, b) M-DBI estimation c) FE-MSE estimation.

#### 7.4.2 Case – 2

The damage considered in case 2 is type D2 damage, which is about 24% of damage type D1 or 4.5% of the panel area. The position of simulated damage is located on the same lane with the moving axel load path around the mid span of the bridge. Like the first case, comparison between the cumulative and individual sensors' damage index estimation with DBI and modified DBI method from sensors located at the bridge entrance side have been illustrated from Figure 55 to 57 respectively.

The damage location identification from the DBI method estimated index provide several flowed results undermining identification of the actual damage location. In both the individual sensor level and cumulative level estimation several peaks passing the threshold limit provide misleading information about the actual locations of damage. The peak near to the actual damage is even higher in amplitude providing wrong information.

The M-DBI method on the other hand provided the information about the actual location of damage. Even though, the peak near to the actual damage location passes the threshold limit, yet the modified DBI magnifies the damaged section and reduced the magnitude for flawed sections than the DBI method. As a result, we can locate the damage along the longitudinal direction of the bridge with minimized uncertainty level.

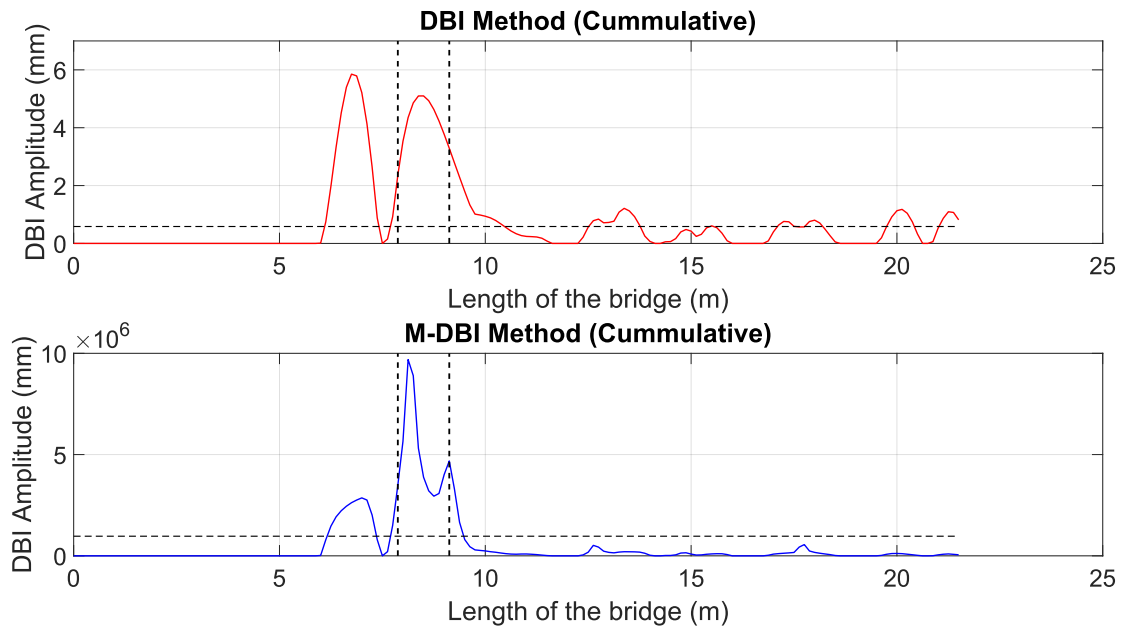


**Fig. 55** Case 2 damage location identification with DBI and MDBI methods

Transversal position of the damage can be estimated from the FE-MSE method. Elements passing the threshold limit are designated as damaged elements. Figure 58 illustrates the estimated damaged elements cluster. The peak of each damaged element cluster numbers are identified as 488, 509, 531, 597, 617, 638, 691, and 724. Since all the damage elements are in the slab region, subtracting 474 will result in local representation of each element on the slab part to identify the estimated positions. Hence, in Figure 59 c), the damaged elements of the slab part can be observed.

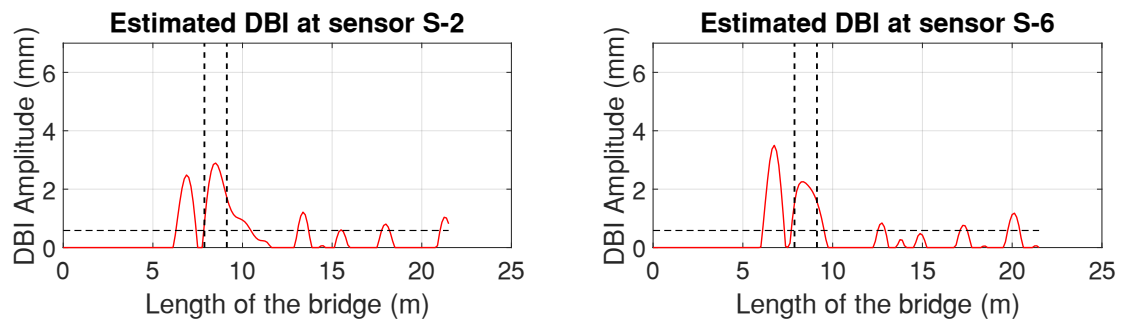


**Fig. 56** Case 2 individual sensors' estimated damage index for DBI method

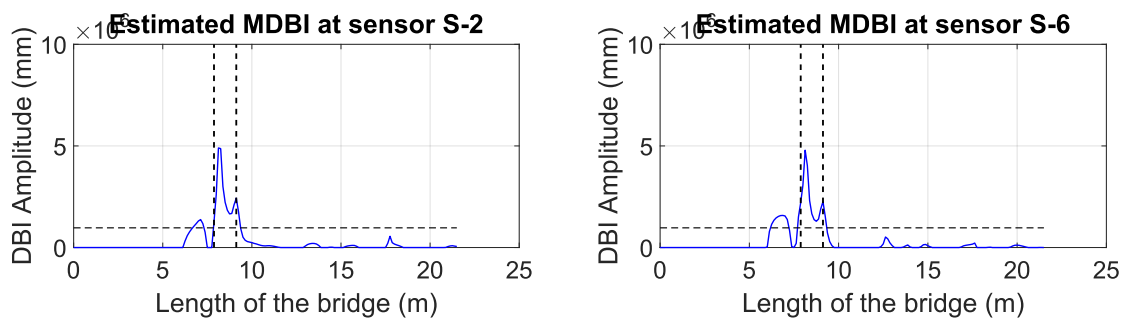


**Fig. 57** Case 2 individual sensors' estimated damage Index for MDBI method

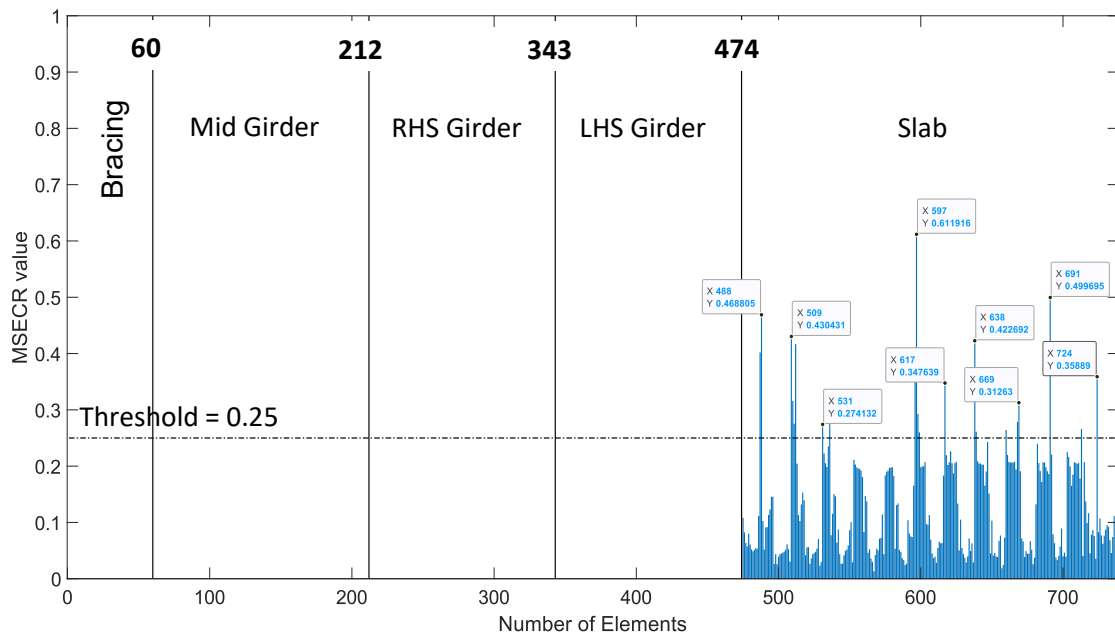


**Fig. 58** Case 2 identified damaged elements using FE-MSE method

Estimation of damage location in case two from the integrated multi approach system provides more accurate result in identifying the actual damaged part and its position. Figure 59 shows visualization of the information provided from the multiple approach where the uncertainty is greatly reduced in locating the actual position.

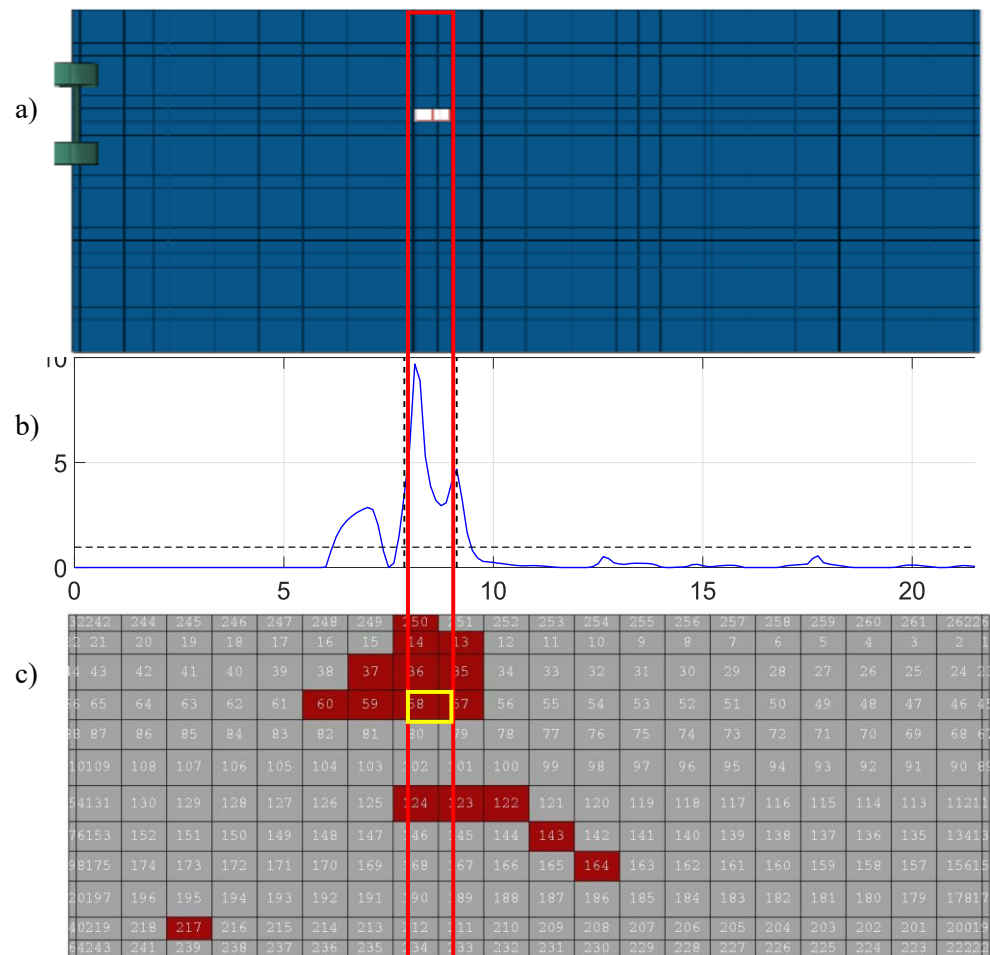


**Fig. 59** Integrated damage location identification for case 2. a) actual simulated damage, b) M-DBI estimation c) FE-MSE estimation.

The integration of MDBI and FE-MSE methods narrows down the estimation of damaged elements close to the actual damage position.

### 7.4.3 Case – 3

The simulate damage in case 3 is type D1 located on the opposite lane of the moving load path near to the bridge entrance. Figure 60 illustrates the cumulative estimated damage index from sensor number 2 and 6. The individual estimated value of each sensor is also presented on the Figure 61 and 62 for DBI method and M-DBI method respectively.



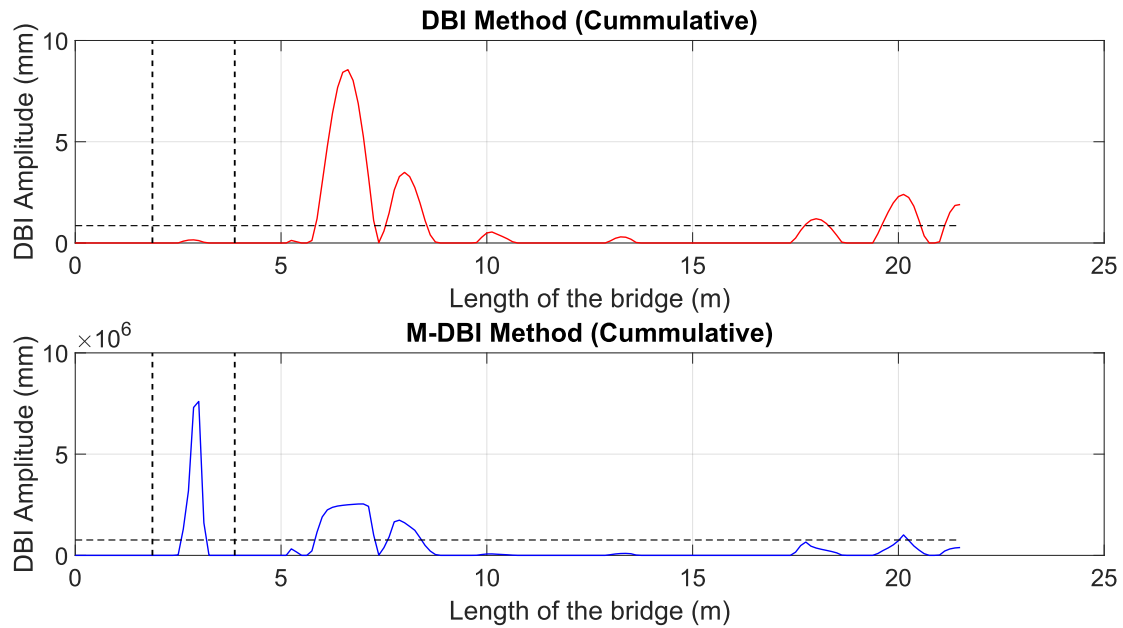


**Fig. 60** Case 3 damage location identification with DBI and MDBI methods

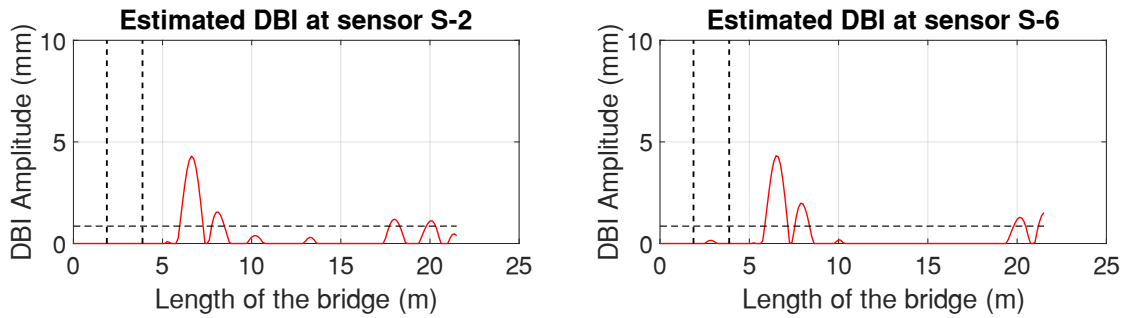


**Fig. 61** Case 3 individual sensors' estimated damage index for DBI method

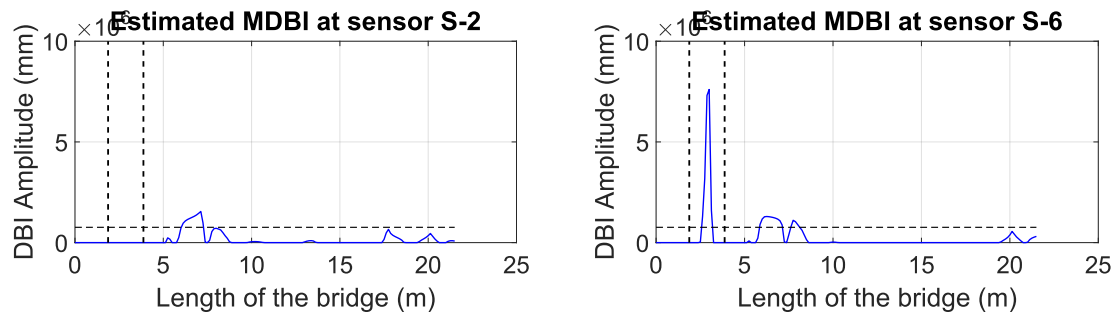


**Fig. 62** Case 3 individual sensors' estimated damage index for MDBI method

We can observe from both individual level and cumulative level estimation in DBI method that the actual damage location is not identified. In fact, wrong position is estimated as damaged location. The modified M-DBI method, on the sensor number 6 and on cumulative level estimation provided the actual position of the damage. However, the two peaks passing the threshold out of the actual damaged region is observed creating some uncertainty.

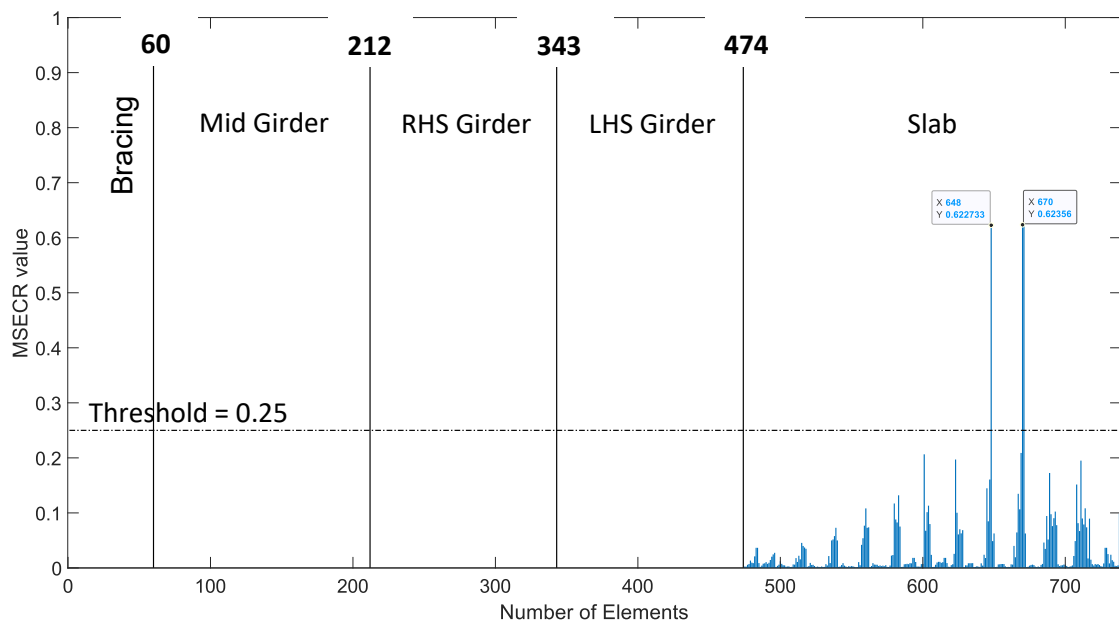


**Fig. 63** Case 3 identified damaged elements using FE-MSE method

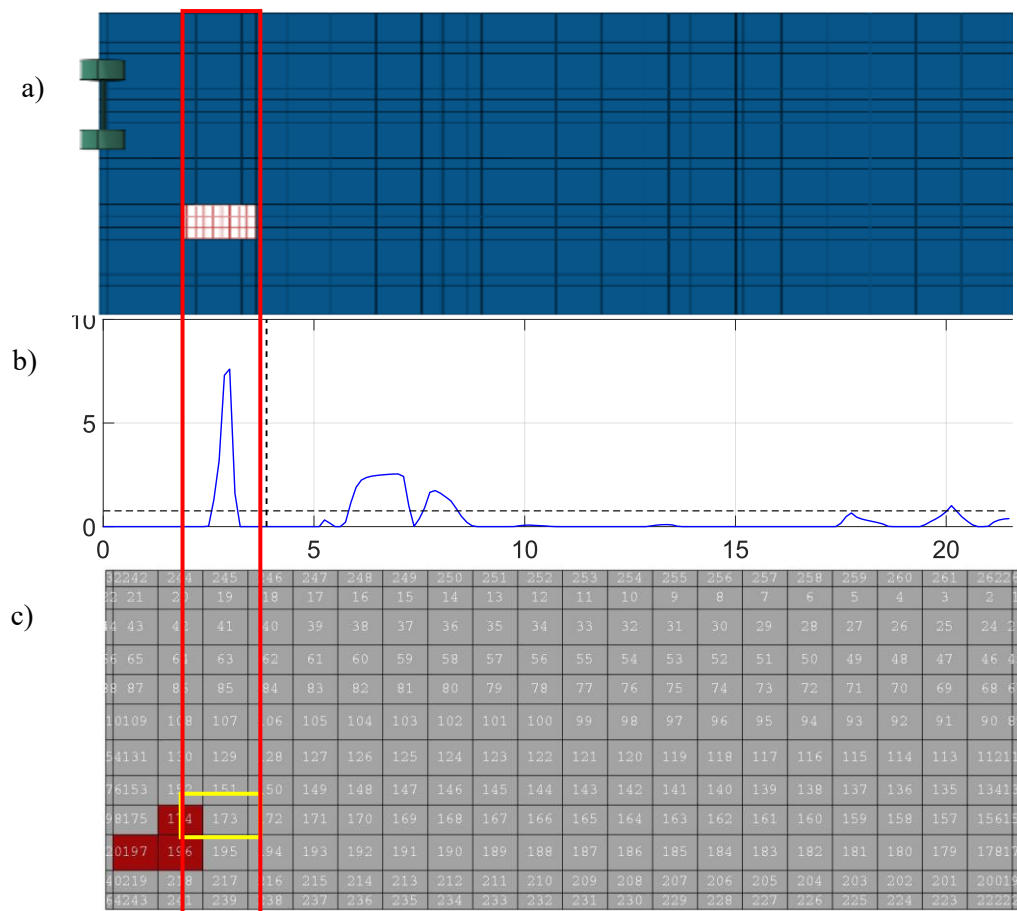


**Fig. 64** Integrated damage location identification for case 3. a) actual simulated damage, b) M-DBI estimation c) FE-MSE estimation.

FE-MSE estimation of case 3 damage identifies two clusters as damaged slab elements. The identified elements with global numbering are 648 and 670, equivalent representation in slab numbering of 174 and 196 respectively. Using the integrated results from the two techniques as shown in Figure 64 we can confirm the position of damage to its actual position.

#### 7.4.4 Case – 4

Multiple damage case is considered in this scenario. The locations of the damages are of different in sizes and types. A combination of damage type D1 and type D2 is simulated. Damage type D1 is clearly identified on MDBI however the damage type D2 could not be identified when examining the cumulative or an individual sensors contribution. Even though, there are some flawed identified locations, sensor #2 by DBI method have identified the location of the second damage.

The major reason observed in case of multiple damage, the displacement response behavior change by the larger damage undermines the effect of the second damage where the damage is smaller than the former.

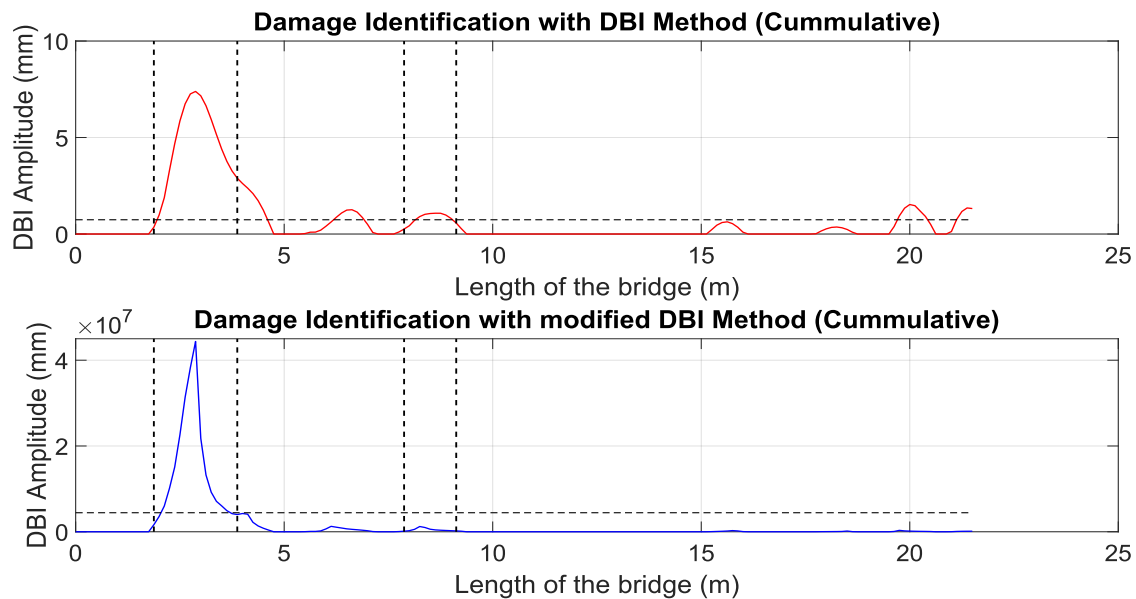


**Fig. 65** Case 4 damage location identification with DBI and MDBI methods

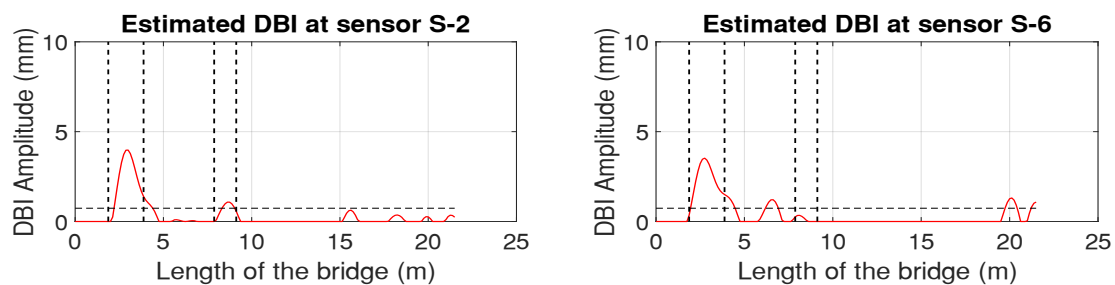


**Fig. 66** Case 4 individual sensors' estimated damage index for DBI method

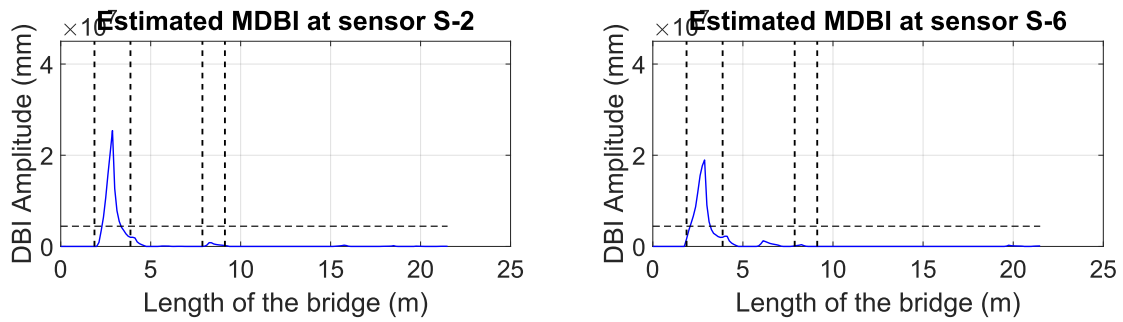


**Fig. 67** Case 4 individual sensors' estimated damage index for MDBI method

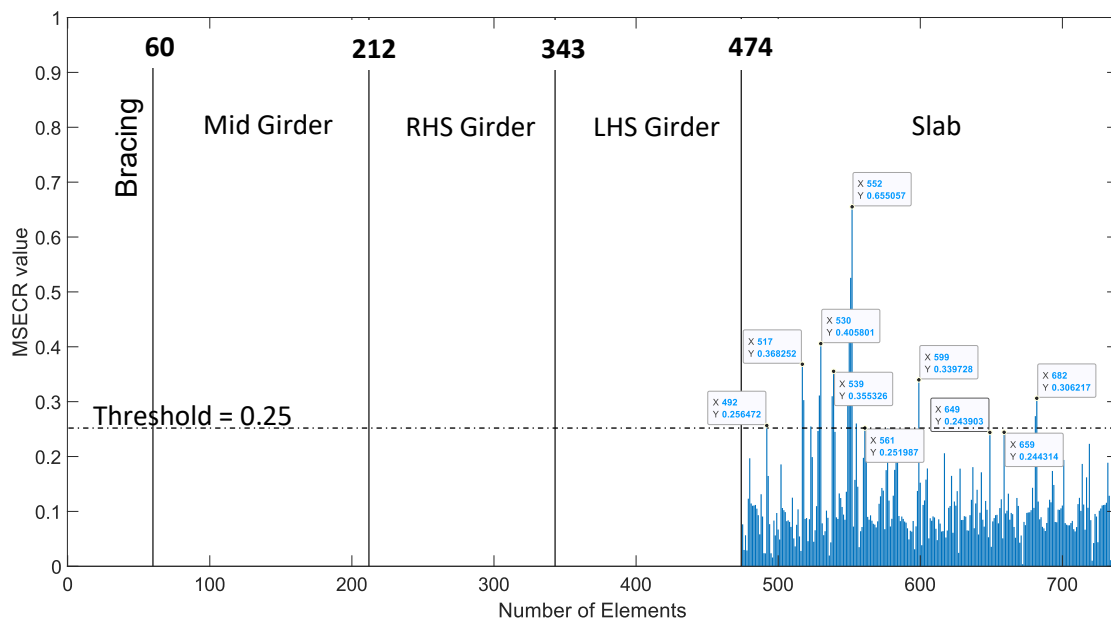


**Fig. 68** Case 4 identified damaged elements using FE-MSE method

FE-MSE estimation of case 4 shows several clusters of damaged elements. All damages are with in the range of slab part. Hence, the damaged part of the bridge is clearly identified. The global numbering of damaged elements are converted to local numbering of the slab part and shown on Figure 69 c). Even though the estimated damaged elements are distributed, there is a concentration of damaged elements around the actual simulated damages. Looking only on the MDBI estimation or FE-MSE estimation it might not be clear information. However, integrating information from both techniques, the damage location identification can be narrowed to the actual position.

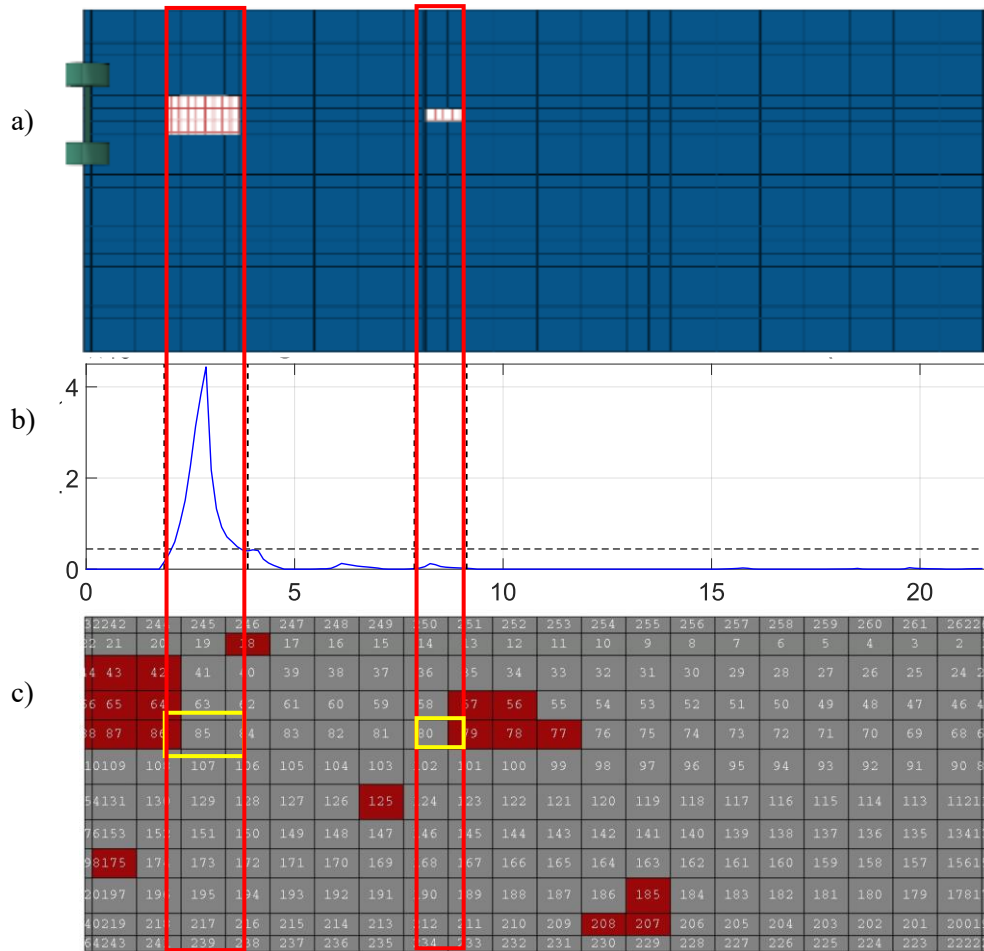


**Fig. 69** Integrated damage location identification for case 4. a) actual simulated damage, b) M-DBI estimation c) FE-MSE estimation.

#### 7.4.5 Case – 5

In case 5, multiple damage scenario is studied, where the damages are located at opposite lane of the moving load path. In this case also the combination of damage type D1 and type D2 are evaluated. Unlike case 4, where the larger damage – type D1 – occurs before the smaller damage – type D2, the occurrence is reversed. It is observed from Figure 70 that both methods identify the location of the smaller damage relatively better than the case where the larger damage occurs before the smaller damage. However, the magnitude of the estimated index at the damaged location is low, which makes it difficult to clearly identify the exact positions.

For individual sensor estimation, the DBI method on Fig 71 shows, sensors #2 and #6 relatively identify the location of the first damage but due to the magnitude is similar with other flawed location its hard to exactly tell the real damaged position. While the M-DBI method, sensor # 6 show relatively better estimation, but still the effect of the noise is not eliminated to the satisfying level.

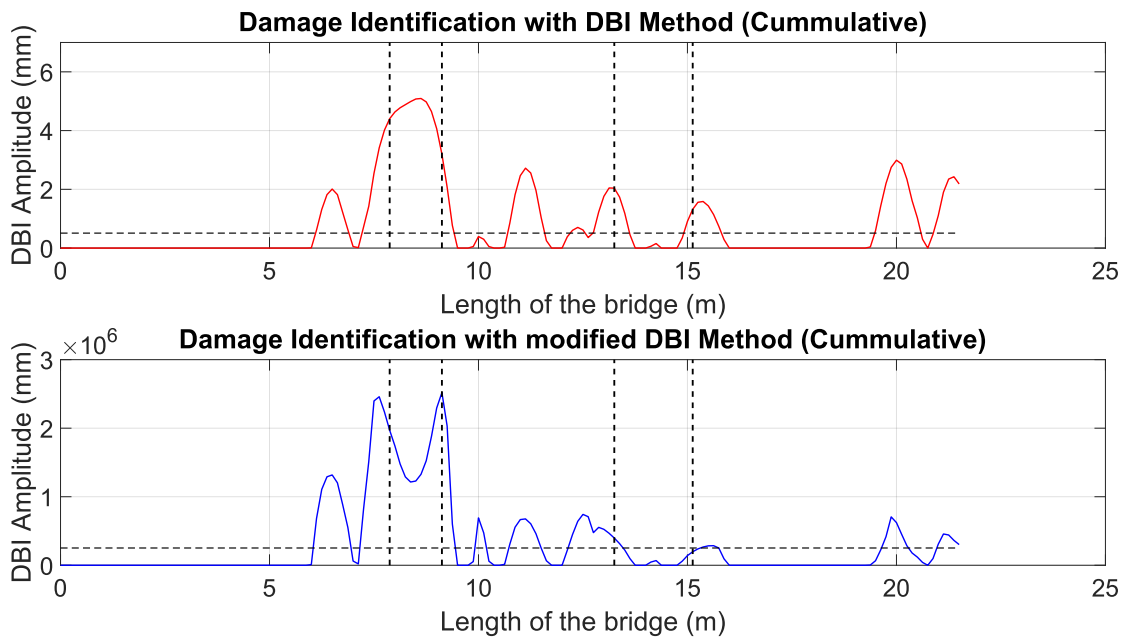


**Fig. 70** Case 5 damage location identification with DBI and MDBI methods

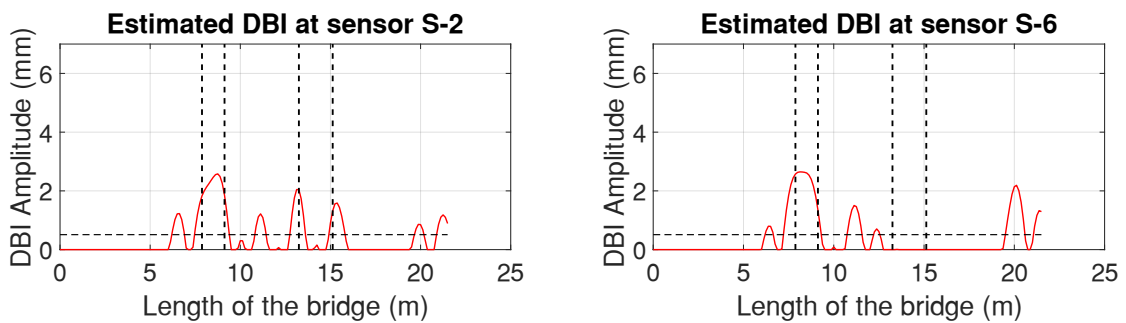


**Fig. 71** Case 5 individual sensors' estimated damage index for DBI method

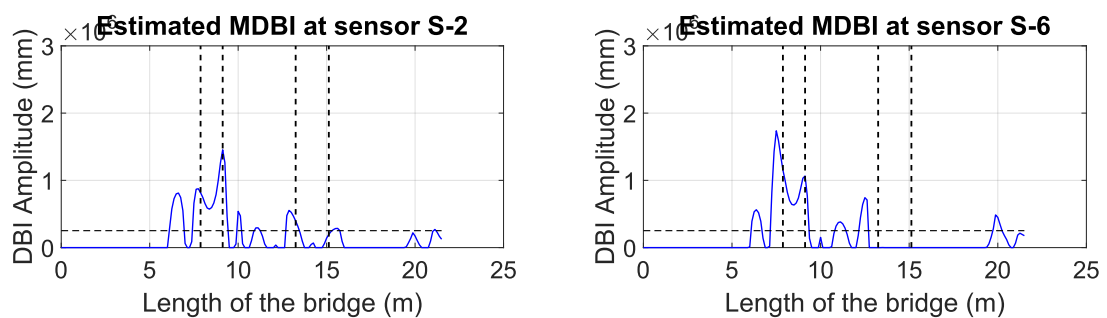


**Fig. 72** Case 5 individual sensors' estimated damage index for MDBI method

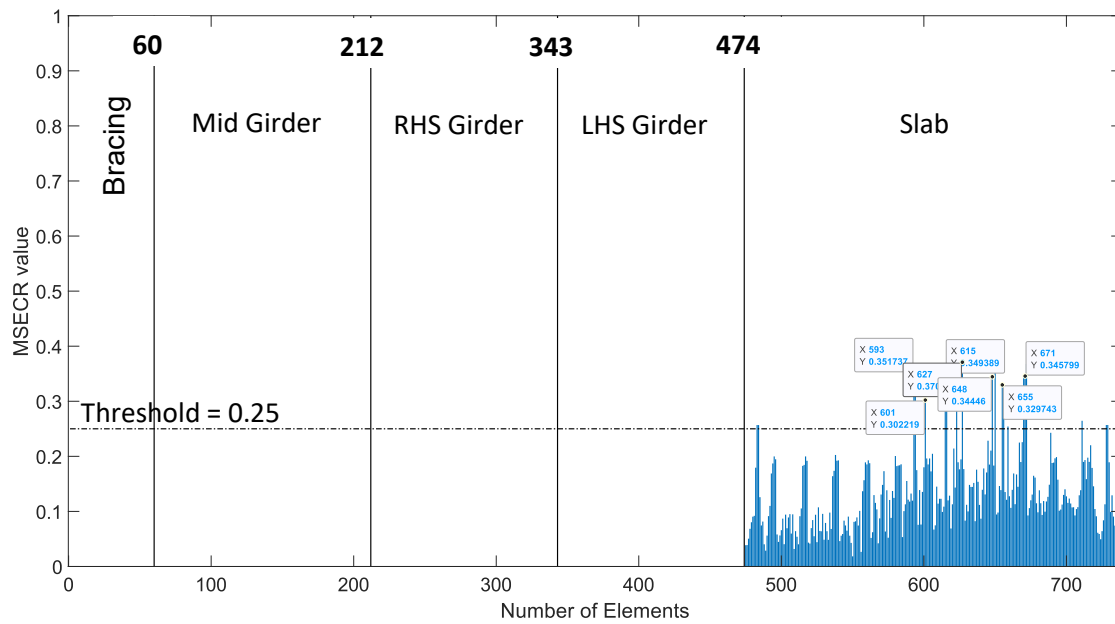


**Fig. 73** Case 5 identified damaged elements using FE-MSE method

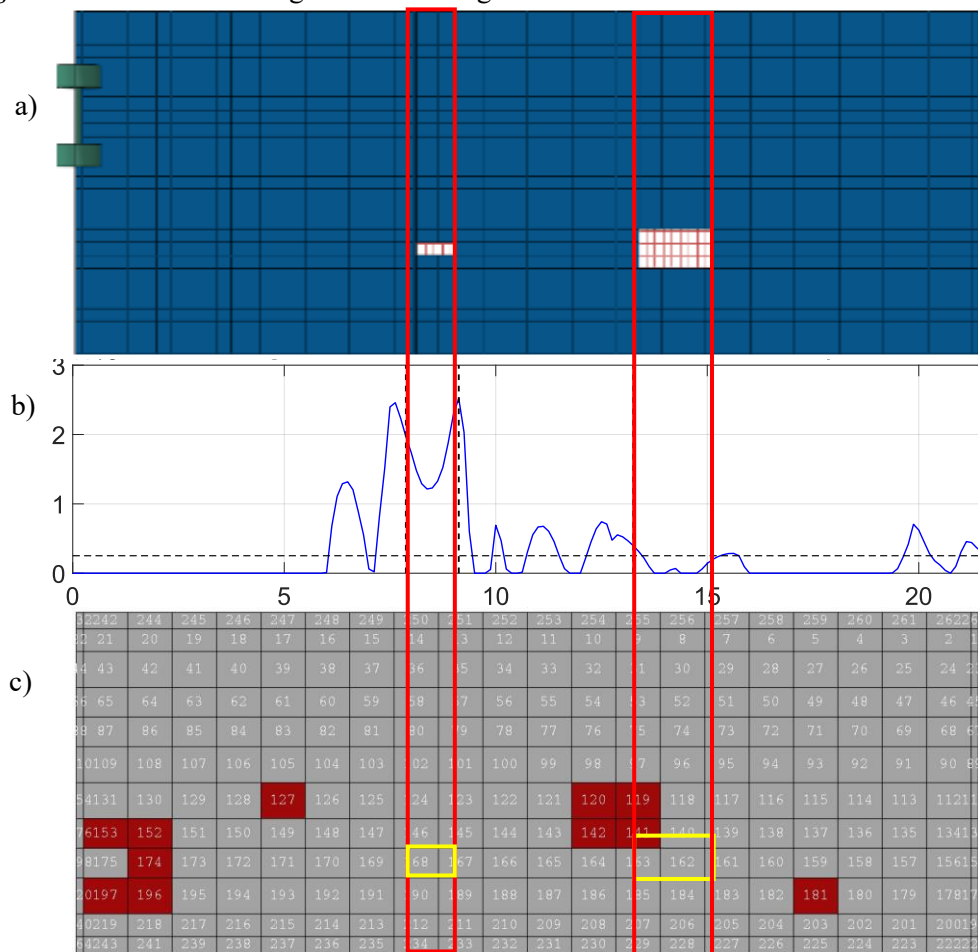


**Fig. 74** Integrated damage location identification for case 5. a) actual simulated damage, b) M-DBI estimation c) FE-MSE estimation.

The FE-MSE estimation provides identified damaged elements. The estimated location is distributed along the slab where the actual damaged elements are approximated at D1 type damage position. Even though the D2 type damage position is identified in MDBI method, it is not identified in FE-MSE estimation. Hence, with the use of integrated mode, there will be a high probability of damage along the transverse direction along the D2 damage. This suggests further investigation to reduce the uncertainty.

#### 7.4.6 Case – 6

The effect of multiple damage at the same position but in different lanes is examined in case 6. It is the combination of case 1 and case 3 occurring together. Due to the added effect from both damages the magnitude of the estimated MDBI index in both cases increased compared to the case one. Hence the location of damage for the DBI methods can also be identified from individual sensors #2 and #6 estimation show on Figure 75.

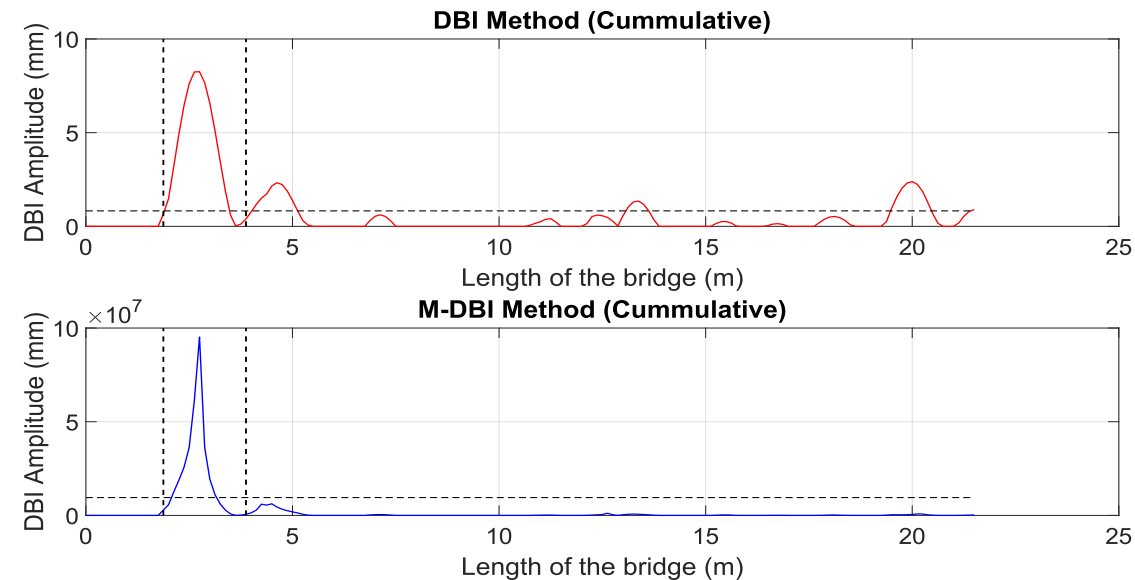


**Fig. 75** Case 6 damage location identification with DBI and MDBI methods

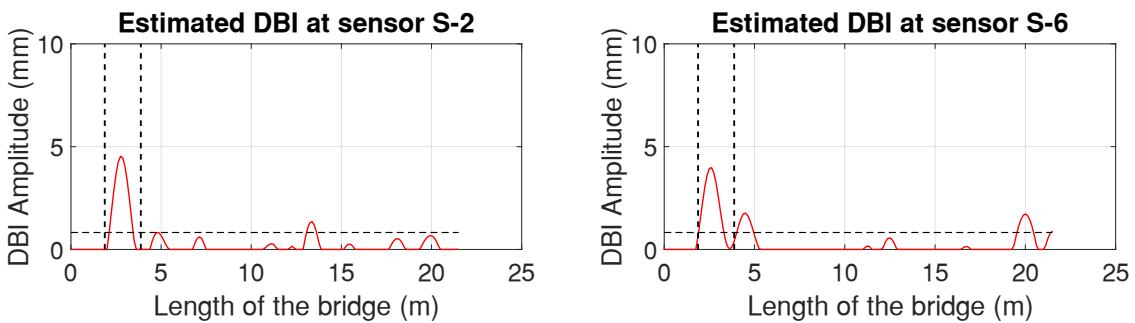


**Fig. 76** Case 6 individual sensors' estimated damage index for DBI method



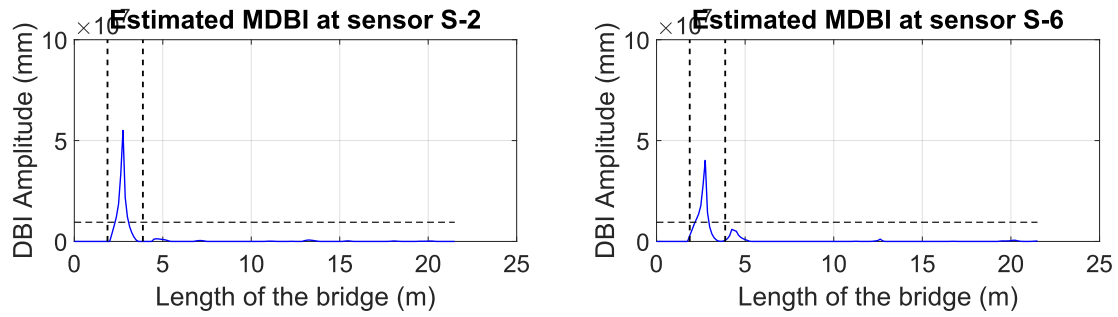


**Fig. 77** Case 6 individual sensors' estimated damage index for MDBI method

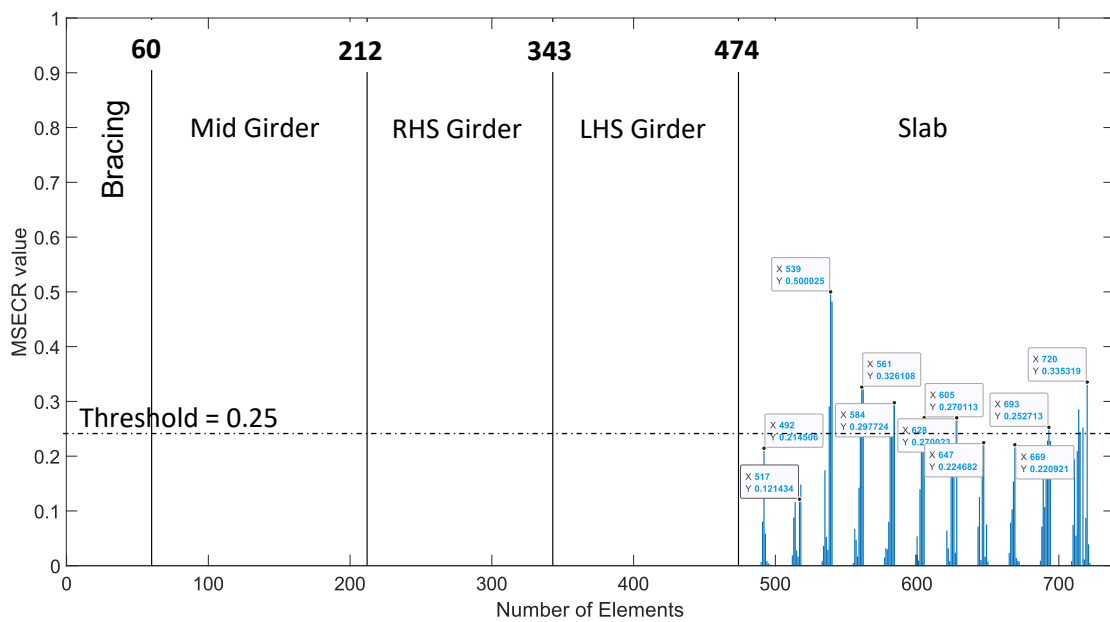


**Fig. 78** Case 6 identified damaged elements using FE-MSE method

The estimated damage elements in FE-MSE are also illustrated in Figure 78. The damaged elements are in the slab. The distributed elements around the cluster can be visualized in Figure 79 c). The estimated damaged elements are spread around the actual positions in both lanes. Hence this also emphasizes the importance of using FE-MSE in identifying the transversal position of the actual damaged position.

Furthermore, the integration of the M-DBI and MSE method narrows the estimated damage to the actual damage positions. Hence, enabling decision makers to minimize the uncertainty in their decision making.

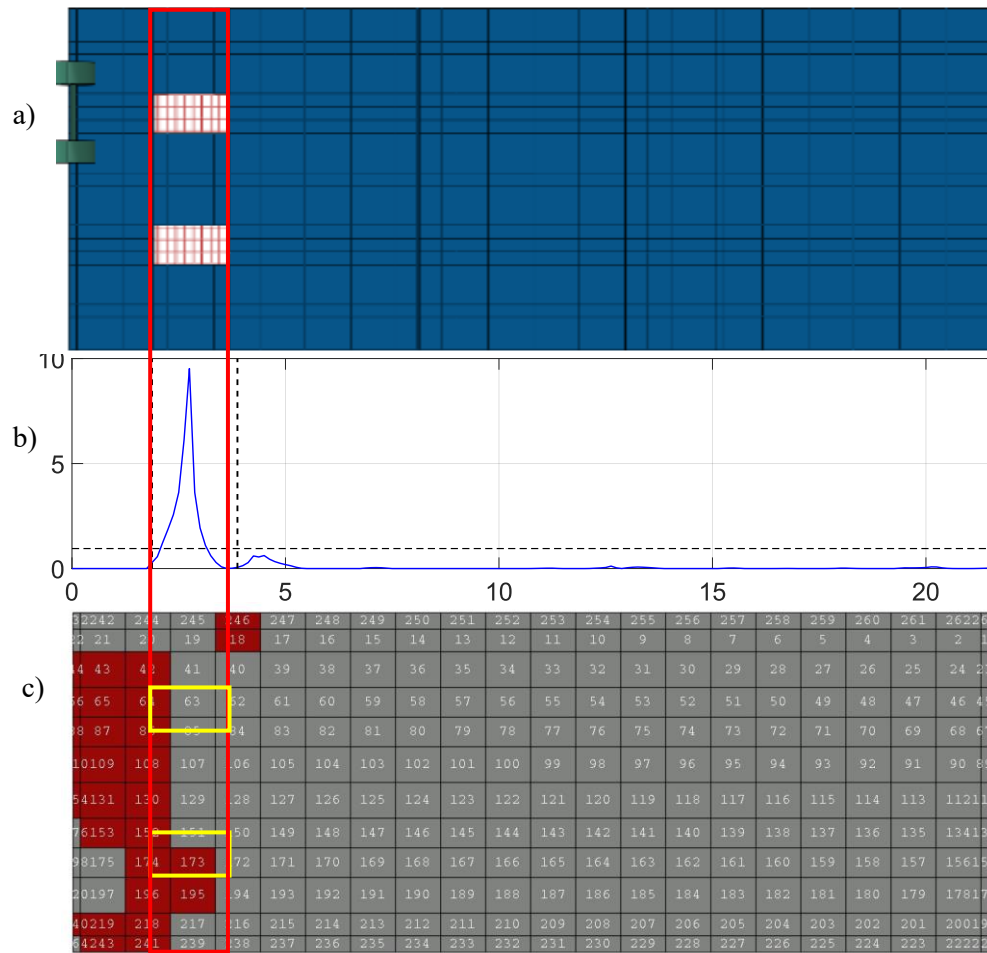


**Fig. 79** Integrated damage location identification for case 6. a) actual simulated damage, b) M-DBI estimation c) FE-MSE estimation.

#### 7.4.7 Case – 7

Damage location analysis with type D3, half the damage size of type D2, is examined in case 7. The position of damage is similar to that of case 1 but the magnitude of damage is reduced. The analysis with MDBI in Figure 80 shows the damage location is identified in the longitudinal direction. However, the extent of damage is somehow extended beyond the range of damage.

Estimated damaged elements with FE-MSE are identified with in the slab part. Figure 84 illustrated the damaged elements are approximately identified around the actual damage position.

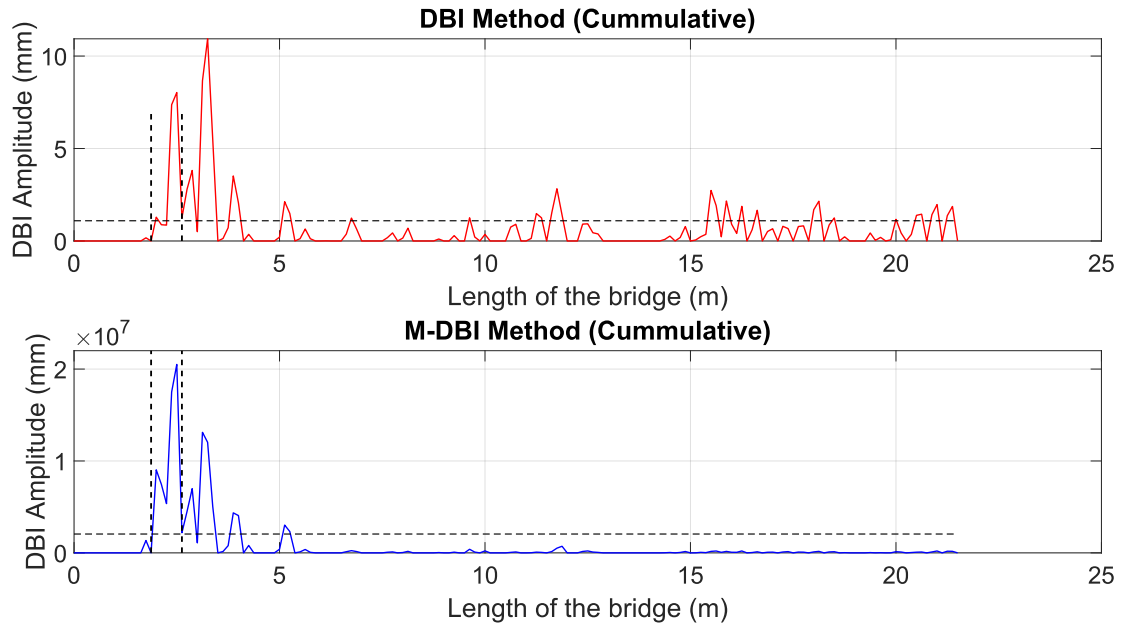


**Fig. 80** Case 7 damage location identification with DBI and MDBI methods

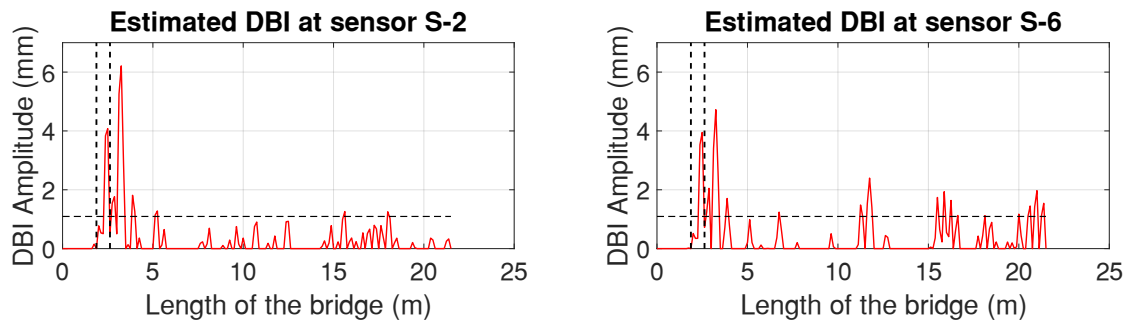


**Fig. 81** Case 7 individual sensors' estimated damage index for DBI method

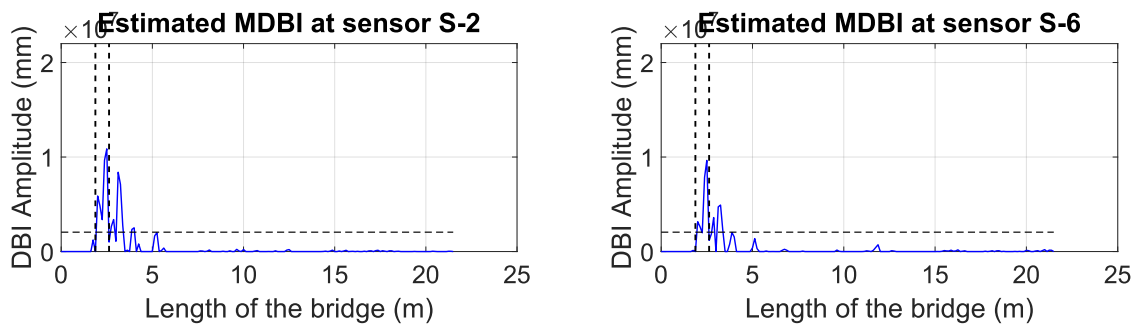


**Fig. 82** Case 7 individual sensors' estimated damage index for MDBI method

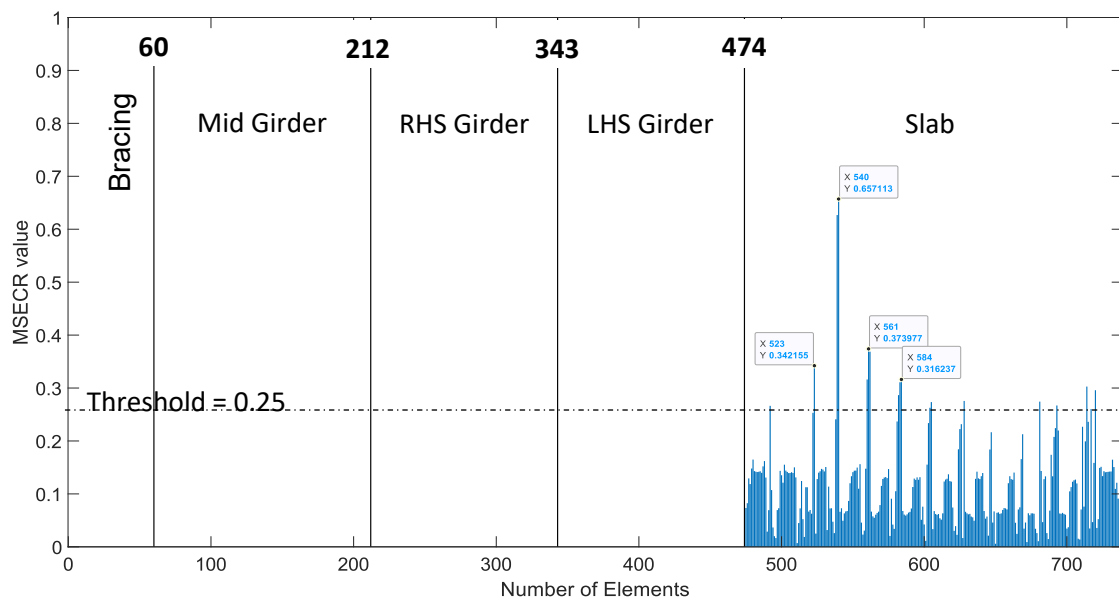


**Fig. 83** Case 7 identified damaged elements using FE-MSE method

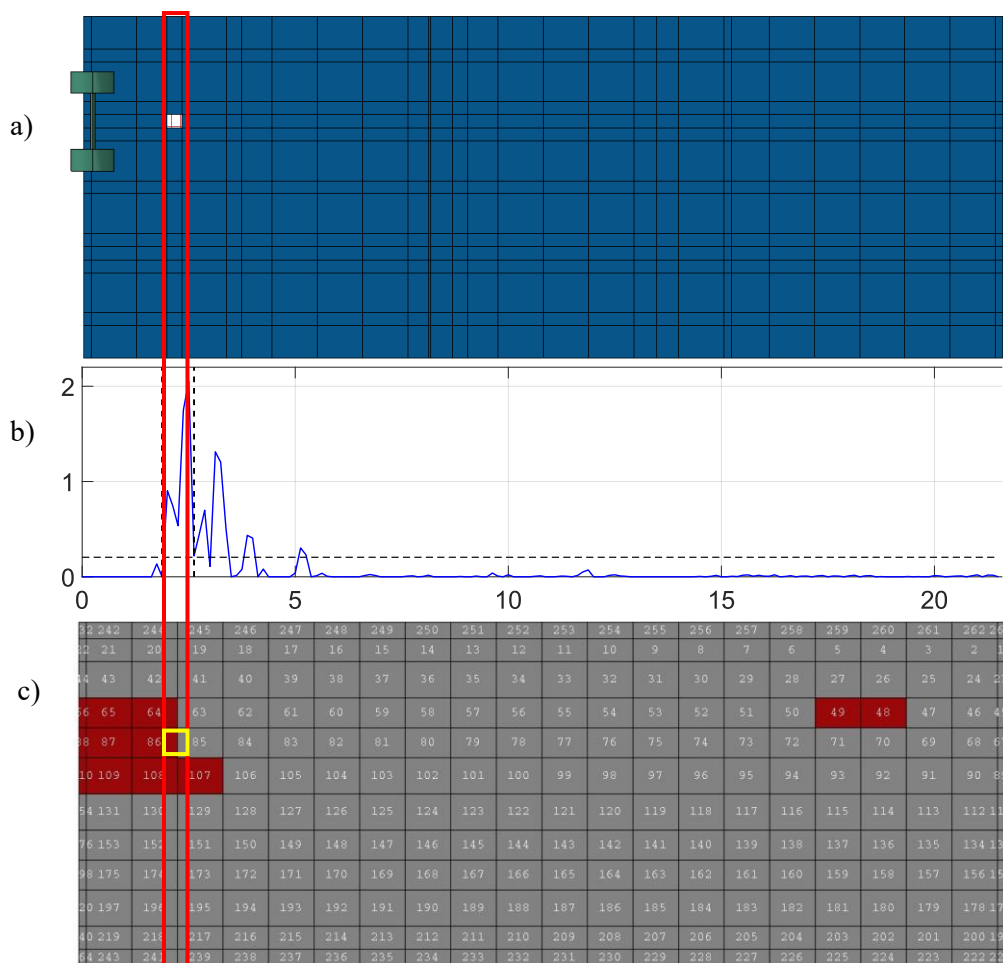


**Fig. 84** Integrated damage location identification for case 7. a) actual simulated damage, b) M-DBI estimation c) FE-MSE estimation.

#### 7.4.8 Case – 8

The case simulated in this scenario demonstrates the application of these approach on analysis of any structural damages. In this particular case a middle girder damage is simulated with 25% stiffness reduction. As shown in the Figure 85, the damaged position is located at the first quarter of the middle girder span. With the MDBI estimation. The actual damage location is identified longitudinally.

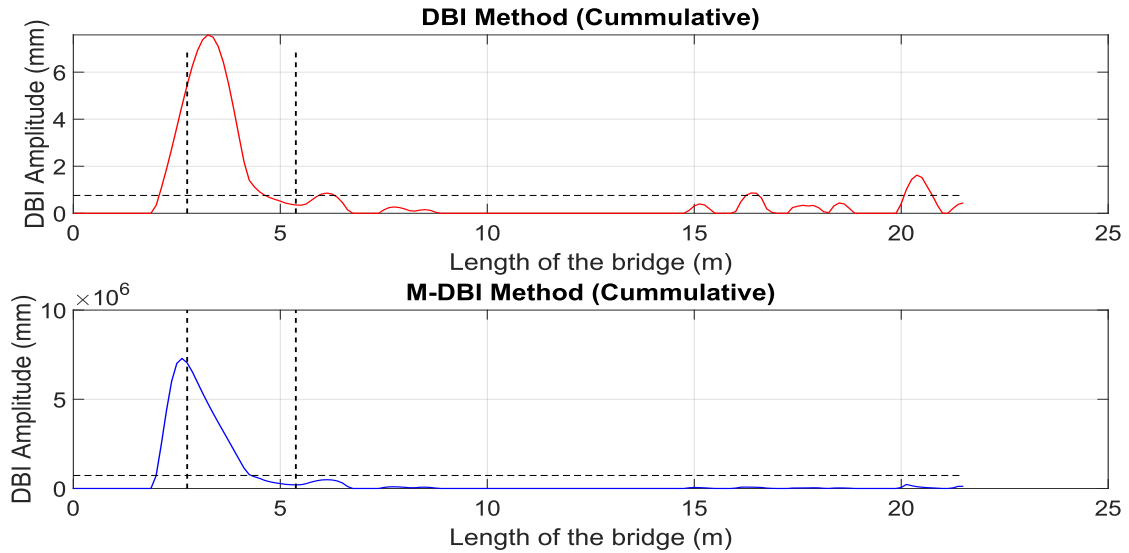


**Fig. 85** Case 8 damage location identification with DBI and MDBI methods

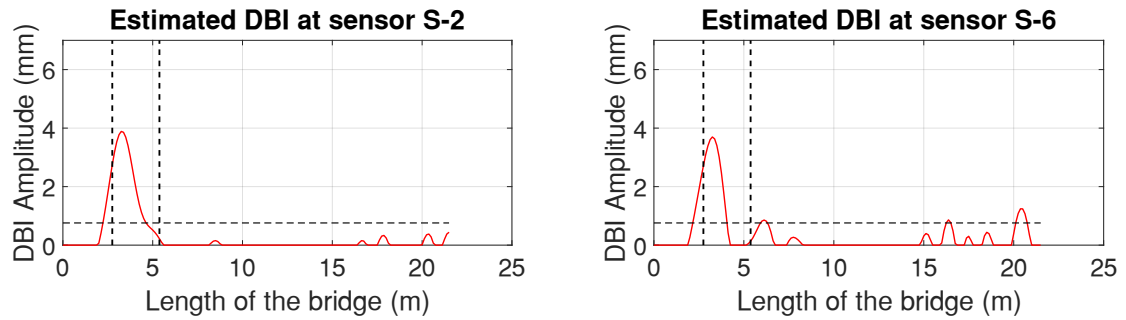


**Fig. 86** Case 8 individual sensors' estimated damage index for DBI method

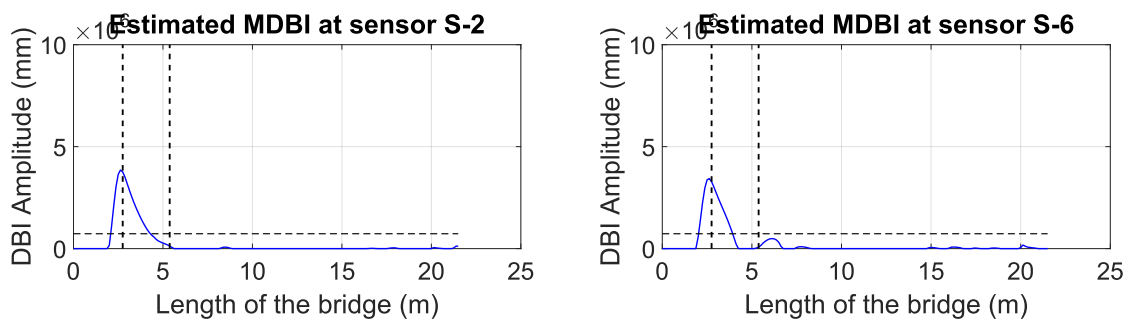


**Fig. 87** Case 8 individual sensors' estimated damage index for MDBI method

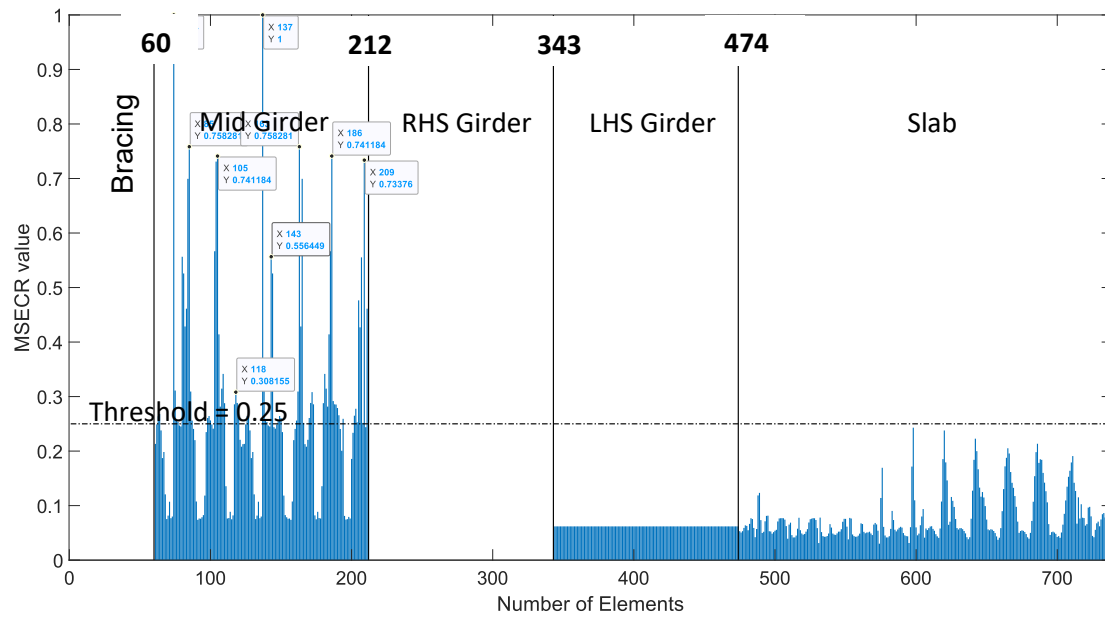


**Fig. 88** Case 8 identified damaged elements using FE-MSE method

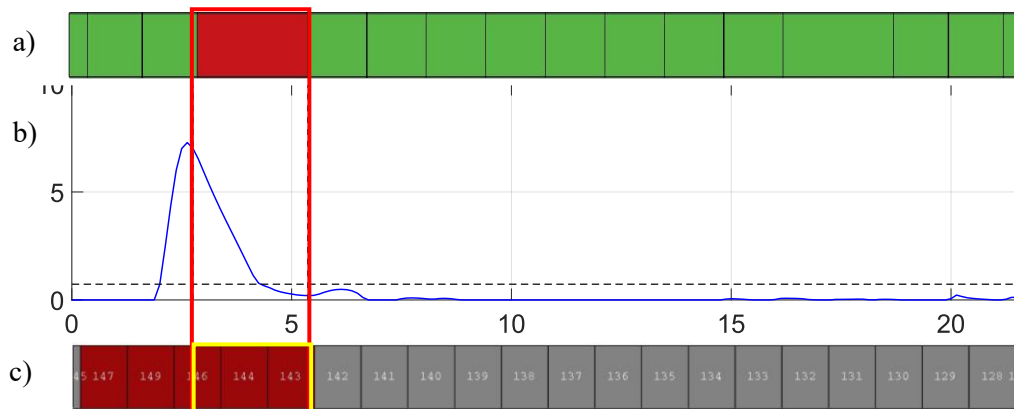


**Fig. 89** Integrated damage location identification for case 8. a) actual simulated damage, b) M-DBI estimation c) FE-MSE estimation.

The FE-MSE estimation shown in Figure 88 demonstrates damaged elements identification in Mid-Girder part of the bridge. There is also nonzero estimation in left hand side girder and slab parts, their values being lower than the threshold value indicates being ineligible to be considered as damaged elements. Hence the estimated damaged elements are shown in Figure 89 c).

## Summary of Case Studies

The results of cases considered in the scenario are summarized in two forms. First, the comparison of MDBI method and DBI method is presented in Table 11 and second, the integration of MDBI method and FE-MSE method is discussed in Table 12.

The summarized results in Table 11 shows the actual location of damage have been identified successfully in both approaches, where the accuracy of identification is expressed as a proportion of the actual damage extent in the longitudinal direction. However, when we consider the flawed damage location identification with both approaches, the MDBI method shows superiority in reducing error results both in terms of the longitudinal damage extent and amplitude of estimated Index.

**Table 11** Comparison of MDBI and DBI based on summary of case scenarios

Case	Actual Damage			Identified Damage Extent			
	Part	Case	Type	M-DBI		DBI	
				Actual	Error	Actual	Error
Case-1	Slab	Single	D1	100%	25%	100%	430%
Case-2	Slab	Single	D2	100%	135%	100%	439%
Case-3	Slab	Single	D1	58%	130%	0	230%
Case-4	Slab	Double	D1 & D2	63%	36%	100%	86%
Case-5	Slab	Double	D1 & D2	54%	169%	61%	196%
Case-6	Slab	Double	D1	73%	0%	85%	146%
Case-7	Slab	Single	D3	100%	205%	100%	542%
Case-8	Girder	Single	G	58%	28%	73%	56%

The integration of MDBI method and FE-MSE method improved damaged bridge part identification, damage position estimation in terms of both longitudinal and transversal directions, and damage extent estimation in areal representation.

In all simulated cases, the actual damaged bridge part is identified successfully. Furthermore, the visual representation of FE-MSE method enabled 3D representation of damage position enabling good user interactive bridge condition assessment.

**Table 12** Summarized results of case scenarios for the integration of MDBI and FE-MSE methods

Case	Actual Damage			Identified Damage						
	Part	Case	Type	Bridge Part	Direction		Extent			
					Long.	Lat.	Actual	Approx.	Incorrect	Integrated
<b>Case-1</b>	Slab	Single	D1	100%	100%	75%	38%	162%	0%	0%
<b>Case-2</b>	Slab	Single	D2	100%	71%	61%	100%	750%	550%	100%
<b>Case-3</b>	Slab	Single	D1	100%	100%	100%	20%	58%	0%	0%
<b>Case-4</b>	Slab	Double	D1 & D2	100%	50%	76%	50%	200%	90%	0%
<b>Case-5</b>	Slab	Double	D1 & D2	100%	20%	100%	20%	70%	140%	0%
<b>Case-6</b>	Slab	Double	D1	100%	100%	100%	56%	187%	13%	6%
<b>Case-7</b>	Slab	Single	D3	100%	70%	100%	75%	1000%	285%	0%
<b>Case-8</b>	Girder	Single	G	100%	71%	100%	100%	100%	0%	0%

Directionally, the estimated damaged elements are within the actual and approximate elements providing good identification results of the damage locations both in the longitudinal and transversal directions.

The accuracy of estimated damage extent is compared with the actual modeled damage area. In most of the cases, the identified damage extents are with in actual and neighborhood elements around the actual simulated damaged elements. However, cases with smaller damaged area and multiple damaged cases are observed to pick incorrect elements in the damage location identification process. The Integration of MDBI and FE-MSE method is observed to reduce estimation error for better identification of the actual damaged position.

### **Effect of Sensor Optimization on SHM Technique**

To examine the effect of optimization of sensors on the damage identification, Case 1 of the damage scenario is investigated here with the sensor arrangement like Ono R et. al. [17] used in their study. The position of sensors show was around the first quarter and third quarter of the slab length. Hence, sensors #48, #52, #180 and #184 are used to estimate the damage index.



As shown in the Figure 90, both the DBI method and the modified DBI method didn't identify the damage location. For individual sensors estimations shown on Figure 91 and 92 also both methods are unable to identify the damage location.

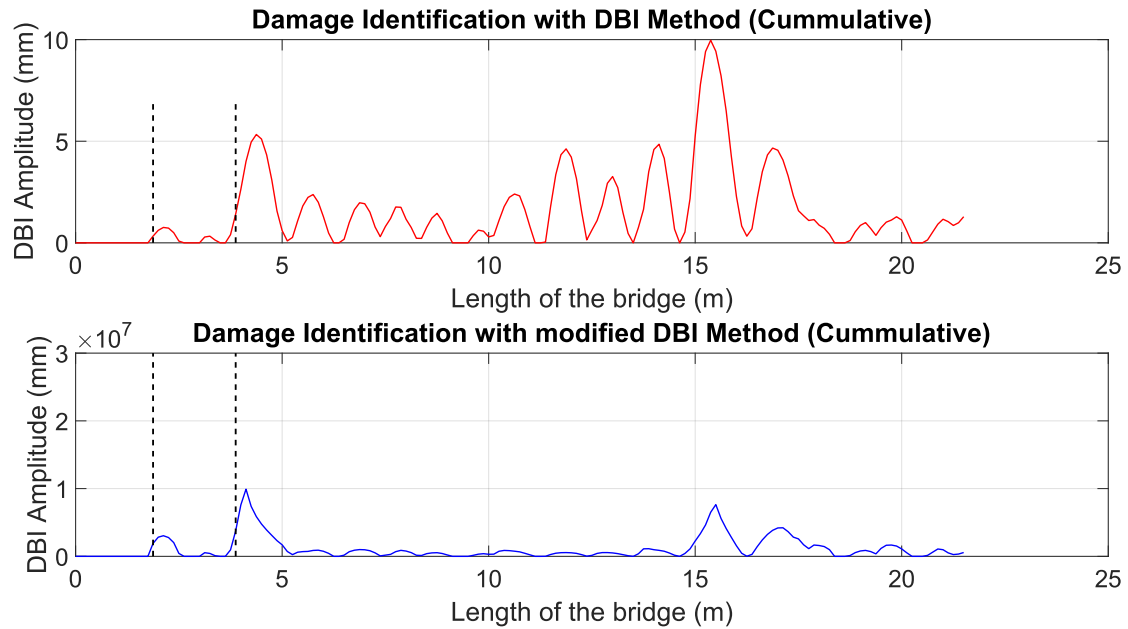


**Fig. 90** Damage location identification for DBI and MDBI methods for evaluating optimized sensor location

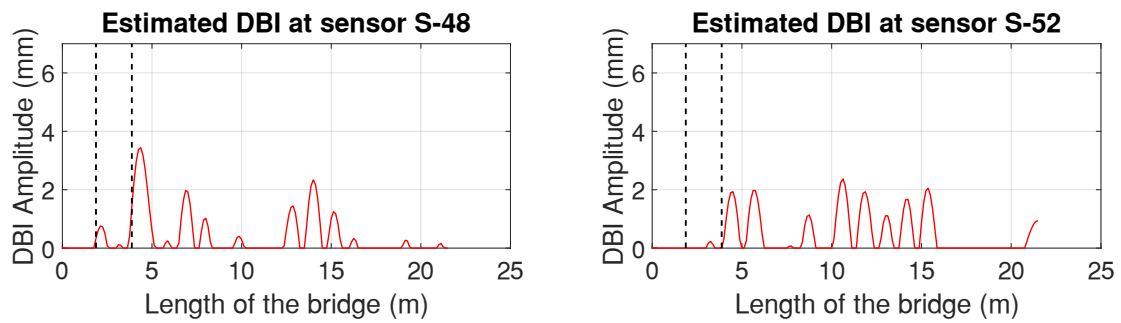


**Fig. 91** Damage location identification using individual sensors' estimation for DBI Method

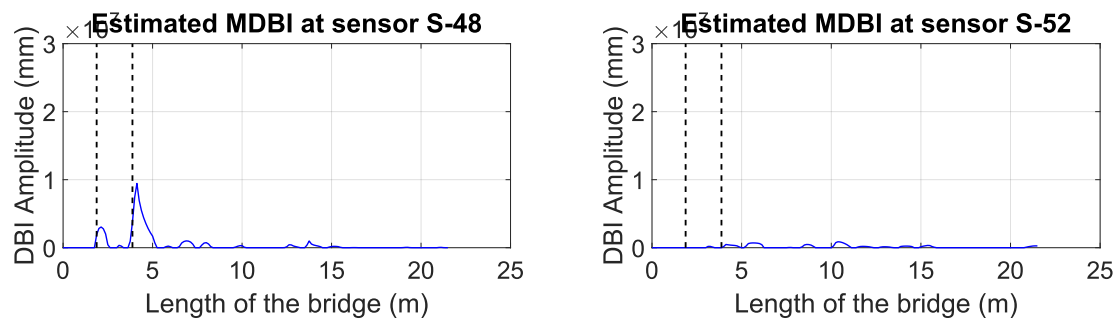


**Fig. 92** Damage location identification using individual sensors' estimation for MDBI Method

### Damage Identification from the Longitudinal Direction Sensors

The movement of the vehicle on the simply supported bridge, where the one end is free to move in the longitudinal direction, creates a vibration for the corresponding direction also. Response of the bridge for the damage type D1 located similar to case 1 is investigated to evaluate its effect. As shown from Figure 93 that, starting from the damage position, there is a variation in displacement response between the original and damaged cases. However, Figure 94 shows, there is no significant relationship between the damage location the estimated indexes.

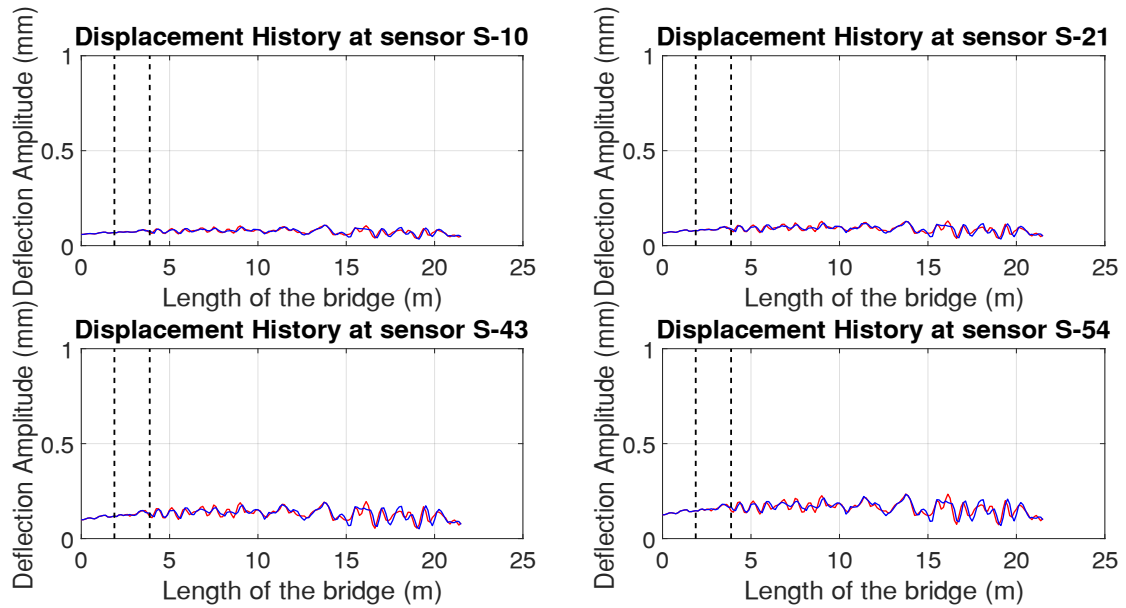


**Fig. 93** Displacement response in the longitudinal direction

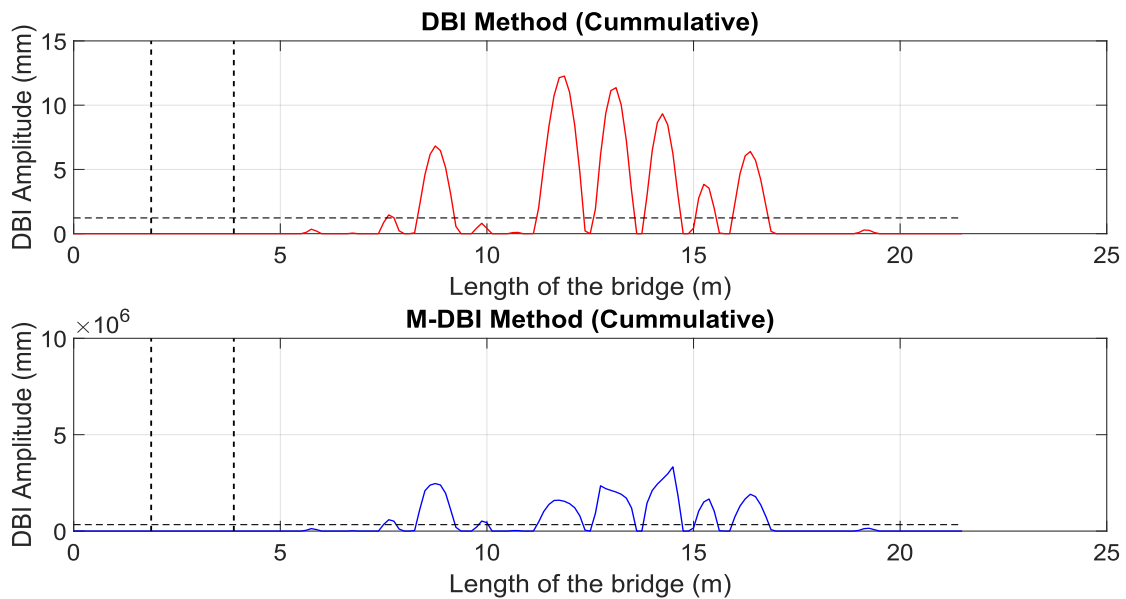


**Fig. 94** Damage location identification for DBI and MDBI methods for evaluating optimized sensor location

## Chapter 8: Conclusion

To summarize, in this research the integration of SHM sensors for damage identification in conjunction with optimization of their placement is studied. The following conclusions are drawn from the study.

- The optimization of displacement sensor improves the damage identification by providing stable location to eliminate the noise disturbance.
- The analyzed damage scenarios show, most of the damage cases are identified by the modified DBI method. Hence, the modification improved the DBI method compatibility to the dynamically excited bridge damage identification
- When using the cumulative damage index, the sensors positioned by the bridge entrance side have better damage identification than the sensors located at the exit side. Hence, evaluating the sensors in line with the direction of movement will eliminate the noise disturbance occurred by the sensor's contribution from the bridge exit side.
- Identification of the transverse position have multiple benefit. First, the measurement error in displacement response at the healthy state and damaged state due to the variation in vehicle position can be minimized. Second, it will be used in the distributing contribution from each sensor to the total DBI index estimation by factorizing the location of sensor with respect to the vehicle position. Furthermore, by examining the transvers position and the lane direction, one can identify the direction of movement and give emphasis to the sensors in the bridge entrance side for more accurate damage detection.
- When a smaller damage occurs after the bigger extent of damage, it will undermine the detectability. Therefore, analyzing damage identification from the vehicle movement in each direction can solve this problem.
- Even though, the longitudinal sensors show variation in displacement response pattern, identification of damage from this direction do not have satisfactory result. Hence, only providing vertical direction displacement sensors are recommended.
- The finite element based modal strain energy method identified the actual damaged part of the bridge and the side in which the damaged elements exit. However, the estimated damage is spread over the actual damage. It shows some degree of over estimation.
- The combination of modified DBI method and MSE method in multi-approach damage identification technique narrows the identification of damage to the actual position. Furthermore, providing user interactive damage location identification.

## **Limitation and Future work**

The research conducted purely from the numerical analysis. Therefore, it's worthwhile to conduct field cases investigations to calibrate the unaddressed issues in the simulation-based approach.

Beyond identifying the position of damage, estimating its severity or the remaining service life of the bridge contribute to the automation of bridge condition assessment using the proposed approach. Hence further studies in the damage severity will greatly enhance the contribution.

The research considers, the cause of dynamic vibration from the perspective of vehicle-bridge-interaction, however, impact generated at the entrance of the bridge are also other cause of dynamic vibration. As a result, the effect of dynamic impact created by the vehicle at the bridge entrance shall be investigated in future studies for its contribution in affecting the efficiency of damage location identification.

Finally, it is recommended that more emphasis shall be given to the application of integrated multiple SHM technique using different approaches to address mass bridge assessment.

## REFERENCES

- [1] J. Zhou, Y. Xu, and T. Zhang, "A Wireless Monitoring System for Cracks on the Surface of Reactor Containment Buildings," pp. 1–13, 2016, doi: 10.3390/s16060883.
- [2] H. Jin, H. Sohn, M. P. Desimio, and K. Brown, "Reference-free fatigue crack detection using nonlinear ultrasonic modulation under various temperature and loading conditions," *Mech. Syst. Signal Process.*, vol. 45, no. 2, pp. 468–478, 2014, doi: 10.1016/j.ymssp.2013.12.001.
- [3] A. Gheitani and D. K. Harris, "Overload flexural distribution behavior of composite steel girder bridges," *J. Bridg. Eng.*, vol. 20, no. 5, 2015, doi: 10.1061/(ASCE)BE.1943-5592.0000671.
- [4] K. Deb and H. Jain, "An Evolutionary Many-Objective Optimization Algorithm Using Reference-point Based Non-dominated Sorting Approach , Part I : Solving Problems with Box Constraints," no. c, pp. 1–23, 2013.
- [5] T. Omar and M. L. Nehdi, "Condition assessment of reinforced concrete bridges: Current practice and research challenges," *Infrastructures*, vol. 3, no. 3, pp. 1–23, 2018, doi: 10.3390/infrastructures3030036.
- [6] T. Omar and M. L. Nehdi, "Resilient infrastructure condition assessment and deterioration prediction tools for concrete bridges: a new look," no. June, 2016.
- [7] B. A. Graybeal, B. M. Phares, D. D. Rolander, M. Moore, and G. Washer, "Visual inspection of highway bridges," *J. Nondestruct. Eval.*, vol. 21, no. 3, pp. 67–83, 2002, doi: 10.1023/A:1022508121821.
- [8] W. Ostachowicz, R. Soman, and P. Malinowski, "Optimization of sensor placement for structural health monitoring: a review," *Struct. Heal. Monit.*, vol. 18, no. 3, pp. 963–988, 2019, doi: 10.1177/1475921719825601.
- [9] E. Ozer, M. Q. Feng, and D. Feng, "Citizen Sensors for SHM: Towards a Crowdsourcing Platform," pp. 14591–14614, 2015, doi: 10.3390/s150614591.
- [10] A. Miyamoto, J. Puttonen, and A. Yabe, "Long Term Application of a Vehicle-Based Health Monitoring System to Short and Medium Span Bridges and Damage Detection Sensitivity," pp. 68–122, 2017, doi: 10.4236/eng.2017.92005.
- [11] G. Comanducci and F. Ubertini, "On vibration-based damage detection by multivariate statistical techniques : application to a long-span arch bridge," no. X, pp. 1–17, 2015, doi: 10.1177/ToBeAssigned.
- [12] A. P. Adewuyi, Z. Wu, and N. H. . K. Serker, "Structural Health Monitoring Assessment of Vibration-based Damage," 2009, doi: 10.1177/1475921709340964.
- [13] P. Cawley and R. D. Adams, "A Vibration Technique for Non-Destructively Assessing the Integrity of Structures," vol. 1982, no. April 1978, 1982, doi: 10.1243/JMES.
- [14] A. Alaimo, A. Milazzo, and C. Orlando, "A strain sensing structural health monitoring system for delaminated composite structures," *Appl. Mech. Mater.*, vol. 249–250, pp. 849–855, 2013, doi: 10.4028/www.scientific.net/AMM.249-250.849.
- [15] R. A. G. Rodrigo *et al.*, "Corrosion-fatigue tests using strain gauges on the specimen to monitoring the load applied under specimen subject to high pressure. Rodrigo R. A. Garcia," 2016.
- [16] M. Yeager, M. Todd, W. Gregory, and C. Key, "Assessment of Embedded Fiber Bragg Grating for Structural Health Monitoring Of Composites," 2017, doi: 10.1177/1475921716665563.

- [17] R. Ono, T. M. Ha, and S. Fukada, "Analytical study on damage detection method using displacement influence lines of road bridge slab," *J. Civ. Struct. Heal. Monit.*, vol. 9, no. 4, pp. 565–577, 2019, doi: 10.1007/s13349-019-00352-9.
- [18] T. M. Ha and S. Fukada, "Nondestructive damage detection in deteriorated girders using changes in nodal displacement," *J. Civ. Struct. Heal. Monit.*, vol. 7, no. 3, pp. 385–403, 2017, doi: 10.1007/s13349-017-0231-x.
- [19] I. Štimac, A. Mihanović, and I. Kožar, "Damage detection from analysis of displacement influence lines," *SICON - Int. Conf. Bridg.*, pp. 1001–1008, 2006.
- [20] S. S. Kessler, "Damage Detection in Composite Materials Using Lamb Wave Methods," no. June 2014, 2002, doi: 10.1088/0964-1726/11/2/310.
- [21] P. Khalili and P. Cawley, "NDT and E International The choice of ultrasonic inspection method for the detection of corrosion at inaccessible locations," *NDT E Int.*, vol. 99, no. March 2017, pp. 80–92, 2018, doi: 10.1016/j.ndteint.2018.06.003.
- [22] V. Giurgiutiu, "Tuned Lamb Wave Excitation and Detection with Piezoelectric Wafer Active Sensors for Structural Health Monitoring," vol. 16, no. April, 2005, doi: 10.1177/1045389X05050106.
- [23] V. Giurgiutiu and A. N. Zagari, "Damage Detection in Thin Plates and Aerospace Structures with the ElectroMechanical Impedance Method Damage Detection in Thin Plates and Aerospace Structures with the Electro-Mechanical Impedance Method," no. June, 2005, doi: 10.1177/1475921705049752.
- [24] D. Roach, "Use of Comparative Vacuum Monitoring Sensors for Automated , Wireless Health Monitoring of Bridges and Infrastructure."
- [25] D. P. Roach and S. N. Laboratories, "Real time crack detection using mountable comparative vacuum monitoring sensors," no. July 2009, 2019, doi: 10.12989/sss.2009.5.4.317.
- [26] Z. Y. Shi, S. S. Law, and L. M. Zhang, "Structural damage localization from modal strain energy change," *J. Sound Vib.*, vol. 218, no. 5, pp. 825–844, 1998, doi: 10.1006/jsvi.1998.1878.
- [27] P. Dewangan, A. Parey, A. Hammami, F. Chaari, and M. Haddar, "Damage detection in wind turbine gearbox using modal strain energy," *Eng. Fail. Anal.*, vol. 107, no. September 2019, p. 104228, 2020, doi: 10.1016/j.engfailanal.2019.104228.
- [28] S. . Jang, S. H. Sim, and B. F. Spencer Jr., "Structural damage detection using static strain data," *Appl. Mech. Mater.*, vol. 501–504, pp. 852–855, 2014, doi: 10.4028/www.scientific.net/AMM.501-504.852.
- [29] Z. Sun, T. Nagayama, D. Su, and Y. Fujino, "A Damage Detection Algorithm Utilizing Dynamic Displacement of Bridge under Moving Vehicle," *Shock Vib.*, vol. 2016, no. March, 2016, doi: 10.1155/2016/8454567.
- [30] T. Vo-Duy, D. Duong-Gia, V. Ho-Huu, H. C. Vu-Do, and T. Nguyen-Thoi, "Multi-objective optimization of laminated composite beam structures using NSGA-II algorithm," *Compos. Struct.*, vol. 168, pp. 498–509, 2017, doi: 10.1016/j.compstruct.2017.02.038.
- [31] W. Khan Mashwani, A. Salhi, O. Yeniay, H. Hussian, and M. A. Jan, "Hybrid non-dominated sorting genetic algorithm with adaptive operators selection," *Appl. Soft Comput. J.*, vol. 56, pp. 1–18, 2017, doi: 10.1016/j.asoc.2017.01.056.
- [32] Y. Wang, Y. Shen, X. Zhang, G. Cui, and J. Sun, "An Improved Non-dominated Sorting Genetic Algorithm-II (INSGA-II) applied to the design of DNA codewords," *Math. Comput. Simul.*, vol. 151, pp. 131–139, 2018, doi: 10.1016/j.matcom.2018.03.011.

- [33] Y. Yuan, H. Xu, and B. Wang, “An Improved NSGA-III Procedure for Evolutionary Many-Objective Optimization Categories and Subject Descriptors,” no. July 2014, 2016, doi: 10.1145/2576768.2598342.
- [34] Y. Yu, C. S. Cai, and L. Deng, “Nothing-on-road bridge weigh-in-motion considering the transverse position of the vehicle,” *Struct. Infrastruct. Eng.*, vol. 14, no. 8, pp. 1108–1122, 2018, doi: 10.1080/15732479.2017.1401095.
- [35] M. Agostinacchio, D. Ciampa, and S. Olita, “The vibrations induced by surface irregularities in road pavements – a Matlab ® approach,” no. September 2013, 2015, doi: 10.1007/s12544-013-0127-8.
- [36] Z. Sun and Z. Zou, “Towards an efficient method of predicting vehicle-induced response of bridge,” vol. 33, no. 7, pp. 2067–2089, 2016, doi: 10.1108/EC-02-2015-0034.
- [37] V. Assets, J. Stevens, and I. S. O. S. Order, “INTERNATIONAL STANDARD ISO Mechanical vibration — Road surface profiles — Reporting of measured data,” vol. 2016, 2016.
- [38] D. Julong, “Introduction to grey systems theory,” *J. Grey Syst.*, vol. 1, pp. 1–24, 1989, doi: 10.1007/978-3-642-16158-2\_1.
- [39] D. M. Siringoringo and Y. Fujino, “System identification of suspension bridge from ambient vibration response,” *Eng. Struct.*, vol. 30, no. 2, pp. 462–477, 2008, doi: 10.1016/j.engstruct.2007.03.004.
- [40] C. R. Farrar and G. H. James, “System identification from ambient vibration measurements on a bridge,” *J. Sound Vib.*, vol. 205, no. 1, pp. 1–18, 1997, doi: 10.1006/jsvi.1997.0977.
- [41] K. Yamada, Y. Saito, K. Nankai, T. Nonomura, K. Asai, and D. Tsubakino, “Fast greedy optimization of sensor selection in measurement with correlated noise,” *Mech. Syst. Signal Process.*, vol. 158, 2021, doi: 10.1016/j.ymssp.2021.107619.
- [42] R. E. Kalman, “Effective construction of linear state-variable models from input/output functions 1),” pp. 3–6.
- [43] R. PAPP, K. ELLIOTT, and A. SCHENK, “A consistent-mode indicator for the eigensystem realization algorithm,” no. May 1992, 1992, doi: 10.2514/6.1992-2136.
- [44] Y. Li, J. Zhang, Z. Guan, and Y. Chen, “Experimental Study on the Correlation between Crack Width and Crack Depth of RC Beams,” 2021.